T.R.
GEBZE TECHNICAL UNIVERSITY
GRADUATE SCHOOL OF NATURAL AND APPLIED SCIENCES

EPITAXIAL PtCo ULTRA-THIN FILM STUDY ON SINGLE CRYSTAL AS PRELIMINARY WORK

BAHA SAKAR
A THESIS SUBMITTED FOR THE DEGREE OF
MASTER OF SCIENCE
DEPARTMENT OF PHYSICS

GEBZE
2015

T.R.

GEBZE TECHNICAL UNIVERSITY

GRADUATE SCHOOL OF NATURAL AND APPLIED SCIENCES

EPITAXIAL PtCo ULTRA-THIN FILM STUDY ON SINGLE CRYSTAL AS PRELIMINARY WORK

BAHA SAKAR

A THESIS SUBMITTED FOR THE DEGREE OF

MASTER OF SCIENCE

DEPARTMENT OF PHYSICS

THESIS SUPERVISOR

ASSOC. PROF. DR. OSMAN ÖZTÜRK

GEBZE

2015

T.C.
GEBZE TEKNİK ÜNİVERSİTESİ
FEN BİLİMLERİ ENSTİTÜSÜ

TEK KRİSTAL ÜZERİNE EPİTAKSİYEL PtCo ULTRA-İNCE FİLM ÇALIŞMASI

BAHA SAKAR
YÜKSEK LİSANS TEZİ
FİZİK ANABİLİM DALI

DANIŞMANI
DOÇ. DR. OSMAN ÖZTÜRK

GEBZE
2015

GEBZE TEKNİK ÜNİVERSİTESİ	**YÜKSEK LİSANS JÜRİ ONAY FORMU**

GTÜ Fen Bilimleri Enstitüsü Yönetim Kurulu'nun 24/06/2015 tarih ve 2015/39 sayılı kararıyla oluşturulan jüri tarafından 15/06/2015 tarihinde tez savunma sınavı yapılan Baha Sakar'ın tez çalışması Fizik Anabilim Dalında YÜKSEK LİSANS tezi olarak kabul edilmiştir.

JÜRİ

ÜYE
(TEZ DANIŞMANI) : Doç. Dr. Osman Öztürk

ÜYE : Prof. Dr. Yurii Chumakov

ÜYE : Yrd. Doç. Dr. Mustafa Erkovan

ONAY

Gebze Teknik Üniversitesi Fen Bilimleri Enstitüsü Yönetim Kurulu'nun

...../...../..... tarih ve ...../..... sayılı kararı.

İMZA/MÜHÜR

SUMMARY

PtCo alloys are well known with their high catalytic properties, good corrosion resistance and magnetic properties. The equiatomic $Pt_{50}Co_{50}$ phase with $L1_0$ crystal structure is the best candidate for magnetic storage applications with its high magneto crystalline anisotropy. Achieving such anisotropy lies on well controlled stoichiometry and the structure of the crystal. In order to understand and control its properties, PtCo samples must be prepared with a well controlled manner.

Previous studies reported for a lower Co ratio then expected for the equiatomic PtCo samples prepared with various techniques. This problem result not well controlled manner depositions. Furthermore, due to this problem un-expected physical properties maybe observed in prepared samples. This study focused on the variation of PtCo ratio. Two different type of substrate used in the study are Pt(111) single crystal and a SiO_x (111) wafer. Pure Co and $Pt_{50}Co_{50}$ samples are prepared on these two different substrates by Magnetron Sputtering. In order to investigate the effect of sample preparation temperature on the variation of PtCo ratio, additional samples are prepared for each film and substrate at various temperatures (RT, 300^{o}C, 450^{o}C, 500^{o}C and 550^{o}C).

Elemental composition and stoichiometry of the samples are analyzed by X-Ray Photoelectron Spectroscopy (XPS) and Auger Photoelectron Spectroscopy (AES). Ultraviolet Photoelectron Spectroscopy (UPS) is used to understand the electronic structure of surfaces and the electronic interaction of the Pt and Co under different preparation conditions. To investigate the epitaxial growth and determine the surface symmetry, low energy electron diffraction (LEED) has been used.

Results of samples prepared on Pt(111) indicate for the Co diffusion through the platinum substrate by the increasing temperature. Furthermore, either the Co or PtCo films grown on P(111) above 450°C have the same stoichiometry, surface symmetry and similar electronic properties. Results of the samples prepared on SiO_x indicate for a bonding formation between Pt and Si with the increasing temperature while there is a significant electronic structure change in Co.

Key Words: PtCo, Magnetron Sputtering, XPS, AES, UPS, LEED.

ÖZET

PtCo alaşımlar, güçlü katalitik özellikleri, yüksek korozyon dirençleri ve manyetik özellikleri ile dikkat çekmektedir. Eşit sayıda atom içeren, $L1_0$ kristal yapısındaki $Pt_{50}Co_{50}$ fazı, sahip olduğu yüksek kristal anizotropisi ile manyetik kayıt uygulamaları için güçlü bir adaydır. PtCo alaşımların özelliklerini anlamak ve kontrol etmek için, örnek hazırlama sürecinin hassas bir şekilde kontrol edilmesi gerekmektedir.

Daha önce yapılan çalışmalarda, çeşitli tekniklerle hazırlanan eşit atomlu PtCo örneklerin Co oranlarının beklenenden daha düşük olduğu bildirilmiştir. Bu sorun, kontrollü örnek büyütmeyi engellemektedir. Dahası, bu problemler örneklerde beklenmeyen özelliklerin gözlenmesine neden olabilmektedir.

Bu çalışmada PtCo oranlarındaki değişimlere odaklanılmıştır. Çalışma dahilinde Pt(111) tek kristal ve SiO_x wafer olmak üzere iki farklı alttaş kullanılmıştır. Bu alttaşlar üzerine, magnetron sıçratma tekniği kullanılarak saf Co ve $Pt_{50}Co_{50}$ ince filmleri büyütülmüştür. Örnek hazırlama sıcaklığının PtCo oranlarındaki değişimler üzerindeki etkisinin incelenmesi amacıyla her alttaş üzerine büyütülen her bir örnek için farklı sıcaklıklarda (RT, 300^{o}C, 450^{o}C, 500^{o}C and 550^{o}C) ilave örnekler hazırlanmıştır. Örneklerin elemental kompozisyon ve stokiyometrileri X-ışını Fotoemisyon Spektroskopisi (XPS) ve Auger Elektron Spektroskopisi (AES) ile incelenmiştir. Örnek yüzeylerinin elektronik yapıları ve Pt ile Co'ın farklı örnek hazırlama sıcaklıklarındaki elektronik etkileşimlerinin incelenmesinde ise UV Fotoemisyon Spektroskopisi (UPS) kullanılmıştır. Düşük enerjili elektron kırınımı (LEED) tekniği kullanılarak da epitaksiyel büyüme ve örnek yüzeylerinin kristal simetrileri incelenmiştir.

Pt(111) alttaş üzerine hazırlanan örneklerin analiz sonuçları artan sıcaklık ile beraber kobalt atomlarının alttaşa difüze olduğunu göstermektedir. Ayrıca, 450°C ve üstü sıcaklıklarda hazırlanan saf Co ve PtCo örneklerin her ikisinin de, birbirleriyle aynı stokiyometriye, yüzey simetrisine ve benzer elektronik yapıya sahip oldukları gözlemlenmiştir. SiO_x alttaş üzerine yapılan çalışmalar ise örnek hazırlama sıcaklığı artışı ile beraber Pt ile Si arasında bir bağ oluştuğuna, kobaltın da elektronik yapısının değiştiğine işaret etmektedir.

Anahtar Kelimeler: PtCo, Magnetron Sıçratma, XPS, AES, UPS, LEED.

ACKNOWLEDGEMENTS

Firstly, I would like to express my deep and sincere gratitude to my advisor, Assoc. Prof. Dr. Osman Öztürk, who not only shared his profound scientific knowledge with me but also taught me great lessons of life. His support, suggestions and encouragement gave me the drive and will to complete this work.

I wish to express my warm and sincere thanks to Asst. Prof. Dr. Sibel Tokdemir Öztürk, Asst. Prof. Dr Mustafa Erkovan and Dr. Ali Şems Ahsen for their guidance, helps and encouragement during this work.

I also wish to express my deepest thanks to Melek Türksoy Öcal for her support, encouragement and friendship. By sharing her valuable experience, this work becomes possible.

I also want to thank my colleagues and friends Dilek Taşkın Gazioğlu, Nur Büşra Koçyiğit, Mehmet Emre Aköz and İsmet Gelen for supporting me all this time.

I am grateful to my valuable parents and my brother for their love and endless support.

I dedicate this work to my late uncle Reha Sakar.

TABLE of CONTENTS

LIST of ABBREVIATIONS and ACRONYMS

Abbreviations and Acronyms		**Explanations**
Å	:	Angstrom
E_k	:	Electron Kinetic Energy
E_x	:	Excitation Energy
ϕ_s	:	Sample Work Function
υ	:	Frequency
h	:	Planck Constant
E_b	:	Binding Energy
$\lambda(E)$	:	Inelastic Mean Free Path
λ_f	:	Inelastic Mean Free Path of Film
λ_s	:	Inelastic Mean Free Path of Substrate
d	:	Thickness
I	:	Intensity
a_o	:	Bohr Atomic Radius
q	:	Charge
$\vec{G}_{hkl}$	:	Reciprocal Lattice Vector
$\vec{k}_i$	:	Wave Vector
λ_0	:	De Broglie Wavelength
m_e	:	Electron Mass
A_{focus}	:	Beam Focus Area
E_I	:	Energy of Ion
2D	:	Two Dimension
3D	:	Three Dimension
AES	:	Auger Electron Spectroscopy
Ag	:	Silver
Al	:	Aluminum
Ar	:	Argon
Ar^+	:	Argon Ion
arPES	:	Angular Resolved Photoelectron Spectroscopy

ASF	:	Atomic Sensitivity Factor
BCC	:	Body Centered Cubic
BE	:	Binding Energy
Co	:	Cobalt
DC	:	Direct Current
E	:	Energy
eV	:	Electron Volt
FCC	:	Face Centered Cubic
FCT	:	Face Centered Tetragonal
FWHM	:	Full Width Half Maximum
GTU	:	Gebze Technical University
HCP	:	Hexagonal Close Packed
HSA	:	Hemispherical Analyzer
HWHM	:	Half Width Half Maximum
ISS	:	Ion Scattering Spectroscopy
KE	:	Kinetic Energy
LEED	:	Low Energy Electron Diffraction
m	:	Meter
Mg	:	Magnesium
min	:	Minute(s)
MSD	:	Magnetron Sputter Deposition
nm	:	Nanometer
NRC	:	Nanotechnology Research Center
O	:	Oxygen
PBN	:	Pyrolytic Boron Nitride
pDC	:	Pulsed Direct Current
Pt	:	Platinum
QCM	:	Quartz Crystal Microbalance
RF	:	Radio Frequency
RGA	:	Residual Gas Analyzer
RSF	:	Relative Sensitivity Factor
RT	:	Room Temperature
sec	:	Second

Si	:	Silicon
srvy	:	Survey
STM	:	Scanning Tunneling Microscope
Ta	:	Tantalum
UHV	:	Ultra High Vacuum
UPS	:	Ultraviolet Photoelectron Spectroscopy
UV	:	Ultraviolet
W	:	Watt
XPS	:	X-Ray Photoelectron Spectroscopy

LIST of FIGURES

LIST of TABLES

1. INTRODUCTION

The advancements in characterization and preparation techniques of nanostructures give rise to interest in bimetallic nanoalloys. While the addition of second metal brings out new physical and chemical properties, advanced preparation techniques make these properties controllable and increase the alloys functionality. This controllability in physical properties becomes a promising remedy for magnetic recording field's most substantial problem, need of increased magnetic storage density. In order to increase this density, the size of the magnetic blocks must be reduced [1]. However a crucial problem in the size reduction is the loss of thermal stabilization in magnetization direction [2], [3]. Studies and predictions shows that the alloys formed by a 3d metal and a 4d/5d metal are promising candidates in order to overcome this problem. Due to high spin moment of 3d metals (i.e. Fe, Co) a large orbital moment is induced on 4d/5d metals (i.e. Pt, Pd, Rh). The large orbital moment causes a strong spin orbit coupling on the 4d/5d metal thus the magnetic anisotropy is enhanced, and furthermore the thermal stabilization of the magnetic blocks can be achieved [3].

From this 3d-4d/5d alloys, PtCo nanostructures hold great importance because of their tunable catalytic properties, magnetic moments and anisotropy by changing the elemental composition.

PtCo nanoparticles are known to have a wide range of catalysis applications. Thin films, with different chemical ordered structures and different sample preparation temperatures, show different catalytic properties due to changes in their electronic and mechanic structures [4], [5]. Platinum is an expensive noble metal but a good catalyst, therefore studies are focused to lower the price (i.e. lower Pt composition) and to increase the efficiency of the platinum based fuel cells. It has been showed that the PtCo catalysts have a good catalytic reactivity while the usage of Pt has decreased dramatically in catalyst layer in fuel cell applications. Furthermore, recent studies towards fuel cell show that the PtCo structures are also efficient catalyst for oxygen reduction reactions.

In magnetic storage applications, PtCo equiatomic nanoalloys are the best candidates with the magneto crystalline anisotropy twenty times better than pure cobalt's values [6]. This extremely high magneto crystalline anisotropy is a result of

the pure Co and Pt atomic planes stacked up to [001] direction in a chemically equiatomic ordered $L1_0$ phase.

Due to its various chemical orders, and complexity; controlling and understanding the properties of PtCo is challenging. Furthermore, amorphous or polycrystalline structures increase the level of difficulties. Due to defects and differently oriented crystallographic axes, the information obtained from the whole sample will be complicated. However prepared epitaxial PtCo samples will be identically oriented with respect to the substrate, and it will help to understanding and controlling its properties.

In previous studies, it has been reported that the elemental ratio calculations of PtCo samples prepared with various deposition techniques (e.g. Magnetron Sputtering, E-Beam deposition) showed a Co ratio lower than the expected ratio. Furthermore studies performed by our research group towards to grow PtCo epitaxial film on Pt substrate, showed that this ratio can drop to a value below 1% with increasing temperatures. Especially, this problem in multi-layer ultra-thin films result not well controlled manner depositions and un-expected physical properties. For a controlled sample preparation, the mechanism behind this ratio change must be well understood.

This study focused on the variation of PtCo ratio with samples grown at different temperatures on different substrates. Two different type of substrate used in the study are Pt(111) single crystal and a SiO_x (111) wafer. Samples prepared on these two different substrates are 14 Å Co and 33 Å $Pt_{50}Co_{50}$ (14 Å Co + 19 Å Pt). Furthermore, for each film and substrate, additional samples were prepared at various temperatures (RT, 300^{o}C, 450^{o}C, 500^{o}C and 550^{o}C). Samples were prepared with magnetron sputtering technique with using ultra-pure cobalt and platinum targets. Depositions rates were kept at low values (>0,1 Å/sec) in order to make a layer by layer growth.

The samples are investigated for their chemical stoichiometry, electronic distribution and crystallographic structure. Photoelectron spectroscopies and Auger electron spectroscopy are the best options for stoichiometry and electronic investigation of surfaces because of their high surface sensitivity. Auger electron spectroscopy (AES) and x-ray photoelectron spectroscopy (XPS) are two extremely surface sensitive spectroscopic characterization techniques. In this study, both techniques are used to determine the surface stoichiometry and to understand the

change in Pt/Co ratio with a comparison of different techniques. Furthermore, the other electron spectroscopy technique used in this study is ultraviolet photoelectron spectroscopy (UPS) which is a high resolution electron spectroscopy technique focused on valance electron distribution of the surface. UPS spectra of the samples are used to understand the electronic structure of surfaces and the electronic interaction of the Pt and Co under different preparation conditions. The samples prepared on substrate were expected to grow epitaxially. To investigate the epitaxial growth and determine the surface symmetry, low energy electron diffraction (LEED) has been used. LEED is highly surface sensitive, 2D surface structure determination technique. LEED results helped to determine the surface symmetry, the quality of the surface crystal structure of samples and substrates.

2. LITERATURE REVIEW of Pt/Co

Bimetallic nanoalloys draw great interest for their tunable physical and chemical properties for last decades. Among these nanoalloys 3d-4d/5d combinations (i.e. FePt, CoPt, FePd etc…) take a significant role due to their good magnetic, catalytic and mechanical properties and stability. PtCo, one of these alloys, had attracted much interest.

Cobalt is a 3d metal located at 8th group in periodic table. Such as its neighbors in periodic table, Fe and Ni, Co is a room temperature ferromagnet. Cobalt has a curie temperature of 1115°C [7], and a magnetic moment of 1,6-1,7 bohr magnetron per atom [8]. Due to its 5 different oxidation states and magnetic properties, it's mostly used and corrosion resistance and magnetic applications. Cobalt has two stable and one unstable phase. The first two are HCP and FCC which's dominance is depend to temperature [9], and the third one ε-Co whose has a complex cubic symmetry [10]. It is also stated that the crystal parameters and particle size of Co are closely related [11]. For the particle diameters below 200 Å, Co has a pure FCC β-phase while it has a mixture of FCC β and HCP α phases around 300 Å. Above 400 Å, HCP α becomes the dominant structure while small amount of FCC β is observed [11].

The other element of the alloy, platinum is a 5d noble metal belongs to the 8th group of periodic table. Alongside it's non-reactivity and chemically stable nature, Pt is also highly stable in terms of thermal expansion. Pt is mostly known as a paramagnetic metal. However, pure Pt is non-magnetic by its nature. The paramagnetic behavior of Pt is an outcome of its interaction with ferromagnetic materials (i.e. Fe, Co) [2], [12]. All these features give Pt a high importance and a wide range of application field from fashion, and building trade to electronics and catalysts. Platinum crystal has a crystal structure of face centered cubic with a lattice constant of 3,92Å

Platinum/Cobalt alloys are the binary systems with high solid-solubility [1]. Different chemical orders of Pt/Co give rise for different significant properties, like high catalytic influence, good corrosion resistance and important magnetic features. Because of the various chemical orders and their complexity, controlling and understanding of the properties of Pt/Co requires well studied phase diagrams. Most

common used phase diagram of PtCo alloys were published by Massalski et.al (Figure 2.1) [13].

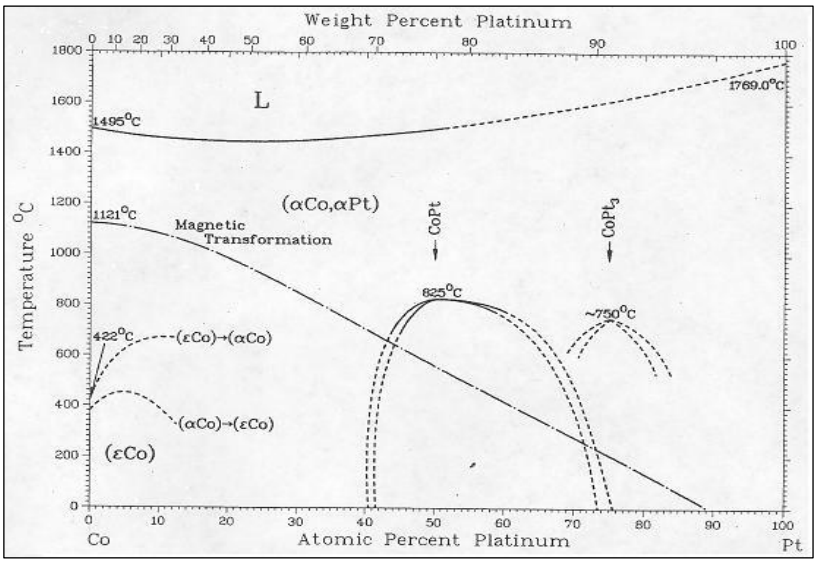

Figure 2.1: Phase Diagram of Platinum Cobalt Alloys Published by Massalski.

Even though pure Co has an hcp phase at room temperature, PtCo phase diagram points out for the fcc-type structure of Pt. According to Massalski's phase diagram, most common phases of PtCo have a face centered cubic (FCC) crystal structure. However, near to room temperature, other phases arise with hexagonal close-packed (HCP) crystal structure. Two ordered phases can be found on Massaslski's phase diagram are; a $L1_0$ and a $L1_2$ phases for elemental ratios of Pt:Co with 1:1 and 1:3 respectively. The alloy PtCo(1:3) was known as a disordered fcc phase at higher temperatures and a disordered hcp phase. However, recent studies indicate for another $L1_2$ phase with an elemental ratio of 1 Pt for 3 Co around 500°C [2], [3], [14]. An extended phase diagram of PtCo is recently published (by Andreazza et.al.) by gathering the results of most recent studies (Figure 2.2). Order formation temperatures are near to 750°C for the $L1_2$ phase with elemental Pt/Co ratio of 3:1 and near 825°C for equiatomic $L1_0$ phase. However these values are for bulk and these won't be totally applicable for ultra-thin films. Artymowicz and his friends obtained a $L1_0$ phase by annealing Pt/Co multilayer at 500°C, and achieved an epitaxial film on a MgO(001) substrate [1].

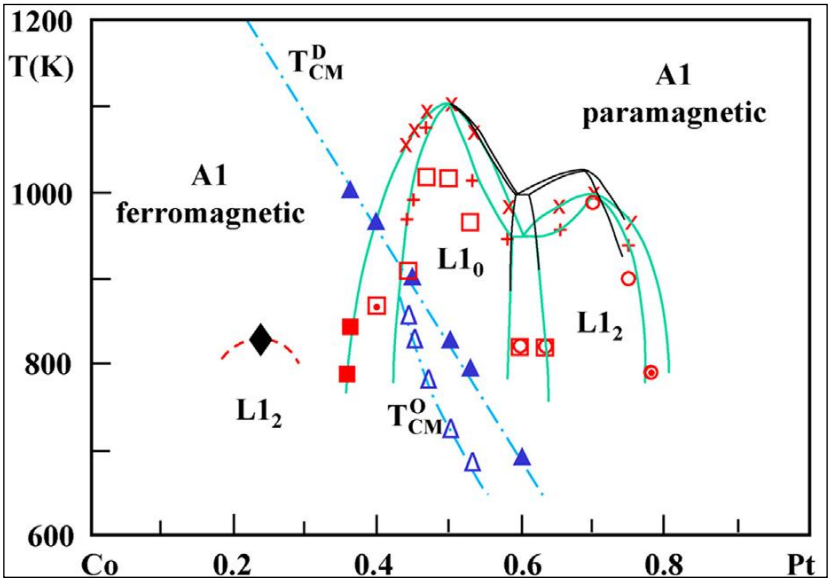

Figure 2.2: Phase Diagram of Platinum Cobalt Alloys Published by Andreazza.

Phase diagram of Pt-Co published by Andreazza and his friends, apart from the $L1_2$ phase of $PtCo_3$, points out slightly different features in curie temperatures. Filled and unfilled blue rectangulars (▲, Δ)are the measured curie temperatures for disordered and ordered structures [15]. A1 phase is a fcc structure with Co and Pt atom distributed randomly on sites. The red rectangulars and circles (■, □, ○) are for the pure phases of A1, $L1_0$ and $L1_2$ respectively. Blue dot-dashed line is the results of T_{cm} calculations with tetrahedron approximation of the cluster variation method for ordered and disordered phases [16]. The ordered, partially ordered and disordered configurations of PtCo is given in Figure 2.3 [3].

$L1_0$ phase (Figure 2.4) is a crystal structure with a symmetry group of p4/mmm (D^1_{4h}) and a lattice complex; $A\ @\ 2e\left(0,\frac{1}{2},\frac{1}{2}\right)$; $B\ @\ 1a(0,0,0)\ and\ 1c\left(\frac{1}{2},\frac{1}{2},0\right)$. This phase is mostly known by the AuCu compound, however there are many other examples for this crystal structure (i.e. CrPd, AgTi, PtFe, PtCo etc..). For PtCo alloys, sites A are filled with a Co atom while the sites B are occupied by Pt atoms. Formation of an ordered phase induces a difference in lattice parameters. $L1_0$ is a face centered tetragonal phase thus this transformation is called tetragonalisation. The value gives the tetragonality of the structure is τ=c/a. Lattice parameters of pure Pt planes are decrease to a=3,803Å where the pure Pt fcc crystal has a lattice parameter of a_{Pt}=3,923Å [17]. Along c axis, the lattice parameters become c=3,701Å [17] where the pure Cobalt fcc crystal's lattice constant is $a_{fcc\text{-}Co}$=3,545Å.

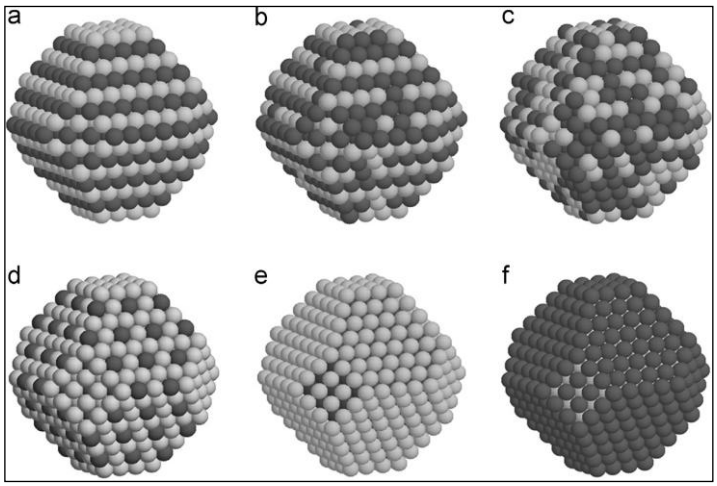

Figure 2.3: Structures of Co-Pt alloys. a) ordered ($L1_0$) , b) partially ordered, c) disordered equiatomic phases, d) ordered Pt_3Co ($L1_2$), and e) Co core, Pt shell and f) Pt core, Co shell clusters.

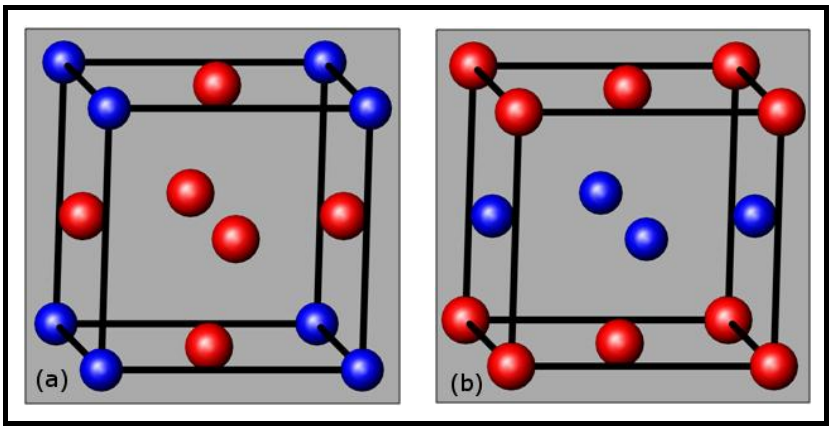

Figure 2.4: Crystal Structure of a) $L1_2$ and b) $L1_0$ Phases.

$L1_2$ phase's symmetry group *Pm3m fom hexoctahedral* class, with lattice complex of; A @ $1a(0,0,0)$; B @ $3c\left(\frac{1}{2},\frac{1}{2},0\right)$. Most common known $L1_2$ phases are $AuCu_3$, $AlPt_3$, $AgPt_3$ and Pt_3Co (Figure 2.3). Disordered A1 phase is a fcc structure with a=b=c=3,751Å [15].

Due to its tunable magnetic features, PtCo received significant attention. The high coercivity and extremely high magneto-crystalline anisotropy (around few MJ/m^3) of its equiatomic $L1_0$ phase make PtCo one of the best suitable candidates for magnetic recording media [2], [3], [18]-[20]. This important magnetic feature is gained by stacking of pure Co and Pt layers among [001] direction. There is also a metastable phase of Co-Pt alloys with a magnetic moment of $2{,}63\mu_B$. This is one of the highest values ever observed in ferromagnetic bulk phase [21].

All these magnetic properties are closely related with the electronic structure of the alloy. Spin polarized band structure calculations of the Pt-Co alloys points out that there is a small charge transfer from Co to Pt [22]-[24]. Furthermore, Lee and his friends suggested an enhancement in Co 3d – Pt 5d hybridization resulting for a loss in Pt d level and an increase in Co d level. Additionally, experimental results and calculations also points out for a loss in p-like conduction electrons while there is a gain in d electrons at Co site with the formation alloy. This redistribution leads for a net charge transfer towards Pt [25].

The properties mentioned above are the result of electronic interactions Understanding these properties a well ordered structure. In order to have a well-known ordered structure, whole of the sample have an identically oriented atomic layers. This ordered structure will eliminate the dispersion of properties due to different orientations. However, Pt-Co alloys have various atomic configurations as shown in Figure 2.3. These kinds of samples are prepared by epitaxial on a single crystal substrate/film. Over decades, various studies performed towards epitaxial PtCo film preparation. Two different way used for epitaxial PtCo preparations are; (a) direct epitaxial by using co-depositions from Pt and Co targets and (b) annealing of Pt-Co multilayers. There are also successful attempts of a single crystal growth with annealing a Co layer grown on Pt single crystal substrate. Techniques used for film depositions are mostly molecular beam epitaxy and sputtering. However, there is also epitaxially grown PtCo films prepared by electrodeposition [26]. Artymowicz and his friends reported that in anneal,ng the Pt-Comultilayers technique ordered phase can occur around 500°C and activation energy of this phase is found around 2,1±0,2 eV which is lower than self-diffusion energy of Pt and Co [1].

3. EXPERIMENTAL TECHNIQUES

In this section, the experimental setup and their technical/theoretical properties are explained. All sample preparations and characterizations are performed at ultra-high vacuum (UHV) cluster system (Figure 3.1) at Gebze Technical University's Nanotechnology Research Center (GTU-NRC). There are several advantages of using a UHV cluster system; possibility of in-situ sample preparation and analysis without exposing the surfaces to atmospheric conditions. Furthermore the high vacuum levels provide a stable and clean environment conditions which increase the quality of the films and information obtained from analysis. The cluster system located at GTU-NRC consist a sputtering chamber, analysis chamber and a loading section.

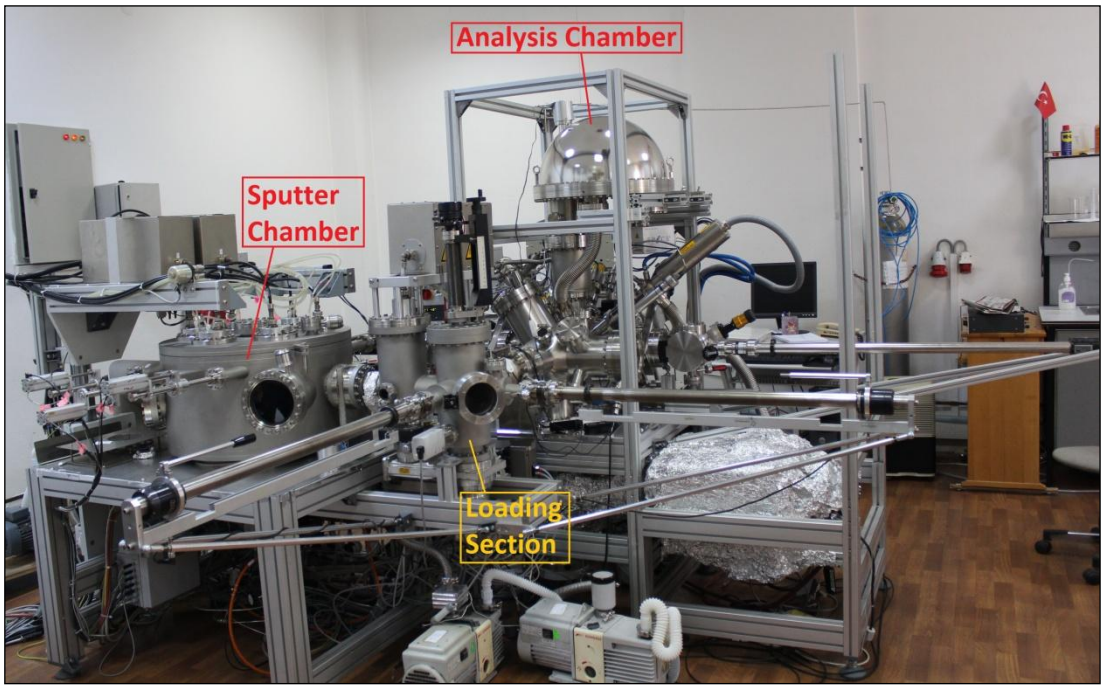

Figure 3.1: Ultra High Vacuum Cluster System Located at GTU-NRC.

First part of this cluster system is sputtering or deposition chamber. This section has a vacuum level of $<5x10^{-9}$ mbar. This vacuum level is supported with a turbo molecular pump and various rotary vane pumps. The chamber is mounted with 3 DC (direct current), 1 pulsed DC, and 2 RF (radio frequency) magnetron sputter guns. The sample manipulator has an ability of azimuthal rotary motion around vertical axis, which allows sequential sputtering. Pyrolytic Boron Nitride (PBN)

Heater on the manipulator allows thermal radiations in UHV conditions for annealing during or before/after depositions. Gas inlets to the chamber are controlled by 3 mass flow meters in range of 0-20sccm with 0.1sccm of sensitivity. These controlled gas inlets make possible to depositions in reactive and inert atmosphere such as for nitride, hydrogenated and oxide samples.

Load section is used for loading and extracting the sample at the system. This is the only section of the system which is exposed to open air. Up to 10 holders can be stored in this section at once. There is also a RF sputter gun mounted on this section. This gun is used for initial surface cleanings. Base pressure of this section is $<10^{-8}$ mbar.

Analysis chamber is the third of the UHV cluster system. This section has a base pressure of $<2x10^{-10}$mbar supported with 3 turbo molecular pump, an ion pump and various rotary vane pumps. This chamber is mounted with numerous analytic systems and two manipulators mounted in two different work directions. Both manipulators have capability of three axis movements and two axis rotations. These manipulators allow transferring the samples from loading section to the analytical chamber in order to analyze within desired angle and position. This capability is essential for most of the analysis techniques (i.e. LEED, AES, arPES…). On the top of the chamber, a Specs® Phoibos 150 hemispherical charge particle analyzer (HSA) is mounted. This analyzer is used for the most of the analytical techniques such as XPS, XPD, UPS, AES and LEIS. XPS is a highly surface sensitive analysis technique and it is used to characterize the surface chemical stoichiometry. The sample manipulator make possible to investigate the same spot of the sample with auger electron spectroscopy (AES) which is also a surface analysis technique in the range of a couple of surface monolayers. There is an ion gun mounted on the chamber and focused to the same spot with x-ray gun and electron gun used for ISS. In addition to use it for ion scattering experiments, this gun also is used for destructive depth profiling by using simultaneously with XPS or AES techniques. The set-up of SED in the analytical chamber is used to image the sample surface within 150micron sensitivity. It is mainly used to synchronize both AES and Ion gun so that both are focused at same spot in order to run the depth profiling experiment. In addition, this ion gun is also used for sensitive surface cleanings. The surface of the Pt(111) crystal is cleaned with the ion source to prepare for experiments. Ion etching with the ion gun is sensitive and effective method. Thus the time of etch and

ion energies need to be selected delicately otherwise the surface of the single crystal is damaged irreversibly. In order to ensure the successful surface cleaning it needs to be checked in-situ by using some surface sensitive analytical technique. AES and XPS are the best candidates in order to check surface cleaning. Ar^+ ions are used for cleaning process and the argon gas is introduced to chamber via a leak valve mounted on the ion source. In order to check the quality of the vacuum and purity of the gases used in the study, a Hidden® residual gas analyzer (RGA) has been used.

Electronic characterizations of the samples are done at the same spot on the sample with an ultraviolet light source focused on the center of the chamber as the x-ray, electron and ion sources do. UV light is acquired with discharging the helium gases. Helium is leaked to the system by a leak valve mounted on the UV source. Capability of analyzing the same spot on the sample with different techniques make possible to investigate the exact same point of the sample in terms of electronic, stoichiometric and chemical structure. A Specs® low energy electron diffraction (LEED) optics is mounted to this chamber. LEED is used to image 2D surface symmetry. Surface symmetry and crystal pattern of the substrate/films grown are investigated with LEED.

Besides the techniques and devices used within this study, there are other axullary equipments on the analytical chamber. Flood gun mounted on the chamber which can be used for electron spectroscopy analysis of the insulator samples. Moreover, a scanning tunneling microscope (STM) probe at the analysis chamber can be used for surface imaging at atomic level. Furthermore, a three-crucible e-beam deposition gun with the capability of co-deposition on the same spot is also mounted to the analysis chamber.

The various analysis and deposition techniques in a cluster system are crucial for this study. Films prepared in the study do not exceed more than 3 nm. However it is known that in atmospheric conditions, a clean surface can be contaminated within seconds. A surface without any contamination is covered by one monolayer of airborne molecular contaminations in $1x10^{-6}$ sec.

Furthermore, the techniques used in the study are extremely surface sensitive. LEED has a surface sensivity of upper 1-2 layer. This sensivity is around 5nm for XPS and 2nm for AES and UPS. According to this surface sensitivity and surface contamination rate, samples exposed to open air, will have a surface contamination thicker than the range of these techniques. Thus the analysis of these surfaces will

not be able to give reliable results. In order to remove the contaminations, samples can be cleaned by ion etching delicately. However this may/will damage the surfaces. These difficulties make a cluster system the best choice for ultra thin film studies. With this kind of cluster system, films can be prepared and analyzed in a controlled manner and in controlled ambient conditions.

3.1. Deposition Technique – Magnetron Sputtering

Magnetron sputtering is a physical deposition method based on ejection of target material onto substrate in a plasma etching process. Plasma etching is an accelerating the gas ions towards a target material. In magnetron sputtering, the plasma is formed in front of the target by the influence of a magnetic field. The direction of the magnetic field is parallel to the target surface and formed by the magnets placed behind the cathode. This magnetic field traps the electrons in front of the target. In the presence of electric field and magnetic field, an electron flux forms a closed circle [27]. The magnitude of magnetic field is in the order of few hundred gauss. This magnitude is enough to affect the electrons but not the ions. Electrons trapped in the area lose their energy by colliding with other electrons (electron heating) or gas atoms (ionization). Dense plasma can be formed by this ionization mechanism. The electric field between anode and cathode formed by the voltage applied, accelerates the gas ions towards target for tear off particles from the target material. Ejecting particles cover the substrate and its around [28]. Inert gases, especially argon, is mostly preferred for magnetron sputtering process, however O_2 and other gases can be used to provide reactive deposition if desired.

Magnetron sputtering deposition can be performed by applying different type of voltages between the anode and cathode. The applied voltage types are direct current (DC), pulsed-direct current (pDC) and radio frequency (RF). Different voltage types are used for different types for the target materials. RF source is used for magnetic materials and insulators and DC source is used for conducting materials. pDC source can be used for both kinds of materials, but it provide faster deposition than rf does but slower than DC does .

During the depositions by DC voltage source, there can be charge formation of target surface if the target material is not conductive enough. This charge might

occur sparks on surface; it shifts electrical potential slowly so that the plasma intensity decreases gradually in result to stop. Therefore semi-conducting or insulating materials are not suitable for DC method. On the other hand a RF source's periodic voltage overcomes this charge problem but it has some disadvantages, such as low deposition rate and power reflections. pDC is an alternative method which has some advantages and disadvantages comparing to other two techniques. A typical range of frequency at pDC source is 10 to 100 kHz.

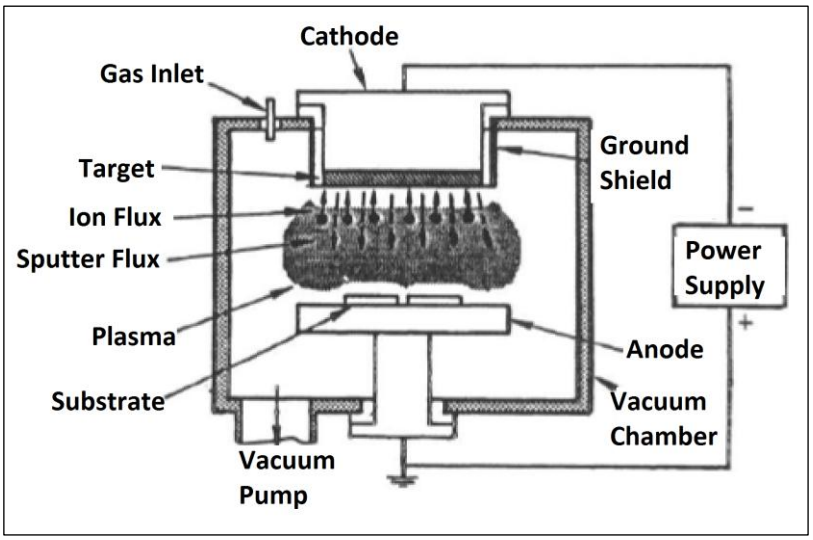

Figure 3.2: Schematic Diagram of a Magnetron Sputtering Process.

Samples are mostly prepared by magnetron sputtering in this work. RF source was chosen for Co while Pt depositions were done by a DC source. Other deposition methods such as e-beam deposition and MBE, maybe more sensitive for thin film growth however they are not suitable for industrial applications. On the other hand, chemical deposition methods may be more applicable for large scale productions. However the chemical waste of the process is hazardous for environment and human health. Magnetron sputtering, as a physical vapor deposition, is harmful for neither the environment nor the human health. Unlike the evaporation based deposition techniques, the target does not to be heated for deposition process. However, targets warm up due to plasma. Furthermore, the deposition rate of the magnetron sputtering using in our laboratory can be adjusted from 0,01 Å/sec to 100 Å /sec. Deposition speed is directly connected to argon flow and the electro power on target. With increasing argon pressure, the concentration of plasma decreases so does the momentum of the Ar ions. Decreasing the voltage also decreases the momentums of

Ar^+ by decreasing magnitude of their acceleration. Momentum of the ions is inversely proportional to the size of the ions, and the ions in plasma worn off the particles from the target material in order to gather on the substrates. Smaller particles decrease the possibility of island growth and allow for layer by layer growth. However there is a lower limit for target voltage and gas flow. Below this limits, plasma becomes unstable.

The lower limits of magnetron sputter system in the GTU-NRC are defined by preliminary works. Depositions are performed on the edge of these limits in order to occur the smaller particle size in the surface of substrate. Deposition parameters are given in the sample preparation section (Chapter 4.1).

3.2. Thin Film Characterization Techniques

Samples prepared by the magnetron sputtering technique are analyzed in situ by using extremely surface sensitive analyze techniques, which are photoemission and electron emission spectroscopies. They are used for the electronic and chemical characterizations of the surfaces. Different techniques of surface electron spectroscopies provide information from different depth ranges and different properties; such as Photoelectron spectroscopies are used for chemical, elemental and electronic investigation of the surfaces, while the auger-emission spectroscopy is used for elemental and chemical investigations in range of a top layer. Low energy electron diffraction is used for investigation of the surface's crystal structure.

3.2.1. Surface Electron Spectroscopies

Surface Electron Spectroscopies are analytical techniques to investigate the electronic structure and its dynamics of atoms and molecules in surface [29], [30]. Surface electron spectroscopy techniques are based on the ejection of an electron by an excitation of electron or photon. Detection of electrons excited by a photon source (i.e. photoelectrons) is called photoelectron spectroscopy or photoemmision. Detecting the auger electrons emitted from an excited atom is called auger electron spectroscopy. In AES, atoms are excited by an incoming electrons to surface and the electron gun is used to produce incoming electron beam in range of 100ev-5keV.

All these techniques require ultra high vacuum conditions, an excitation source and a charge analyzer. Hemispherical Charge Particle Analyzer mounted on the analytical chamber of the GTU-NRC cluster system is used for electron kinetic energy analyzing versus the intensity of charge particles coming from the sample surface. A typical analytical setup for an electron spectroscopy is given in Figure 3.3 [31].

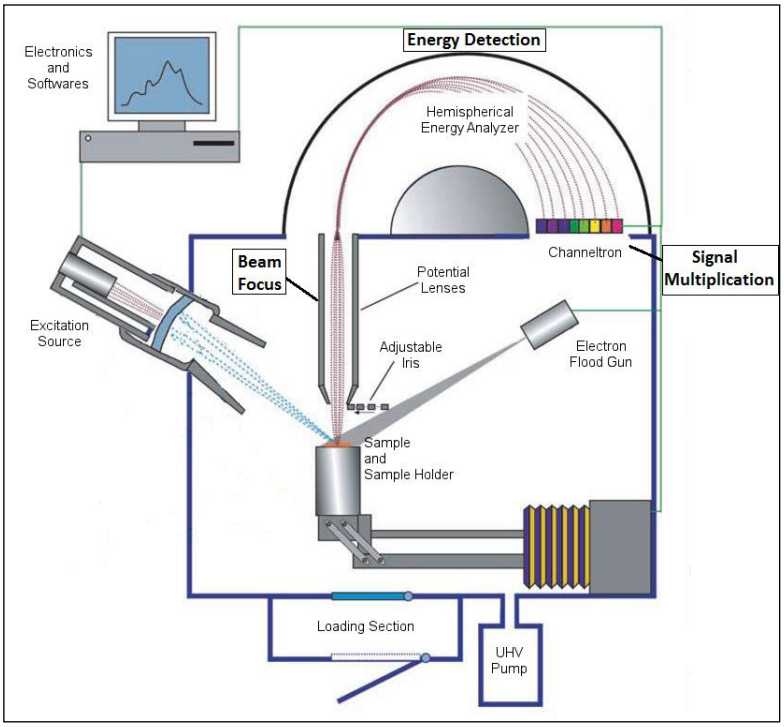

Figure 3.3: Schematic Diagram of an Electron Spectroscopy Experimental Setup.

A Hemispherical Charge Particle Analyzer has three sections, beam focusing, energy detection and signal multiplication. Beam focusing process is carried out with a lens system and an adjustable iris. Lens potentials allow focusing the charged particles reach analyzer's slit entrance. Potential configurations of electro static optic lens system and iris position regulate the acceptance area and the acceptance angle. Both defines the emission area to modify the angle and spatial sensitivity of photoemission analyzing. Energy detection section consists of two parts slits and electrostatic hemispheres. Entrance and exit slits are used to regulate the shape of the beam. Energy analyze is made with the two electrostatic hemisphere, and there is a potential of ΔV between them. The width of this potential is also known as pass energy which is a important parameter for energy resolution and intensity. Signal

multiplication section is consisting of electronics and a channeltron. Channeltron is a charge particle counter, which induces a current and modulate the current detected in order to count the electrons or the ions. The electronics and with a software plot the count rate versus kinetic energy and a spectrum is composed on the screen.

All the electron spectroscopy equations consists a work function which is specific for each material. The spectrometer has also a work function and it needs to be accounted for when calculating the electron kinetic energy. To compensate the spectrometer's and sample's work functions, following equation are used [32];

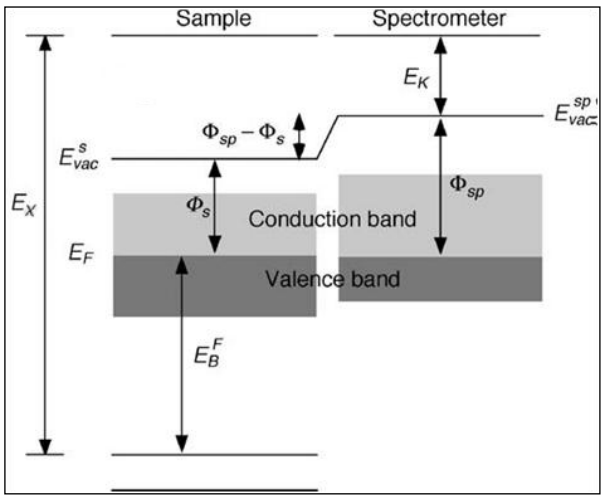

Figure 3.4: Influence of spectrometer work function ϕ_{sp}. E_K is for electron kinetic energy, E_x for excitation energy and ϕ_s for work function of sample.

$$E_K = E_x - E_B - \phi_{sp} \tag{3.1}$$

$$E_{K,max} = E_x - \phi_{sp} \tag{3.2}$$

$$E_{K,min} = \phi - \phi_{sp} \tag{3.3}$$

$$\Delta E = E_{K,max} - E_{K,min} = E_x - \phi \tag{3.4}$$

$$\phi = E_x - \Delta E \tag{3.5}$$

Photoelectron spectroscopy is an electron spectroscopy technique based on detection of electrons excited by a photon source. Theory behind this process is Einstein's photoelectric effect [33]. According to photoelectric effect, energy of a

photoelectron depends on the wavelength of the photon [34]. This effect is observed by Thomas Hertz for the first time at 1887 as an electric spark triggered by a previous spark [35]. In Hertz observation, the first spark has enough energy to excite the atoms for a secondary photon emission. In the photon emission process, a photon is absorbed by an atom, and an electron with lower binding energy than the photon is ejected. This ejected electron is called photoelectron. The relaxation of this excited atom emits a photon and this process is called photoemission. During 1960's Dr. Siegbahn and his team used this photoemission phenomena with using X-Ray source and electron spectroscopy for the first X-Ray Photoelectron Spectroscopy (or Electron Spectroscopy for Chemical Analysis). This invention becomes commercial around 1970's and Dr.Siegbahn earned the Nobel prize (at 1981) for his research in this area [35].

Nowadays, photoelectron spectroscopies are used to determine the elemental compositions, oxidation states and electron densities of surfaces. Formalism of the photoelectron spectroscopy can be given with the Einstein equation [31];

$$E_k = h\upsilon - E_b - \varphi \tag{3.6}$$

,where $h\upsilon$ holds for energy of exciting photon and φ is for the work function calculated above. A photon can reach down to μm's of depth in a solid. However the electron excited by photon, called photoelectron cannot travel more than 10nm in solids. Photoelectrons elastic movement in a solid can be given with the following graph (Figure 3.5) and equations;

$$I_f(d) = I_f(\infty)\left(1 - e^{-d/\lambda_f}\right) \tag{3.7}$$

$$I_s(d) = I_s(0)\left(e^{-d/\lambda_s}\right) \tag{3.8}$$

These equations will be used to calculate film thickness, etching rates and deposition rates.

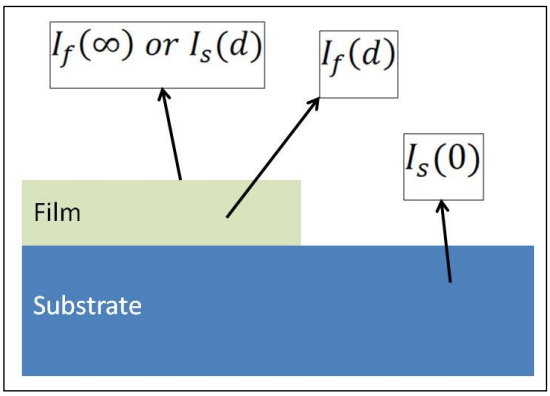

Figure 3.5: Diagram of the Photoelectron Intensity From a Substrate and Film.

3.2.1.1. X-ray Photoelectron Spectroscopy (XPS)

X-ray photoelectron spectroscopy is a qualitative electron spectroscopy technique measures the elemental composition, empirical formula, chemical and electronic state of the elements within a material.

A standard XPS spectrum can be analyzed by using the primary and secondary information. The primary information is core levels, valance levels and auger series. The secondary information of the spectrum is secondary peaks, tails and satellites.

Core level peaks origin is the core energy levels of the element. They can show up in two form; singlet and doublets. While the s-levels are singlet, non s-levels show a doublet feature. The doublet shape is a result of spin orbit coupling which is a shift in electron's binding energy due to electromagnetic interaction between the electron's spin and the magnetic field generated by the electron's orbit around the nucleus. The magnitude of separation is related with β.

$$\Delta E = \frac{\beta}{2}\big(j(j+1) - l(l+1) - s(s+1)\big) \tag{3.9}$$

$$\beta(n,l) = Z^4 \frac{\mu_0}{4\pi}\, g_s \mu_B^2 \frac{1}{n^3 a_o^3 l(l+1/2)(l+1)} \tag{3.10}$$

, where a_o holds for Bohr radius. The electron population at shells is given in the Table 3.1 [36].

Table 3.1: Spin Orbit Splitting and Its Effect on Photoelectron Lines.

Subshell	j values	Area ratio
s	1/2	-
p	1/2 , 3/2	1:2
d	3/2 , 5/2	2:3
f	5/2 , 7/2	3:4

These peaks area is used for stoichiometry calculations. Stoichiometry of films is calculated by the following formula;

$$R_a = \frac{\frac{I_a}{ASF_a}}{\sum_i \frac{I_i}{ASF_i}}, \quad 0 < R_a < 1 \tag{3.11}$$

, where R holds for the ratio, I is for the intensity (or the area of the peak in our case) and ASF is for the atomic sensivity factor, which is a scale factor depending on photoemission cross-section- to calculate the atomic concentration. So the peak intensities depend on atomic photoemission cross-section and electron population , peak width (can be defined as Full Width Half Maximum – FWHM) ΔE depends on three fundamental features [36];

$$\Delta E = \sqrt{\Delta E_n^2 + \Delta E_p^2 + \Delta E_a^2} \tag{3.12}$$

, where ΔE_n holds for inherent width of core level, which is a direct reflection of uncertainty in life time of ion state remaining after photoemission, ΔE_p for width of photon source and ΔE_a for analyzer resolution [36].

Binding energy of electron can also change with chemical bond or any potential change in solid. The fluctuation in the electron charge density, alters the potential inside the solid. Equation giving the relation between binding energy and charge density can be given as [33, 36];

$$E_i = E_i^0 + kq_i + \sum_{i \neq j} \frac{q_i}{r_{ij}} \tag{3.13}$$

This shift can lead to understand the chemical state of an element. As it can be clearly seen from Figure 3.6 [36], C atoms forming different bonding have different binding energies. N ions composed of two N^- and one N^+ give different intensities (2 to 1 for 2 negative ions against one positive as long as their photoemission cross-section stays same) at different energies.

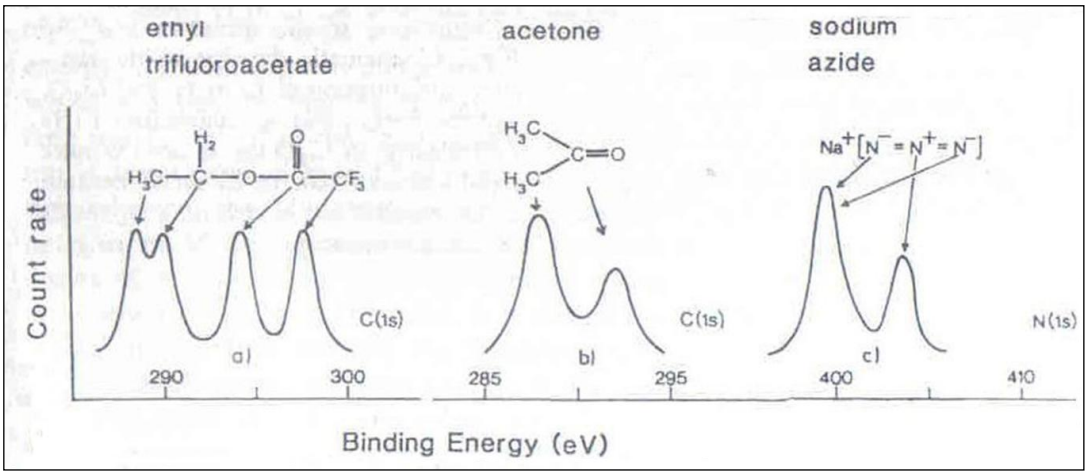

Figure 3.6: Chemical shift of C1s and N1s for different chemical bonding.

The second and third of the primary information in a XPS spectrum are valance level and auger series. Auger peaks are formed by an auger transition explained in further section. Valance levels are used to investigate the electronic structure of the sample. In order to have a higher resolution valance structure, ultra-violet light source can be used as excitation source. This technique is called ultra-violet photoelectron spectroscopy. UPS and the analysis of a valance structure is also explained in further sections.

Most common satellite peaks in XPS spectra are due to x-ray source. X-ray obtained from an anode such as Mg, Al, Cu, has a characteristic spectrum. This spectrum consists of bremsstrahlung radiation peak (or braking radiation) and two characteristic peaks caused by kα and kβ transitions of the anode material (Figure 3.7). An aluminum screen in front of the x-ray source reduces the intensity of bremsstrahlung radiation, but the two other peaks stand still. While first and the highest peak -kα- is used as the main x-ray source, second and short one -kβ- is ignored. However, it still can excite photoelectrons with a specific energy shift. The width of this shift is equal to the energy difference of the kα and kβ.

These satellites are called x-ray satellite and they appear in near every peak in spectrum unless the spectrum is taken with a synchrotron or a cyclotron light sources. There can be another satellite with the same characteristics of x-ray satellite if the source anode has some impurity. These are called x-ray ghost peaks [36].

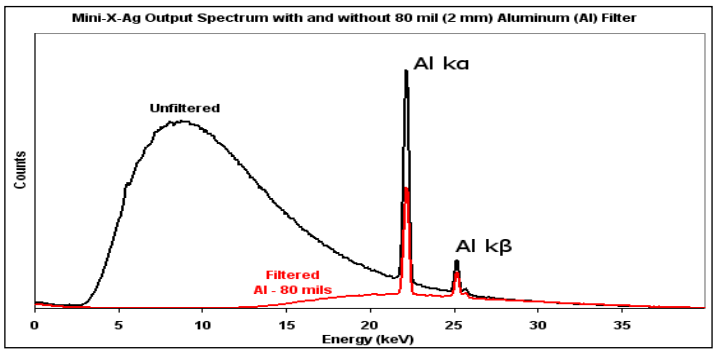

Figure 3.7: Characteristic & Bremsstrahlung radiation of aluminum with and without a filter.

Other most common secondary feature in a spectrum is called the tail of core peaks. This occurs due to unoccupied electron levels above Fermi in metals and called asymmetric metal core level. The spectrum windows for platinum and a cobalt can be shown these features as an example in Figure 3.8. While Co2p shows a tail like peak, Pt4f stands as a Gaussian/lorentzian shaped function [33], [36], [37].

There are also shake off and shake up satellite peaks due to photoelectron-valance interaction. These features can hold great importance in elemental analysis of metal-oxide films with multiple oxidation states.

An XPS spectrum seems like to have a step like shape rising towards high binding energy side of the spectrum. This characteristic background is a consequence of electrons inelastic scattering through the solid. These scatterings can be summarized in two; Extrinsic and Intrinsic effects. Scatterings away from the atomic center , through the response of the loosely bound electrons to the probing electron are called Extrinsic and scatterings in the close vicinity of the emitting atomic center, through the response of the core hole are called Intrinsic scatterings [36], [38].

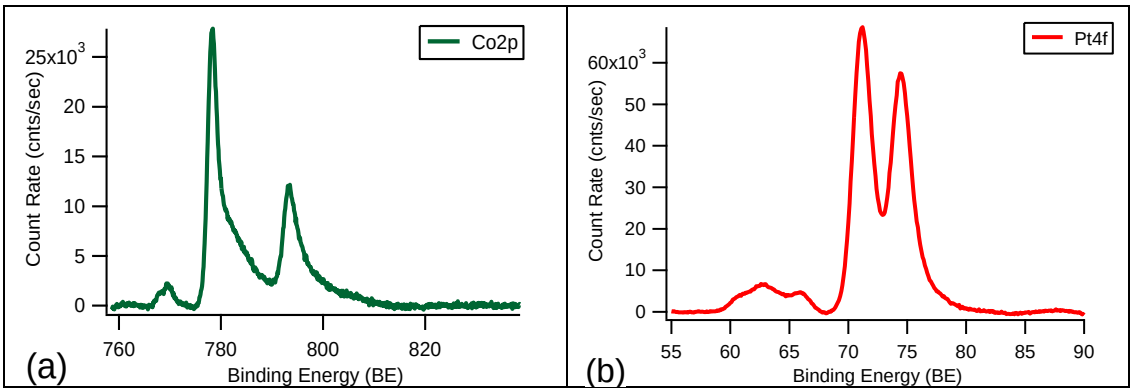

Figure 3.8: a) Co2p and b) Pt4f high resolution XPS scans.

Calculating and subtracting the background function from spectrum is crucial for quantitative analysis. There are several ways to calculate the function. Most crude and easier one is linear background. It can be used when there is a little change in background. Higher order polynomial curve is another method for calculating the background function. Due to its step like shape, it gives better results than linear function. The third and fourth is integral functions. Shirley function, as a common background function, is a S-type function, which considers the energy loss function as a constant. Shirley calculating requires an iterative method. Shirley's function is given by [36], [39].

$$B(E) = A^{(i)} \int_{E}^{\infty} P(E')dE' = A^{(i)} \int_{E}^{\infty} \left(M(E') - B(E')\right)dE' \tag{3.14}$$

$$B_N = B_{N-1} = M_N \ , \quad \left|B_i^{(k+1)} - B_i^{(k)}\right| < Tolerence \tag{3.15}$$

$$A^{(1)} = A^{(0)}\left(1 - \left|\frac{M_1 - B_1^{(0)}}{M_1}\right|\right) \tag{3.16}$$

, where "A" stands for iteration constant and "i" is for number of iteration. "M" holds for the intensity of raw data and "B" stands for the intensity of background.

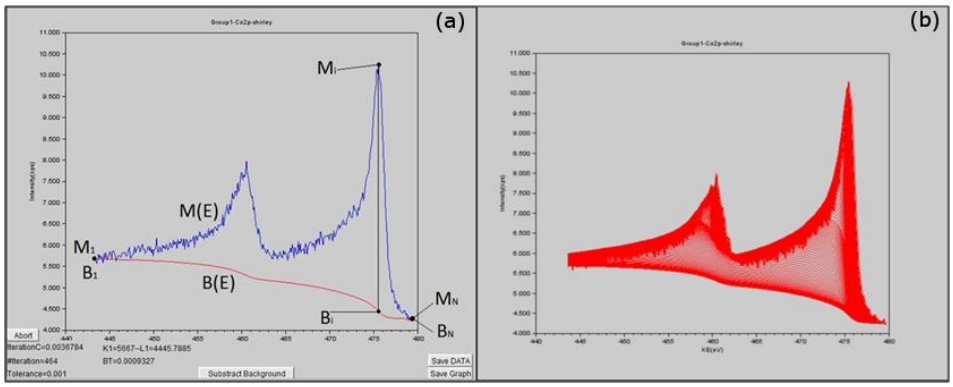

Figure 3.9: Shirley Background of a Co2p Line for a) Each Iteration and b) Final iteration.

```
while BT>=tolerance
   N=size(MI(string(y)));
   N=N(1);     TAP=0;
   while N >= 2
      TOP=MI(string(y))(N)-Bg(string(y))(N);
      TAP=TAP+TOP;     KAP=Ai*TAP;
      Bg(string(y))(N-1)=TEK+KAP;
      N=N-1;
   end
   Btop=Bg(string(y))(maxi);      BT=Btop-Bex;
   BT=abs(BT);                    Bex=Btop;
   delete(hf.children($).children(1));
   plot(ME(string(y)),Bg(string(y)),'r');
   Ai=Ai*(1-abs((MI(string(y))(1)-Bg(string(y))(1))/MI(string(y))(1)))
   hf2.string="IterationC="+string(Ai);
   hf4.string="#Iteration="+string(k);
   K1=MI(string(y))(1);      L1=Bg(string(y))(maxi);
   hf7.string="K1="+string(K1)+"--L1="+string(L1);
   if L1>K1 then Ai=Ai-0.001; end
   hf8.string="BT="+string(BT);
   k=k+1;
end
```

Figure 3.10: Algorithm used in order to calculate the Shirley background.

Shirley background functions are calculated by an algorithm coded in SciLAB workplace. Codes and an example of calculation is given in Figure 3.9 - 3.10.

Tougard is the last and the most successful background function. It's also an integral background function and it separates the extrinsic and intrinsic energy loss process. It considers the intrinsic energy loss function as constant. However, in Tougard assumptions, the extrinsic losses depend on the type of the element and sample. The Tougard Function can be given as [39], [40];

$$F(E) = j(E) - \lambda(E) \int_{E}^{\infty} K(E, E' - E) j(E) dE' \qquad (3.17)$$

, where $F(E)$ holds for spectrum, $\lambda(E)$ for inelastic mean free path for an electron of energy E,and $K(E,T)$ for differential inelastic scattering cross-section for an energy loss T. Function can be simplified by replacing the $K(E,T)$ with a universal cross-section [39];

$$F(E) \approx j(E) - \lambda(E) \int_{E}^{\infty} \frac{E - E'}{(C + (E' - E)^2)^2} j(E) dE' \qquad (3.18)$$

Due to Tougard's calculation difficulties and dependency on the type of samples, we preferred Shirley function. A comparison of Shirley background functions with polynomials are given in the Figure 3.11 .

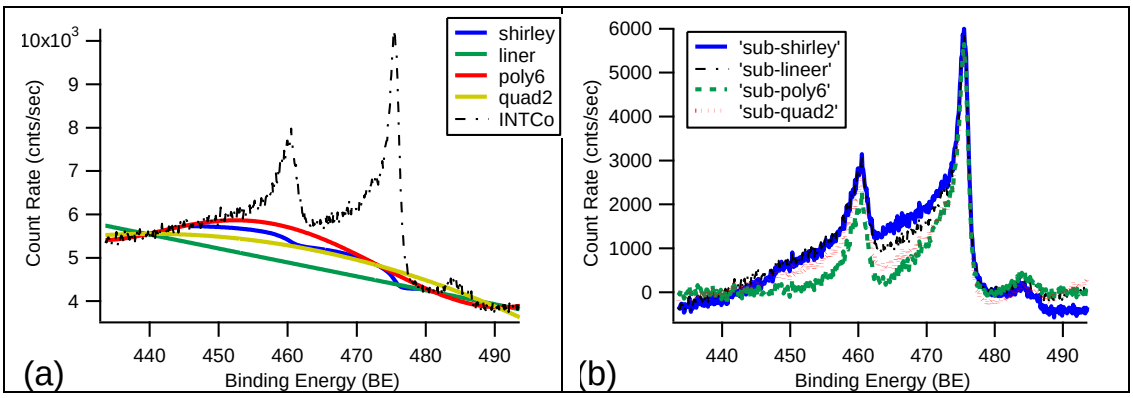

Figure 3.11: Co2p spectrum with different type of background. On the left, a) the spectra are given without background subtraction while on the right, b) the background spectra subtracted are given.

The comparison shows that the effect of backgrounds is minor on the main and secondary peaks intensities. On the other hand, with different subtraction methods, the shape and intensity of the tails change dramatically. It is also clear that the results after the subtraction of linear background method is similar to the method of Shirley subtracted curve.

XPS data acquired in the study is processed by licensed IGOR 4.0 and SciLAB workplaces. IGOR has been used to draw the XPS graphs and for fitting processes.

Before the fitting processes, secondary electron backgrounds of spectrum are subtracted by using Shirley Function. The algorithm and secondary electron backgrounds are explained above. Curve fitting procedure is used to calculate the stoichiometry of films and film thicknesses. Fitting procedures are performed using a voigt functions. Voight functions are Gaussian instrument response function convolved in the intrinsic Lorentzian core-level line shape. A Voigt function is given as;

$$V(x;\sigma,\gamma) = \int_{-\infty}^{\infty} G(x';\sigma)L(x-x';\sigma,\gamma)dx' \qquad (3.19)$$

, where σ and γ hold for half-widths at full maximum (HWHM). The shape of voigt fucntion is chosen as η=0,1 in our study. A Lorentzian, Gaussian and voigt functions are given in Figure 3.12 [41].

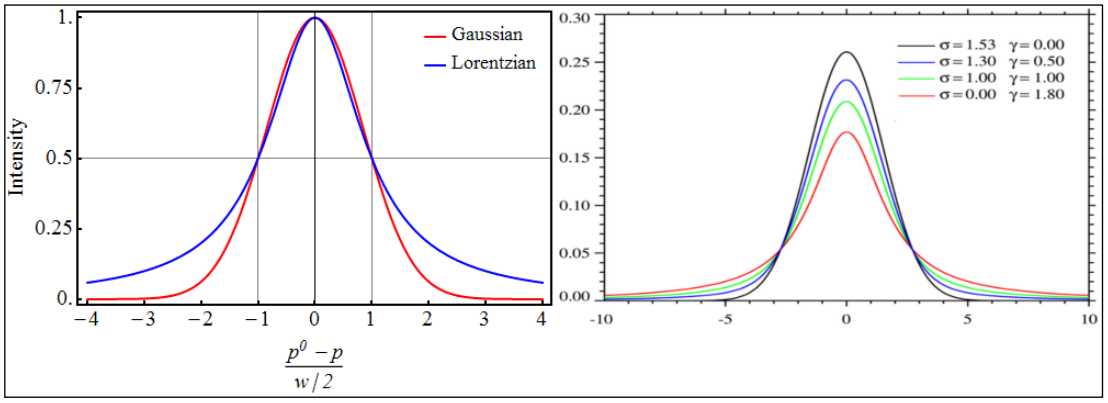

Figure 3.12: Comparison of Gaussian and Lorentzian lines and comparison of voigt lines for different shape values.

Measurements have been made with a 2xAnode Specs® X-Ray Source and Specs® Phoibos 150 HSA (Hemispherical Charge Particle Analyzer) in a vacuum chamber with 1 x 10-^{10}mbar base pressure. As excitation source Mg-kα (1253,6 eV) anode has been chosen at most of the measurements. X-ray gun's schematic is given in the Figure 3.13 [33].

This is a standard dual anode x-ray gun. Electrons produced at filament are accelerated towards desired anode by a high voltage. This electron bombardment on

anode, produces the x-ray. Al foils screen in front of the x-ray source works as a filter for bremsstrahlung light and undesired other low energy radiations [31].

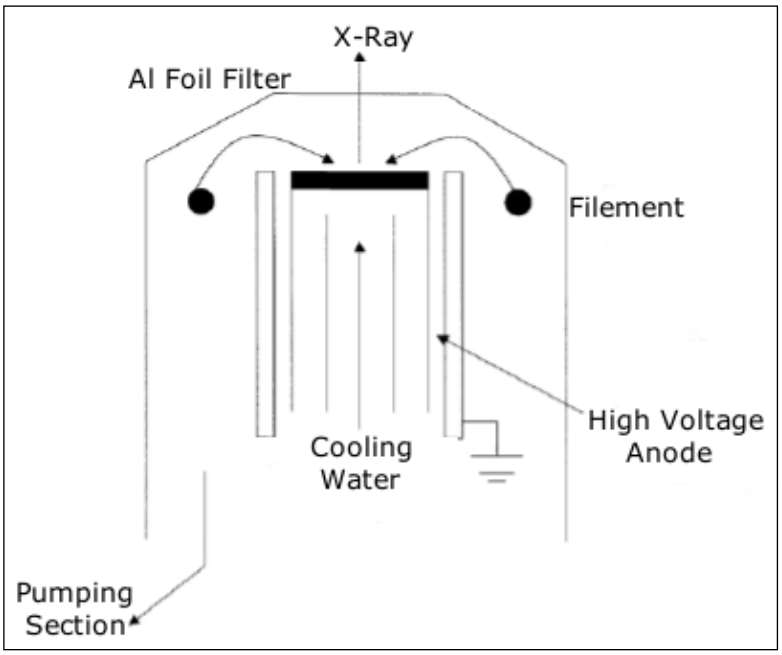

Figure 3.13: Schematic diagram of a standard dual anode X-Ray Gun.

3.2.1.2. Ultraviolet Photoelectron Spectroscopy (UPS)

UPS has a photoelectron emission spectroscopy mechanism just like XPS does, and the ultraviolet light source (incident photon source), having the low energy range up to 45 eV, is used to excite the electrons around the valance band. UV photons can excite electrons from valance levels. On the contrary of XPS, UPS cannot be used for qualitative analysis easily. Since valence electrons are involved in chemical bonding, UPS is a well suited technique to study bonding on surfaces. In addition, UPS can be used to define the surface work function, the band structure of surfaces and adsorbed layers.

Most common UV light source used for UPS technique is produced by Helium discharge gun. It allows to produce He I (21,2 eV) and He II (40,8 eV) UV lights. These energies can barely excite valance levels. XPS can also give information about valance level. However, x-ray with energy of more than 1keV will easily excite the valance electron and transfer nearly all of its energy, and it results to poor cross sections of emission process. Investigating energy levels with tens of eV by electrons

with thousands of eV energy will reduce the resolution. Thus UPS is much more suitable for valance electrons than XPS does [32].

UPS spectrum is more complex then XPS spectra because of the superposition of the numerous energy levels around Fermi. This effect is increased by the number of the elements and phases in samples. This complexity increases the difficulty of the interpretation of spectrum. However, the electron distribution of surface can be interpreted by comparison of different samples core level and valance level spectra. Furthermore, the density of state calculations is also suitable for UPS investigations.

3.2.1.3. Auger-Electron Spectroscopy (AES)

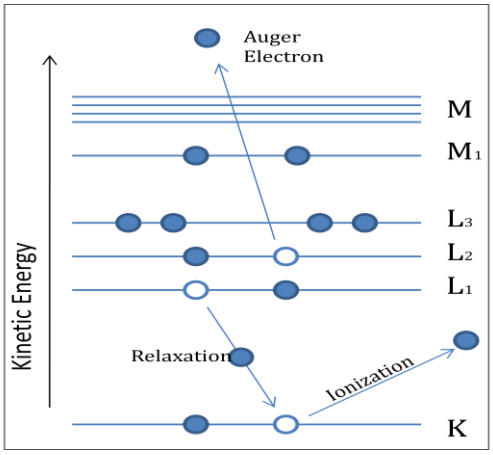

Figure 3.14: Auger – KL_2L_3 transition diagram.

Auger electron spectroscopy is an electron spectroscopy based on Auger effect. This effect is named after the Pierre Victor Auger.

Auger effect is a phenomenon where an ion relaxation emits another electron instead of an electro-magnetic radiation (Figure 3.14). Auger peaks, are called with the transitions occurred in the process. For example, if the relaxation occurs from a shell L to shell K and the auger electron gets emitted from shell M, this transition is called KLM.

Emission probability of an auger electron or an electromagnetic radiation depends on quantum selection rules. For lower atomic numbers, auger transition is much more probable while a photon emission is dominant at higher atomic numbers (Figure 3.15) [42].

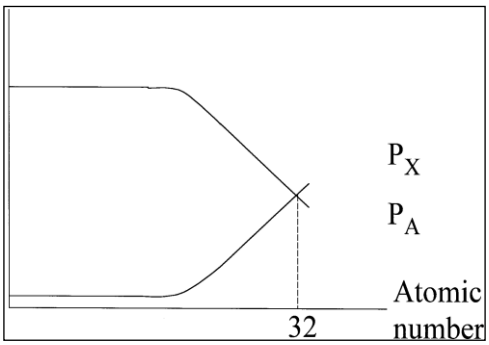

Figure 3.15: Emission Probability of an Auger electron (A) or photon (X).

Alongside to Auger peaks AES spectrum consists of low energy secondary electrons, additional of auger electrons and photons. These additional features are caused by the inelastic collisions and it contributes to the spectrum as a background level. Due to the inelastic background, Auger transitions can be found in spectrum as small peaks (Figure 3.16).

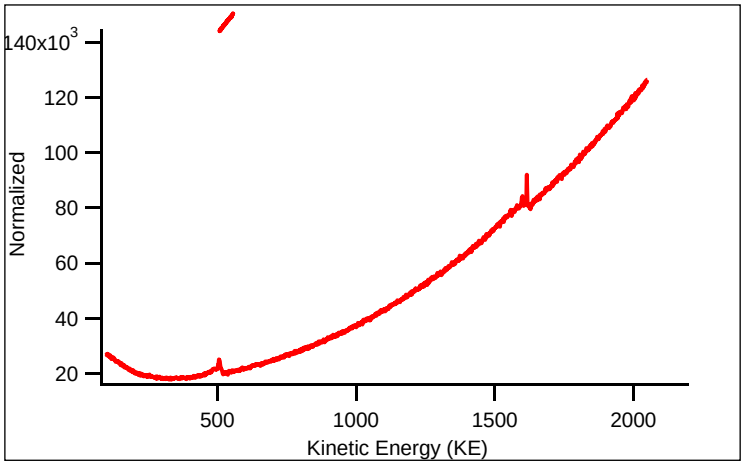

Figure 3.16: Auger-Survey spectrum of Co sample on SiO_x substrate.

Due to this high background, it's hard to calculate the area of peaks for stoichiometry calculations. To handle this problem, the spectra are mostly differentiated. Instead of area calculations, peak to peak intensities of differentiated spectra are used in elemental ratio calculations. On the contrary of photoemission, in auger process, there are two vacancies instead of one. This "two" vacancies –or holes- can shift the energy of an auger peak due to a hole-hole interaction [33], [43]. This process is also sensitive to chemical and electronic state of an element, but due to this hole-hole interaction, AES is not preferred for chemical shift investigations. As in XPS, the intensity of each element depends on a value called relative sensivity

function (RSF) based on emission cross-section. For calculation of elemental ratios, the intensities measured should be divided by this RSF value which is calculated empirically. Stoichiometry of samples is calculated with the following formulation;

$$R_k = \frac{I_{T_k}}{\sum_i I_{T_i}} \quad , \quad I_{T_k} = \frac{I_{R_k}}{RSF_k} \tag{3.20}$$

, where R_k holds for ratio and I_{R_k} holds for measured intensity of element k.

The electron spectroscopy based on this phenomenon is called AES. Unlike to photoelectron spectroscopies, AES uses electron as excitation source. X-ray photoelectron spectroscopy gives information around tens of angstroms but, due to electrons penetration depth, and their energy used for technique, AES gives information from the upper 2-3 layers of surface [36], [43]. It makes AES a much more surface sensitive characterization technique than XPS does.

3.2.2. Low Energy Electron Diffraction (LEED)

Low Energy Electron Diffraction (LEED) is an extremely surface sensitive electron diffraction technique. LEED is based on investigation of the elastically scattered electron's 2-D diffraction pattern. Energy of the electrons varies from 0 to 500eV [44]-[46]. Electrons with these energies will have penetration depth less than 10Å [47]. Because of these two facts, only the upper few atomic layers can be investigated with this technique [44]-[46]. LEED can be for both quantitative and qualitative experiments. Qualitatively, surfaces can be investigated in terms of diffraction pattern which gives the information about the surface symmetry in two dimensions. On the other hand, intensities of the diffraction beams can be analyzed as a function of the incident electron energy. This process is called I-V curve calculations. Atomic positions of the structure can accurately be acquired by comparing I-V results with theoretical calculations [46].

The LEED setup used in this study is specs ErLEED optics mounted on the analysis chamber by an 8″ conflat flange. A CCD camera is used for image capture. In Figure 3.17, the schematic diagram of LEED is shown [47]. The electron gun located in the central axis is aligned towards to the fluorescent screen.

Monochromatic electron beam produced by this electron gun is directed to the sample. Grids are mostly adjusted for the potential values around 95-99% of the incident electrons in order to filter the in-elastically scattered [44]. Filtering is also reducing the energy of the elastically scattered electrons that hit the fluorescent screen with leaving bright spots. Sharpness of the spots depends also on surface's uniformity as it depends on grid potentials but not the electron.

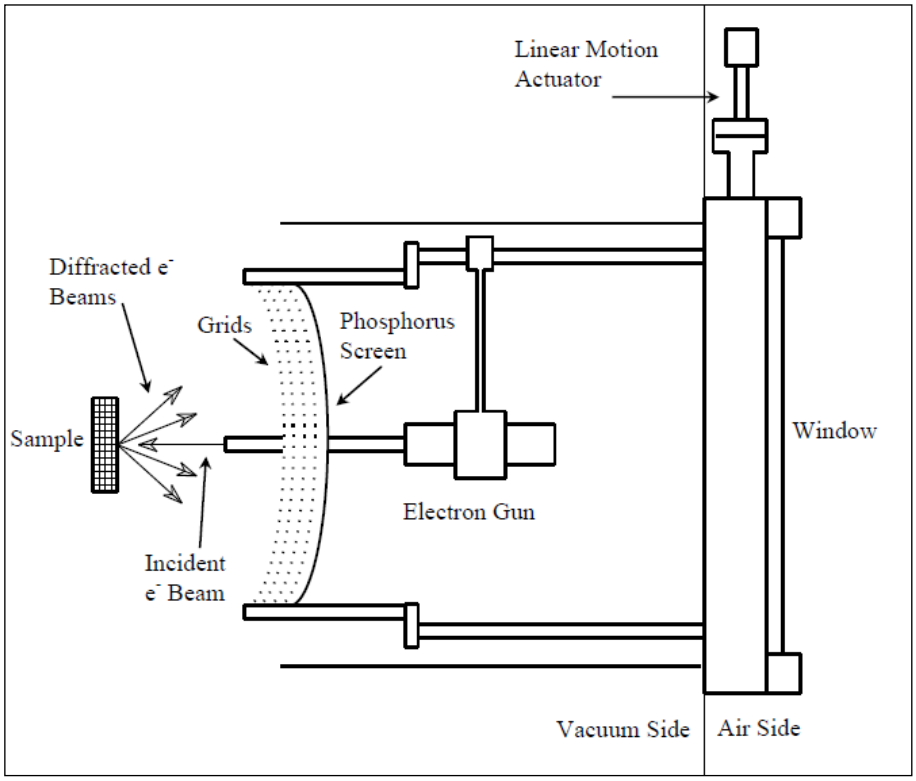

Figure 3.17: Schematic diagram of a LEED system.

Surface sensitivity of the LEED allows to consider the diffraction mechanism as a scattering of an electron from a two dimensional lattice. The interaction between crystal and electrons is mostly described in reciprocal space. The lattice vectors in real and reciprocal spaces are given by;

$$\vec{a}^* = \frac{2\pi\vec{b} \times \vec{c}}{\vec{a} \cdot (\vec{b} \times \vec{c})'} \tag{3.21}$$

$$\vec{b}^* = \frac{2\pi\vec{c} \times \vec{a}}{\vec{b} \cdot (\vec{c} \times \vec{a})'} \tag{3.22}$$

$$\vec{c}^* = \frac{2\pi\vec{a} \times \vec{b}}{\vec{c} \cdot (\vec{a} \times \vec{b})'} \tag{3.23}$$

, where the $(\vec{a}, \vec{b}, \vec{c})$ holds for primitive real space vectors and $(\vec{a}^*, \vec{b}^*, \vec{c}^*)$ holds for primitive reciprocal space vectors. Laue condition is used for calculations of scatterings of electrons from atoms. Laue condition given with reciprocal space vectors is [44];

$$\vec{G}_{hkl} = h\vec{a}^* + k\vec{b}^* + l\vec{c}^* \tag{3.24}$$

, wave vectors of electrons are given by;

$$k_0 = \frac{2\pi}{\lambda_0} \quad , \quad k = \frac{2\pi}{\lambda} \tag{3.24}$$

, where k_0 holds for wave vector of incident electron and k for scattered electron as λ and λ_0 holds for their's de Broglie wavelengths. Laue condition can also be given with this wave vectors as;

$$\vec{G}_{hkl} = \vec{k} - \vec{k}_0 \tag{3.24}$$

These two equations give

$$\vec{k} - \vec{k}_0 = \vec{G}_{hkl} = h\vec{a}^* + k\vec{b}^* + l\vec{c}^* \tag{3.24}$$

, for 2D approximation

$$\vec{k} - \vec{k}_0 = \vec{G}_{hk} = h\vec{a}^* + k\vec{b}^* \tag{3.24}$$

, so now the reciprocal space vectors can be given as

$$\vec{a}^* = \frac{2\pi\vec{b} \times \hat{n}}{|\vec{a} \times \vec{b}|} \tag{3.24}$$

$$\vec{b}^* = \frac{2\pi\hat{n} \times \vec{a}}{|\vec{a} \times \vec{b}|} \tag{3.24}$$

This Laue condition can be visualized by a diagram called Ewald's sphere (Figure 3.18). For construction of Ewald sphere, from an origin, $\vec{k}_0$ the wave verctor of incident electron is drawn to reciprocal point.

The sphere with the same origin with $\vec{k}_0$ and with the radius equal to $|\vec{k}_0| = k_0$ is called Ewald's sphere. It is known that the magnitude of $\vec{k}$ depends;

$$\lambda = \frac{h}{\sqrt{2m_e E}} \quad , \quad k = \frac{2\pi}{\lambda} \tag{3.25}$$

$$k = \frac{2\pi\sqrt{2m_e E}}{h} \cong 2\pi\sqrt{\frac{E(eV)}{150}} \tag{3.26}$$

It can be clearly seen that the magnitude of k is not affected in scattering process and

$$\frac{|\vec{k}_i|}{|\vec{k}_j|} = 1 \tag{3.27}$$

So every $\vec{k}_i$ will end on the edge of the Ewald's sphere. The Ewald sphere is represented as the fluorescent screen in LEED experiment. It means that if an occupied reciprocal lattice points cross the Ewald sphere, it will leave a spot for LEED pattern. With the construction of Ewald sphere, LEED pattern can be simulated for any known real space (Figure 3.19).

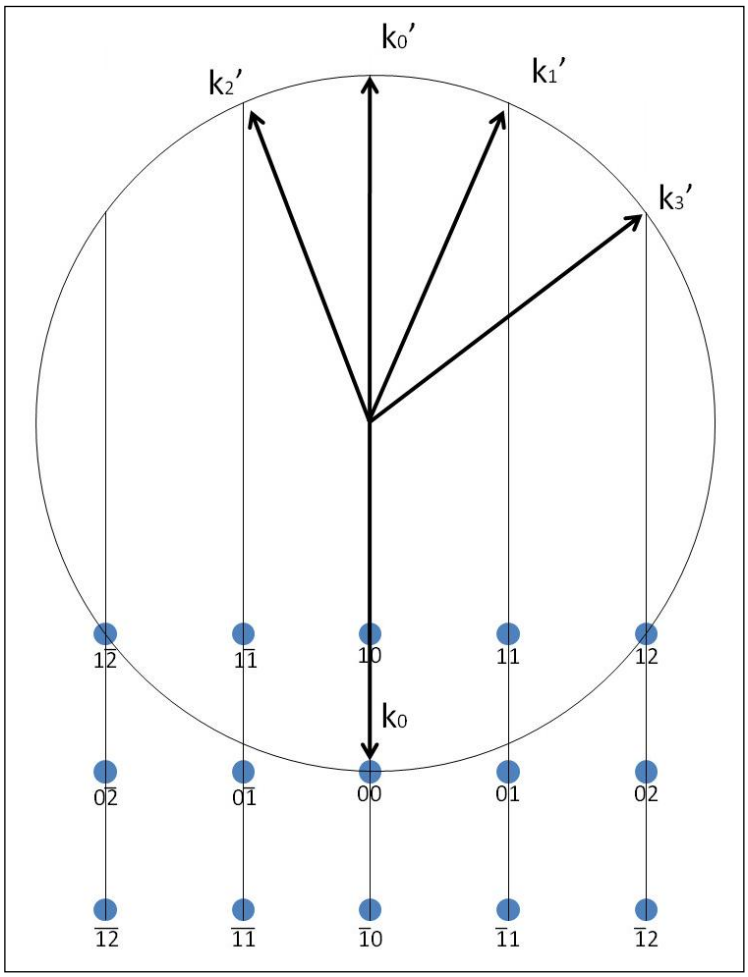

Figure 3.18: Ewald's sphere construction for diffraction from 2D-lattice.

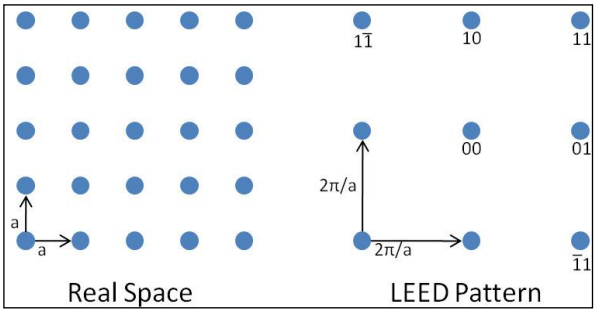

Figure 3.19: Real space and reciprocal lattice of a (1x1) lattice.

LEED patterns for simple lattices (Figure 3.19) are easier to simulate. However an essential problem for LEED patterns is the existence symmetrically equivalent domains. These domains may lead to a diffraction pattern with a higher symmetry than defined surface. In order to have observe these domains in LEED, their size needs to be bigger than the incident beam area. This leads for a superposition of the diffracted beams which gives new LEED pattern with complex domain(s) structures

[45], [46]. An example for a superposition of (2x1) and (1x2) surfaces is given in Figure 3.20.

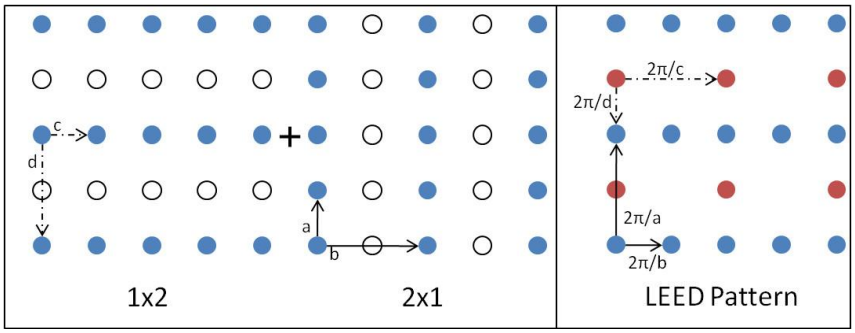

Figure 3.20: LEED pattern of a super position of two orthogonal domains (2x1) and (1x2).

4. EXPERIMENTS AND RESULTS

4.1. Sample Preparations

The well-defined surface and surface sensitive characterization are essential for repeatable and control-manner epitaxial depositions. The aim of the work is to practice repeatable deposition as possible as more sensitive. The magnetron sputtering deposition was used to grow the ultra-thin films on well-defined substrates; although it does not have common usages on epitaxial thin films. On the other hand, it is used to grow the multilayer and composite films for the state-art technologies. Some of applications demands even more complex and thinner layers and it causes elemental problems, which the quantum physics and the in-commensurate structures involved to. In this study, the surface sensitive analyzes techniques based on electron were used to characterize the growth thin films and to define the surface of the substrates. PtCo alloy films were grow on two different substrates to study for the comparison of the growth mechanism, on what it is well-known that the substrates and growth techniques effect. Two different films and two different substrates have been chosen in order to investigate the relation and interaction between substrates and films in growth process and to understand the reason behind the change in stoichiometry ratios.

4.1.1. Substrate Preparation and Reconstruction

The two type of substrate used in the study are naturally oxidized silicon wafer (SiO_x) and a platinum single crystal Pt (111). Platinum crystal has been used repeatedly after the application of certain reconstruction procedure, while SiO_x substrates have been prepared from silicon wafer freshly for the each film preparation. These are essential for a stable surface cleaning.

Surface cleaning of the each SiO_x substrates is annealed at 550^oC for 15minutes. The annealing process removed the carbon type contaminations from the surface. The cleanness of the substrates was confirmed by XPS shown in Figure 4.1.

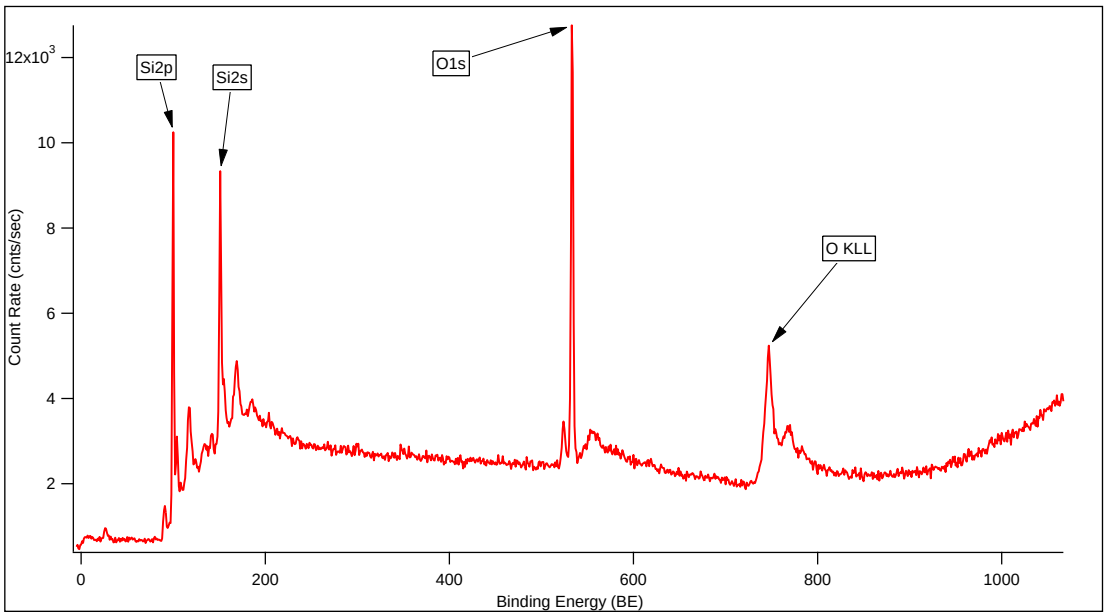

Figure 4.1: XPS-Survey spectrum of a clean Si(111) surface.

The reconstruction of Pt(111) which is performed within two steps; the restoration of the clean platinum surface and reconstruction of the Pt (111) surface. The restoration of the clean surface was performed by etching with energetic argon ions. A standard Ion gun (made by SPECS) was used for the etching process. However, the surface of the single crystal is delicate material and excessive etching may damage the surface structure. Therefore, the parameters such as ion energy, etching rate and etching time need to be optimized carefully. In order to find the best parameters for ion gun, it is necessary the calibrations work.

The growth rate was calibrated by removal of a platinum film grown on a Ta foil substrate and it was observed by XPS. First, Ta substrate was polished mechanically in order to minimize the surface roughness and it was welded to a holder. Additionally, the surface of Ta foil was cleaned with a rf- etching gun mounted of the loading section being part of UHV cluster system. Following to the confirmation of surface cleanness by XPS, the 16Å platinum was deposited on the surface by DC magnetron sputtering gun. Afterward, ion etchings were performed for different time spans and XPS spectra were taken before and after each etching period (Figure 4.2). Argon pressure for the etching was adjusted to 1,3-1,6 x 10^{-7} mbar in analytical chamber. Ion energy and focus area were chosen as 3keV and 1mm x 1mm respectively.

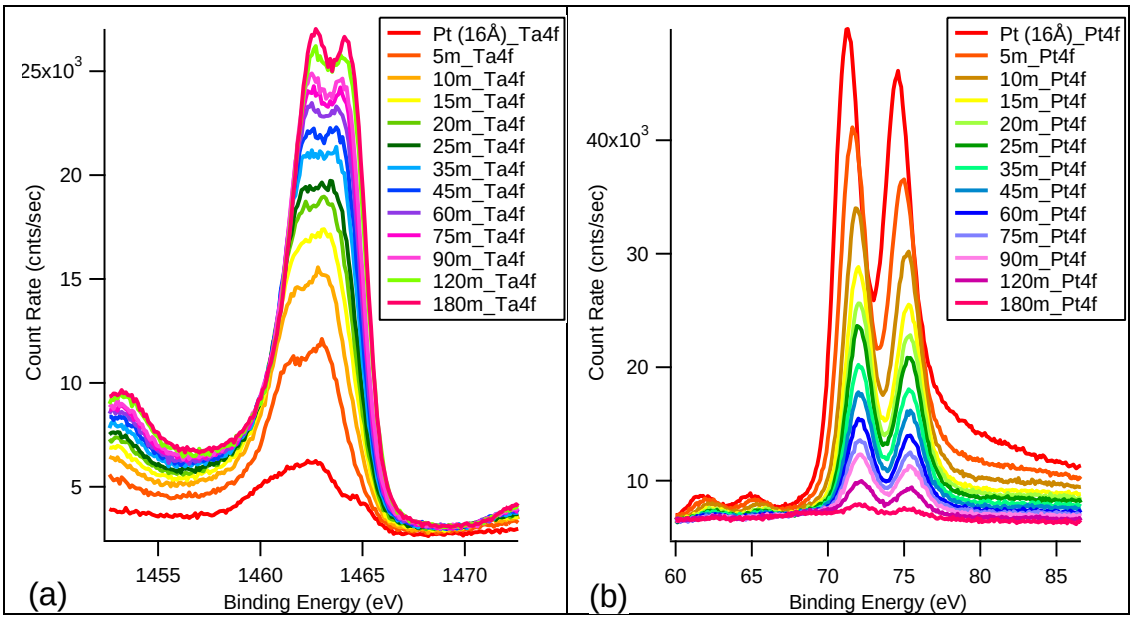

Figure 4.2: Ta4f and Pt4f XPS spectra taken after each etching step.

Ta 4f peak intensities (Figure 4.2) were used for the calculation of Pt film thickness after each etching by using the equation (4.1).

$$I = I_0 . e^{-d/\lambda} \tag{4.1}$$

The film thickness as a function of etching time is given in the Figure 4.3. This calibration results an etching speed of 3,33 Å/min for certain gas pressure, ion energy and focus area.

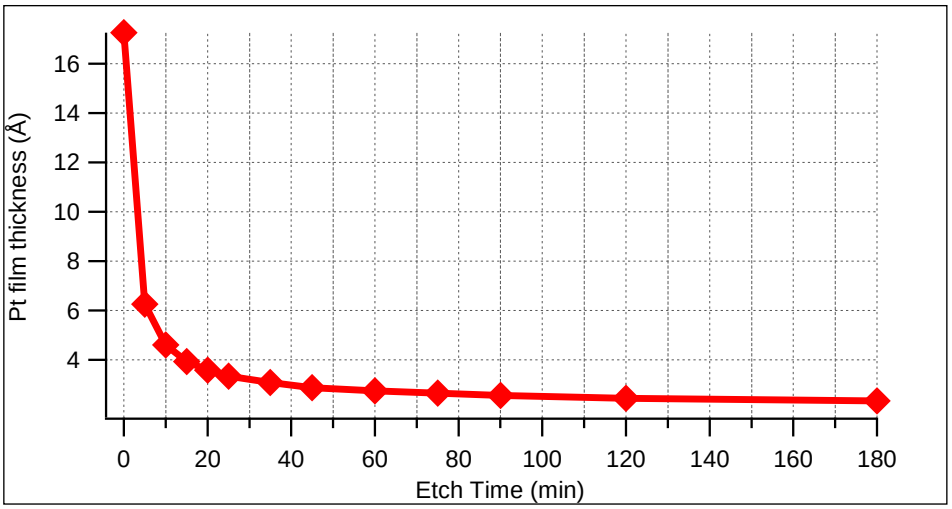

Figure 4.3: Platinum thickness over etching time.

I and the I_0 are the intensity of the Ta 4f peak. Film thickness and inelastic mean free path (IMFP) are given by d and λ(E) respectively. IMFP is the distance of how far an electron on average can travel within a solid without losing its energy. It is a function of energy and it also depends on the electronic and the physical structure of the solid. IMFP values can be obtained from experimental data or theoretical calculations. Values used in this study are obtained from NIST data base. Inelastic mean free path of an electron depends on the electron energy and the physical properties of the material, where electron travels. IMFP values of the Pt4f and Ta4f electrons travelling through platinum are taken as [48];

- $\lambda(E_{Pt}=1415,3eV)$ throughout Pt =16,84Å
- $\lambda(E_{Ta}=1463,4eV)$ throughout Pt =17,26Å

Cleanness of the argon gas used for depositions or etching processes is also essential for an efficient cleaning and purity of the films. Commercially purchased argon gas has a purity of %99,999. However additional purification by a gas filter is performed before exposing the argon to the vacuum system during deposition process. The cleanness of the argon gas exposed to the chamber is checked by using a Hidden® Residual Gas Analyzer (RGA). RGA spectrum of the argon is given by the Figure 4.4.

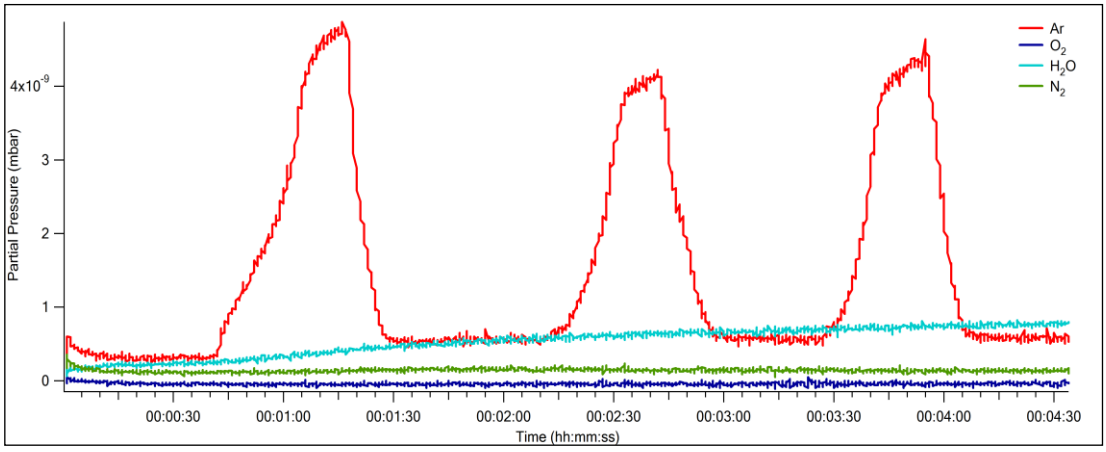

Figure 4.4: Change in partial pressure of Ar, O_2, H_2O and N_2 in analytical chamber.

RGA is a mass spectrometer used for monitoring the quality of the vacuum, detection leak and chemical reaction experiments. RGA can measure the desired element down to 10^{-14} mbar levels within sub-ppm detectability.

Purity checking of the argon was performed while exposing through the vacuum chamber periodically. At the same time, the RGA is run to measure differentiated distribution of argon, oxygen, water and nitrogen in the chamber. Purity of the Ar gas is crucial for both sample preparation and etching process. Samples prepared with low-purity Ar will have impurities. Furthermore, substrate cleaning with low purity Ar may contaminate the crystal surface.

Figure 4.5: Pt(111) single crystal mounted on a holder.

The surface of Pt(111) single crystal was reconstructed in two steps; surface cleaning and annealing. Pt (111) crystal was mounted on a molybdenum holder (Figure 4.5), and then it was loaded to the UHV system through the load-lock chamber. As first test after introducing the Pt(111), XPS was used to characterize the single crystal surface. According to the impurities on the surface base on the result of photoemission characterization, the crystal surface was etched by ion gun with the calibrated parameters (E_I=3keV, A_{focus}=1 mm x 1mm, P= 1,3-1,6 x 10^{-7} mbar). The preliminary etching process is used for the removal of the contaminations on the surface. It repeated until the surface cleanness which is also confirmed by XPS after each etching step. In Figure 4.6, an XPS spectrum of the Pt (111) substrate before and after cleaning process is shown for comparing reason.

In order to use the Pt substrate repeatedly, the films grown on the substrate are also need to be removed. For these film removal processes, same cleaning process mentioned above is used but with different etching parameters such as power, time,

temperature, and the partial pressure of Ar^+. The time interval of etching process is also varied while changing the sample preparation temperature. The films grown at room temperature can be removed in 15-30 min, and it was observed that etching time increases up to several hours with increasing preparation temperature.

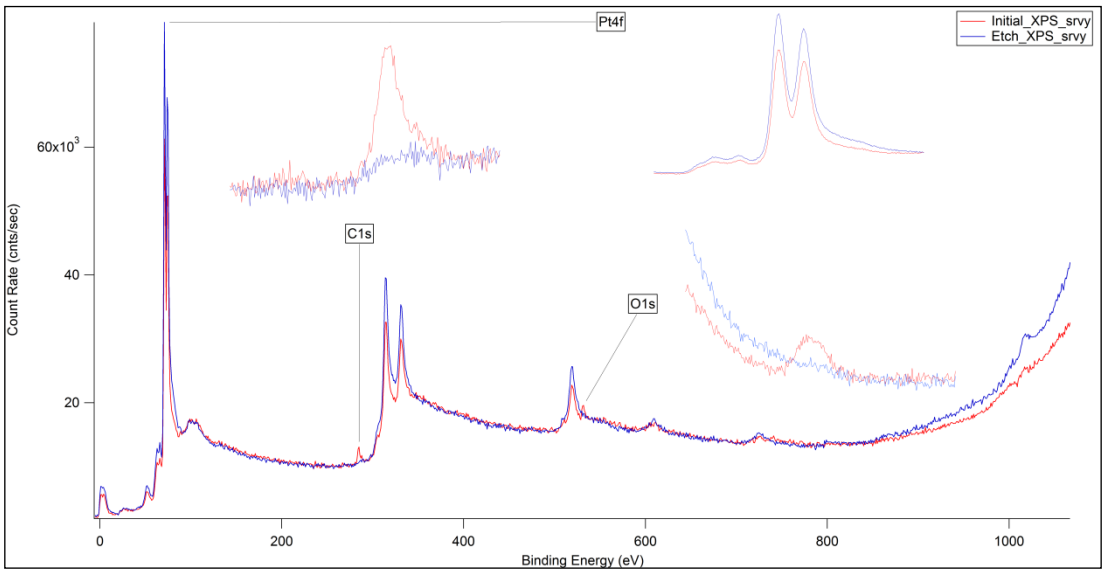

Figure 4.6: XPS-spectra of Pt(111) substrate before (red) and after (blue) cleaning process.

Surface cleaning of the single crystal is followed by an annealing process. For optimal annealing temperatures, various temperatures were used. After each reconstruction attempt, the surface symmetry was checked with LEED. The best results were obtained with 1100°C (Figure 4.7). This temperature is high enough the reformation of the surface symmetry for platinum crystal. Annealing time for all reconstructions was chosen as 15 min in order to achieve a stable surface. After each reconstruction, same LEED pattern, surface elemental composition was obtained.

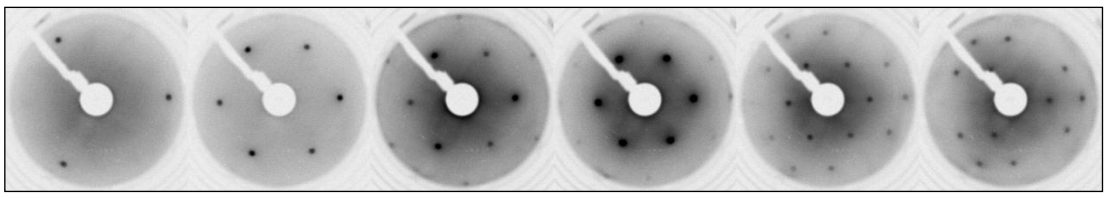

Figure 4.7: LEED pattern of reconstructed Pt(111) crystal (E=90eV, 135eV, 185eV, 220eV, 305eV and 370eV respectively).

4.1.2. Film Depositions

All the samples studied were prepared by magnetron sputtering technique in the sputtering chamber which is a part of the UHV cluster system. Chamber's base pressure is lower than $1x10^{-8}$ mbar. All the samples were prepared with 2,3 sccm argon flow. The thicknesses of films were monitored by a Quartz Micro-Balance system which was calibrated by XPS. The calibration is explained in the following section. Annealing processes were carried out by a PBN heater mounted on the chamber's manipulator. Manipulator was cooled constantly by a recirculation chilling system in closed cycle. Cooling water kept in a constant flow with 16-17^{o}C temperature.

The samples prepared can be separated by the film deposited; Co and PtCo. On different substrates, these two different films are grown for different preparation temperatures shown in Table 4.1.

Table 4.1: Schematic illustrations of the samples prepared.

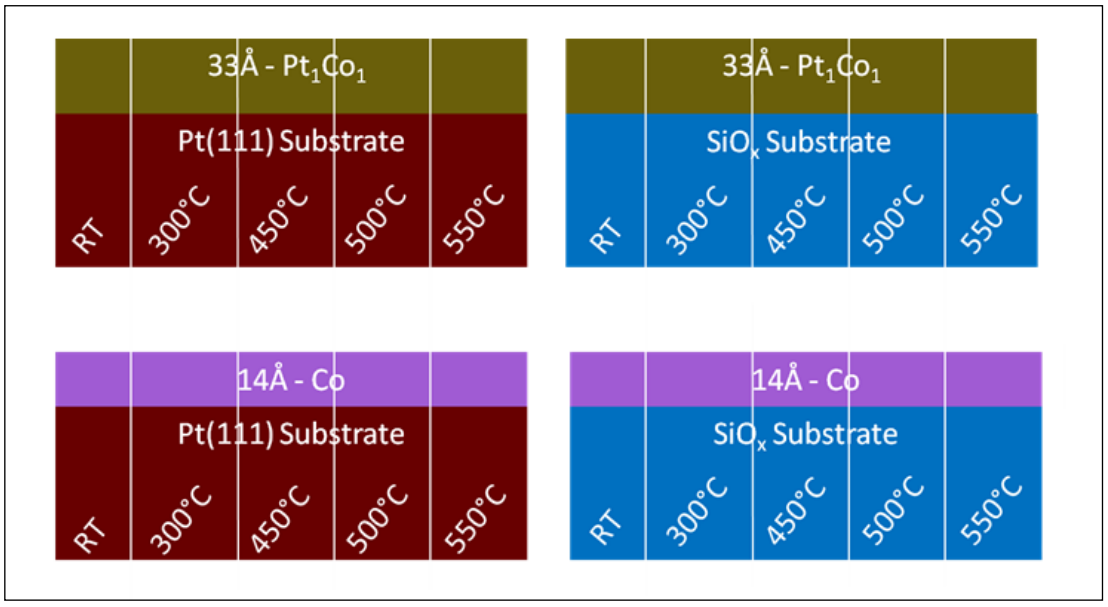

First set of films were prepared with a thickness of 14Å Co on SiO_x and Pt(111) substrates at Room Temperature, 300^{o}C, 450^{o}C, 500^{o}C and 550^{o}C. Before the deposition started, substrates were kept at preparation temperature for an extra 15 minutes so that they reach the targeted temperature. SiO_x wafer substrates were clamped on different holders and each holder can have different thermal

conductivity. Furthermore, the size of the substrates may vary. The extra annealing was essential to eliminate the thermal instabilities caused by these different conditions. For cobalt film depositions, RF source was the most suitable option due to magnetic properties of Co. Films were prepared with the lowest possible power so that the stability of the argon plasma was stayed hold. This value was found as 15W. Thicknesses of the films are monitored with a QCM in-situ and it was found 14Å.

The second set of films are PtCo with an atomic ratio of Pt/Co = 1/1 on same substrates and the same temperatures is used above. Deposition is carried out by using two different magnetron sputter guns run at the same time. During the deposition, the substrate mounted on the manipulator travels under the both gun sequentially while both guns are flushing. This technique is called sequential deposition. For the platinum deposition sequences a DC source is used. Co depositions are done by the RF source with the same parameters used in pure Co film preparations. DC source used in platinum depositions is adjusted to 2V. Each film preparation took a total 79 sequences of platinum and cobalt depositions. Number of the sequence is calculated by taking account of a film growth of ≤ quarter monolayer for each sequence. The lower deposition rate and the large number of sequences ensure the homogeneity of the films and it enables to grow epitaxial thin films layer by layer. The thickness of the film is measured by the calculation of the total amount of atoms deposited on the substrate. The calculations results a 19Å Pt film and 14Å Co film for equal-atomic 1:1 ratio. The calculation gives the thickness of 33 Å for PtCo film.

4.1.3. Calibration of Deposition

For control manner deposition, the guns used for sputtering should be calibrated. During sputtering depositions, QCM is used in-situ, even though the photoemission spectroscopy (XPS) is used to measure the thickness of the growth film for confirmation; and the result of XPS is sensitive for ultra-thin layer as long as the thickness of layer is around the attenuation length of electron emitted the atoms of films. QCM, in other words Quartz Crystal Microbalance measures the change in frequency of a quartz crystal resonator which gives information about the mass variation on surface. This mass variation is triggered with oxide growth/decay or film

deposition. This measurement in “change of balance” gives QCM a wide range of working temperature and application field from gravimetric to gas sensors.

QCM reader analyzes the change in quartz crystal oscillations and calculates the thickness from this analysis. The QCM tooling factor is an essential parameter for this calculation and it needs to be calibrated periodically for each element and/or the sputter gun. Tooling calibration is performed by consecutive film depositions followed by a thickness measurement with a different technique than QCM. With the comparison of the deposition rates, the tooling factor is adjusted for the 95.0. Our research group uses the X-Ray Photoemission Spectroscopy for QCM calibrations to eliminate the errors distributions since it is very delicate to minimize the error distribution of thickness. For calibrations, Co and Pt films are grown of Ag and SiO_x substrates respectively with different deposition times. Each deposition is followed by a XPS measurement (Figure 4.8).

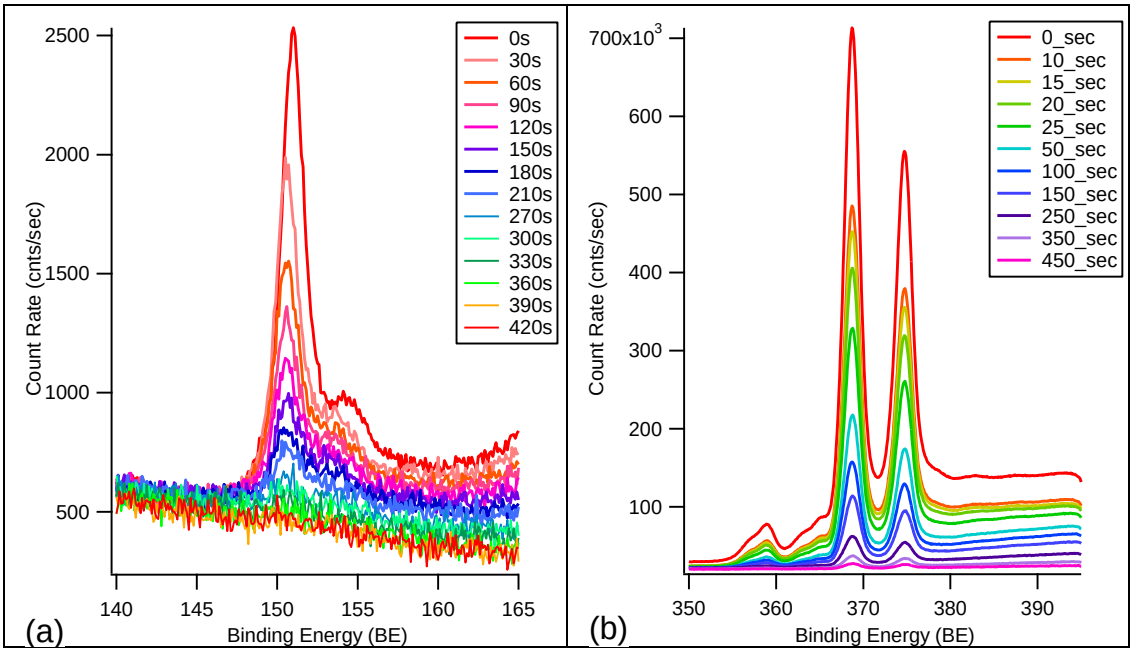

Figure 4.8: a) Si2s and b) Ag3d photoelectron lines for different deposition times.

Thickness of the films grown at each deposition is calculated with the equation (4.1), where I and I_0 holds for the final and initial intensities, d for film thickness and $\lambda(E)$ for IMFP. From these values, the film thickness has been calculated as a function of deposition time. The derivation of this function yields for deposition rate for each target. These deposition rates have been used to calibrate the tooling factor of QCM.

Deposition rate used in our study are calculated as;

- $V_{Pt} = 0{,}04\ \text{Å}/sec$
- $V_{Co} = 0{,}036\ \text{Å}/sec$

There are two ways for an epitaxy film preparation for alloys; annealing of multilayer films or codeposition from different targets [26]. The co-deposition methods require layer by layer growth can be done by simultaneous or sequential depositions. Layer by layer growth, in sequential deposition can be achieved by stacking atoms with a thickness lower than quarter monolayer at each sequence.
A quarter monolayer of a Pt film holds for 0,98Å and Co for 0,63Å. The thicknesses of Pt and Co at each sequence are calculated as;

- $d_{Pt} = 0{,}04\ \text{Å}/s\ \times\ 6\ s = 0{,}24\ \text{Å}$
- $d_{Co} = 0{,}036\ \text{Å}/s\ \times\ 5\ s = 0{,}18\ \text{Å}$

4.2. XPS Results for Surface Characterizations

XPS experiments are performed in the analytical chamber which is part of the UHV cluster system. The excitation source is chosen as the Mg Kα to prevent the convergence of cobalt auger peaks with cobalt core level peaks. Analyzer's iris opening, slit mode and pass energy are adjusted for the best values for the measurements. In order to minimize the deviations, the sample-analyzer distance and x-ray source power were not changed during this study for comparable results.

XPS spectra are used to calculate the surface stoichiometry and the thickness of the films beside electronic properties. Furthermore the behavior of the peaks (i.e. energy shifts, shape changes) is used to interpret the interaction of the substrate-film and cobalt- platinum. Survey apectra are investigated with including the background effects but for the high resolution window scans and curve fittings, the background removal method is applied by using the Shirley algorithm given in equation (3.14-16) and Figure 3.9-3.10.

• The Samples Prepared on Pt(111)

The survey spectra from 14Å Co and 33Å PtCo films grown on Pt(111) at different temperatures are given in the Figure 4.9.

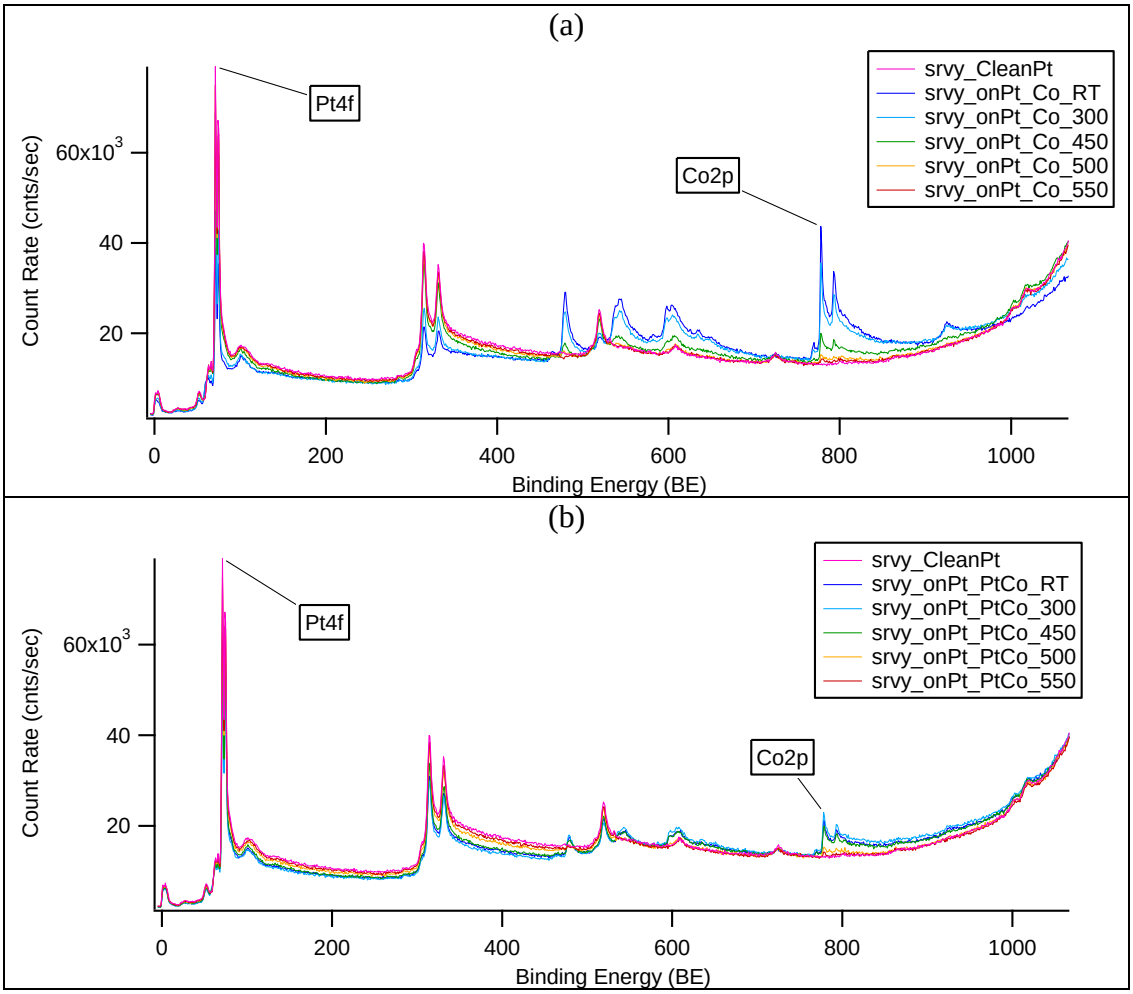

Figure 4.9: XPS-Survey spectra of a) Co and b) PtCo films prepared on Pt substrate at different temperatures.

Survey investigation of the wide range XPS shows that the surface content occurs only platinum and cobalt elements. The existence of platinum in XPS from Co Sample is because of the thickness of film. The thickness is not high enough to suppress the Pt signal coming from the substrate. Furthermore, decreasing in the intensity of Co peak is observed with the increasing in sample preparation temperature. For more detailed analysis, high resolution window scans are studied.

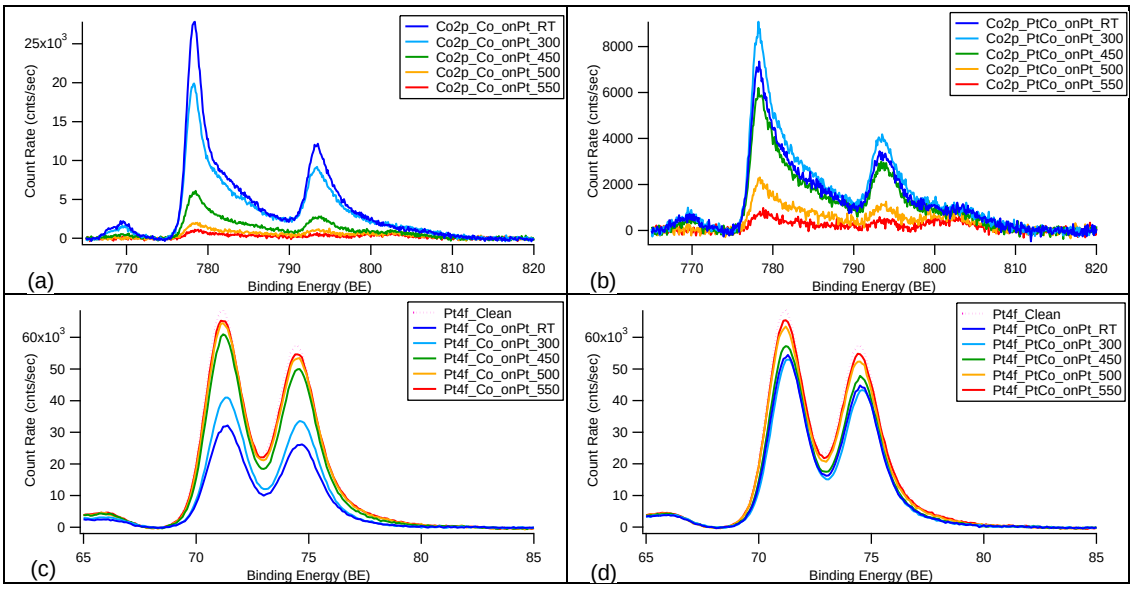

Figure 4.10: Co2p and Pt4f photoelectron lines of Co and PtCosamples grown on Pt(111) substrate. a) Co2p of Co sample, b) Co2p of PtCo sample, c) Pt4f of Co sample, d) Pt4f of PtCo sample.

In the high resolution spectrum, the spectral lines of Co2p and Pt4f at each temperature (Figure 4.10 and Table 4.2) are used to calculate the elemental stoichiometry for the growth films, and the results mostly match with aimed the elemental ratio in the growth films. However, in PtCo sample grown on Pt (111) substrate, while the temperature is increased, the intensity of Co2p is decreased in spectrum. The increament in PtCo samples is interpreted that the surfaces become more and more homogeneous as a function of the increasing temperature up to 300°C. Peak fitting of these spectral lines are essential to support this interpretation. However, cobalt curve fitting can be difficult due to the asymmetric tail at the higher binding energy side of the 2p core peaks since the photoemission spectral peaks of the transition metal and transition metal oxide has, generally, unique tail properties. The tail on the photoemission peak is formed because of the unfilled electron level above Fermi. Furthermore, platinum shows a small peak around 795 – 805 eV. Normally this small peak can be ignored since it is proportional to the main core peak. However the samples prepared at higher temperature have lower cobalt and higher platinum intensities. There by platinum peak at 795 – 805 eV energies becomes more dominant in Co2p line at higher temperatures. This non-cobalt peak in Co2p line, make difficulties in Co curve fitting process. In order to overcome these difficulties in Co curve fitting, only the $2p_{3/2}$ line of Co is fitted easily and the area of the $2p_{1/2}$ curve is calculated from this value, since the peak $2p_{3/2}$ is proportional to

$2p_{1/2}$. The electron population ratio of $p_{1/2}$ and $p_{3/2}$ is 1:2 (table 3.1). This ratio is directly related to the intensities of photoelectron peaks. This means the intensity and the area of a $p_{1/2}$ peak must be the half of the $p_{3/2}$ peak. For stoichiometry calculations, the area of the $Co2p_{3/2}$ is multiplied by 1.5 in order to have the total area under the Co2p curve. Curve fittings are given in Figure 4.11 and Figure 4.12.

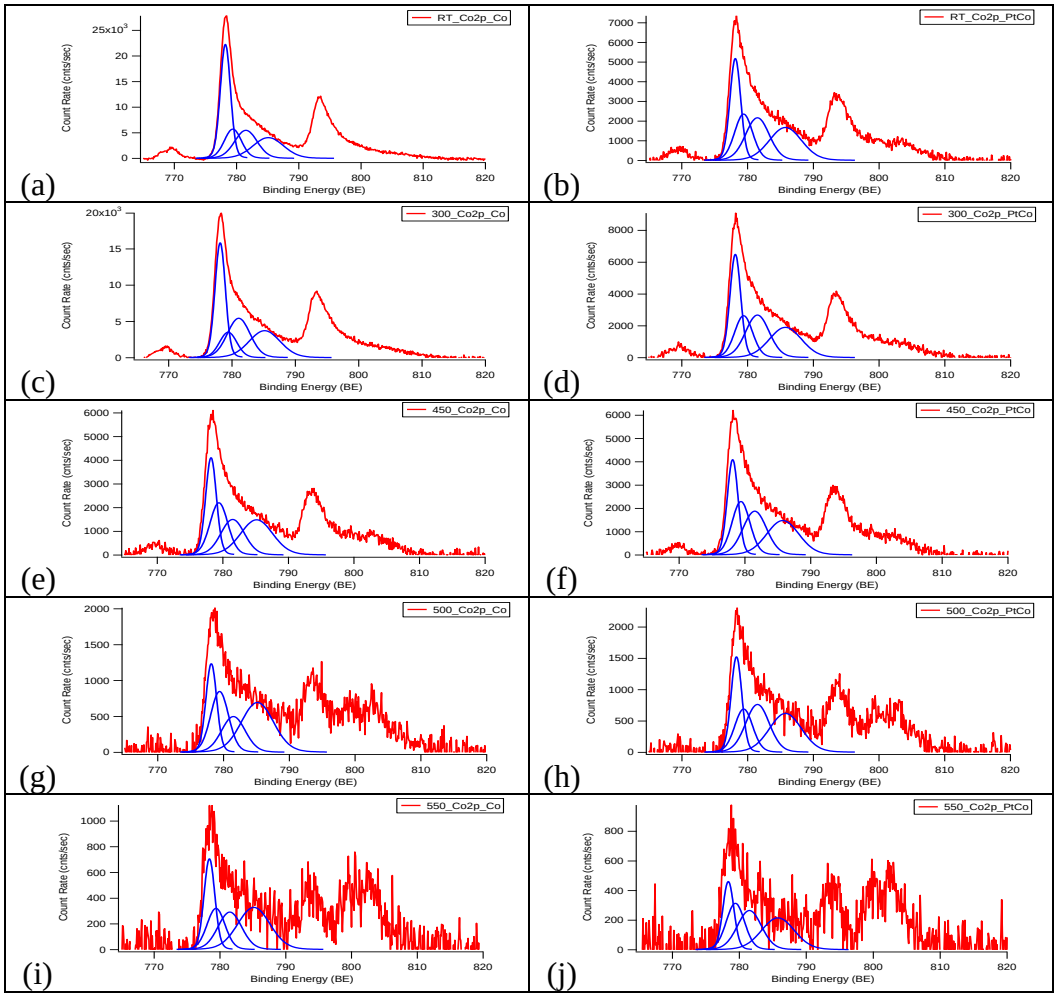

Figure 4.11: Curve fittings of Co2p lines of Co (left column) and PtCo (right column) samples on Pt(111) for increasing substrate temperature (up to down).

Atomic sensivity factors of the elements used for stoichiometry calculations are taken as [49];

- ASF_{Co2p} =3,59
- ASF_{Pt4f} =5,575

The stoichiometries of the films are calculated by using the equation (3.11). The elemental stoichiometry of samples and the energy shifts of core lines are given in Table 4.2. Energy shifts are calculated by substracting the peak's energy from default binding energy. Default Binding Energies has been chosen as 778,2eV for Co2p and 71,15eV for Pt4f [49].

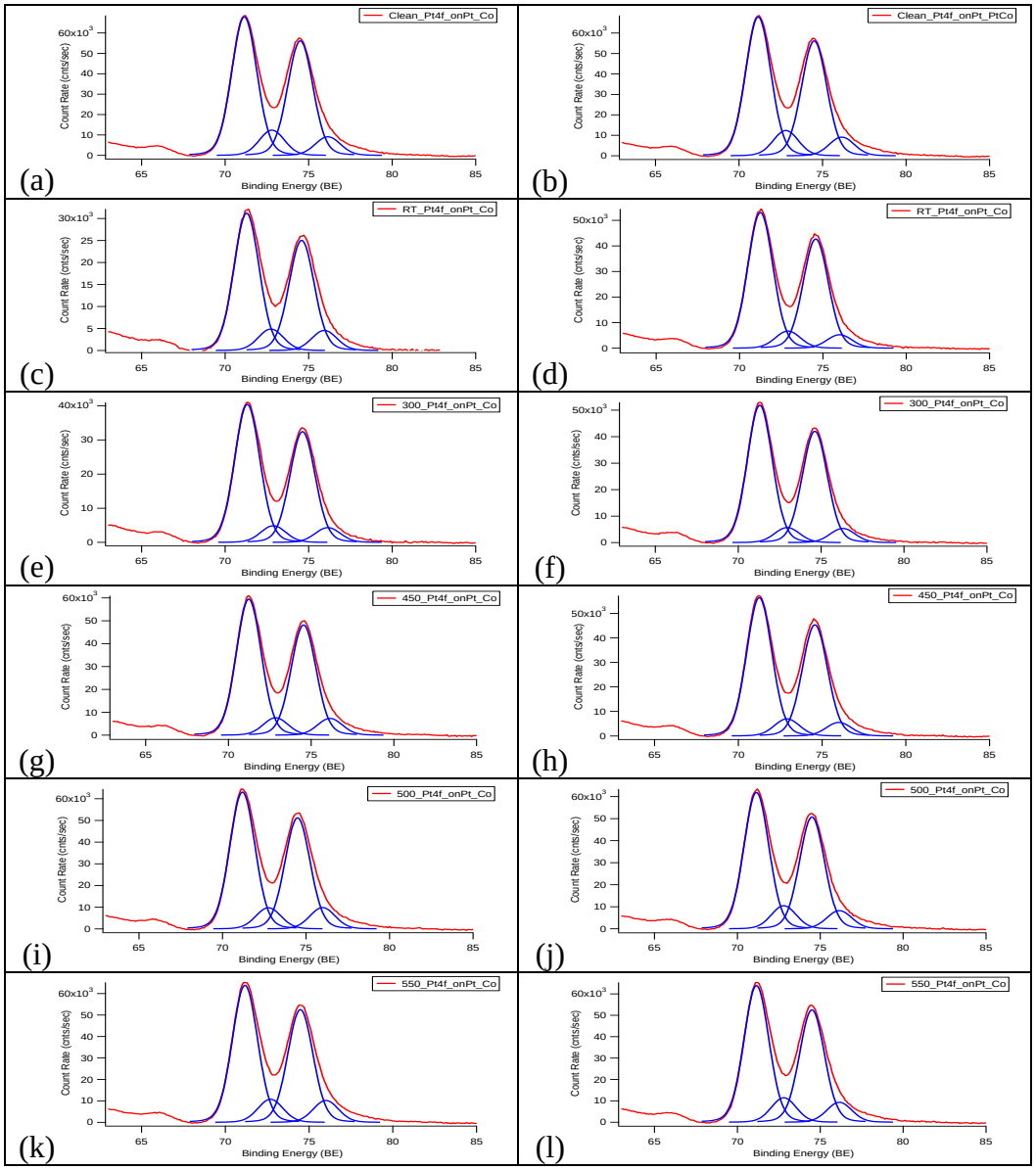

Figure 4.12: Curve fittings of Pt4f lines of Co (left column) and PtCo (right column) samples on Pt(111) for increasing substrate temperature (up to down).

Stoichiometry of the Co films calculated by using fitting results shows a nearly 5% of increase in Co ratio with the increase in temperature to 300°C. On the other hand, PtCo films calculations shows a decrease in Co composition with this

temperature increase. This changes in Co ratio in Co sample prepared on Pt substrate, indicates for the expansion of Pt/Co interface by Co diffusions through the substrate. As it is mentioned earlier, PtCo samples are prepared by sequentially Co and Pt depositions, started with Co, ended with Pt sequences. This final step of Pt sequence forms a Pt rich surface. With the increasing temperature up to 300°C, Co and Pt atoms lied in their sequential layer mobilize and the diffusion occurs in some lavel in order to form a more homogeneous surface. However, the surface stoichiometry of the PtCo films prepared at RT does not show a fifty percentage of Pt over Co. On the other hand, it may be due to the contribution of the Pt substrates to the platinum peak.

Table 4.2: Curve Fitting results and Energy shifts of Co and PtCo samples grown on Pt(111) substrate.

	onPt				ΔBE			
	PtCo		Co		PtCo		Co	
	Pt	Co	Pt	Co	Pt	Co	Pt	Co
Clean	100,00%	0,00%	100,00%	0,00%	0	-	0	-
RT	69,65%	30,35%	32,00%	68,00%	0,1	-0,6	0,13	0
300	65,06%	34,94%	42,21%	57,79%	0,15	-0,6	0,18	-0,06
450	71,75%	28,25%	75,95%	24,05%	0,15	-0,6	0,08	0
500	89,46%	10,54%	90,25%	9,75%	0	0,1	0,04	-0,06
550	96,15%	3,85%	95,08%	4,92%	0	0,15	0,02	0,2

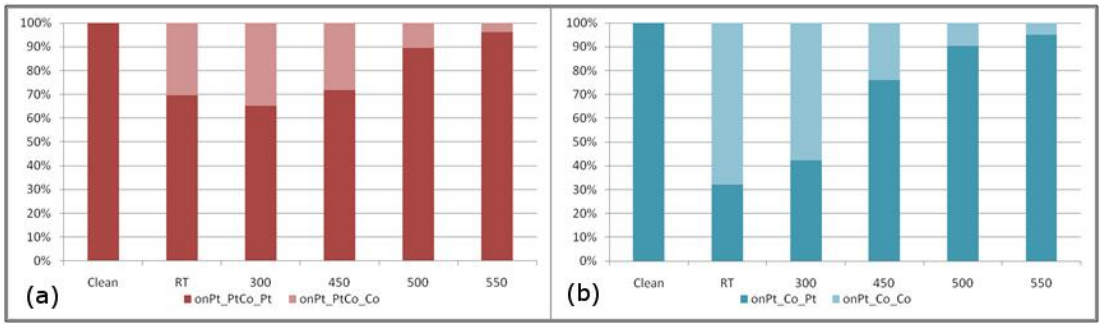

Figure 4.13: Elemental ratio of a) PtCo and b) Co films on Pt(111). Calculated by XPS results.

The stoichiometry of the pure Co and PtCo films prepared on Pt(111) are given in the Figure 4.13. The results indicate for a similar Pt-Co ratio above 450°C. These similarities at higher temperatures can be explained in two ways; the disappearance of cobalt by vaporization or the diffusion of cobalt atoms through platinum crystal. In the sample preparation section, the increase in etching times for higher preparation temperature has been emphasized. Cobalt atoms diffused through the crystal will be

harder to remove by etching comparing to the atoms rest on the surface. This increase in the etching time supports the diffusion explanation. However, in order to understand this mechanism profoundly, further studies must be done such as using alternative analysis techniques and alternative substrates. It is necessary to investigate the behavior of cobalt on a different substrate. Comparison of Co behavior on different substrates will help to understand the diffusion mechanism.

• The Samples Prepared on Naturally Oxidized Si(111)

14Å Co and 33Å PtCo films prepared on the SiO_x substrates are investigated by using the same parameters used for platinum substrate. Survey spectra of these samples are given in Figure 4.14.

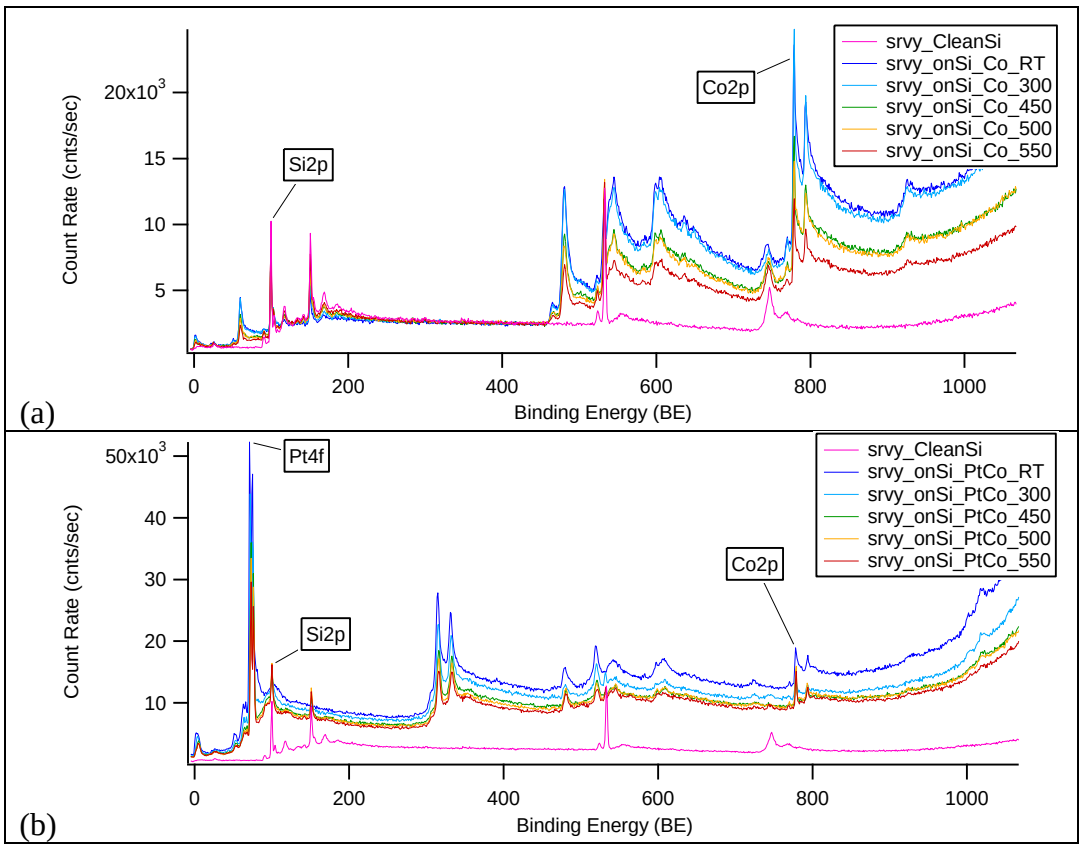

Figure.14: XPS-Survey spectra of a) Co and b) PtCo films prepared on SiO_x substrate at different temperatures.

Survey spectra's elemental analyzes shows the existence of cobalt, silicon and oxygen in Co films, and the existence of cobalt, silicon, oxygen and platinum in PtCo films at each preparation temperatures. The trend in the survey spectra of samples prepared on SiO_x is similar to the samples prepared on Pt(111) substrate; as shown a

decrease in Co intensities. However the decrease in background spectrum is much stronger than the samples grown on Pt(111) substrate. It points out a stronger change in the electronic structure of the samples by increasing sample preparation temperature. On the other hand, for more understanding, the window scans with high resolution are needed to be analyzed (Figure 4.15 - 4.18).

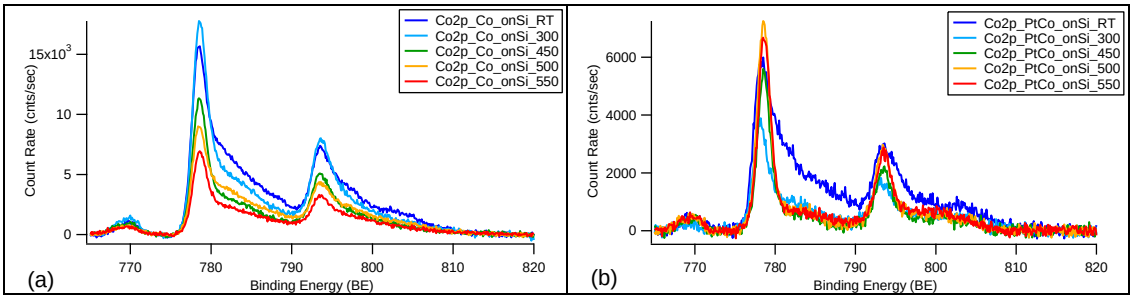

Figure 4.15: Co2p photoelectron lines of a) Co and b) PtCo samples grown on SiO_x substrate.

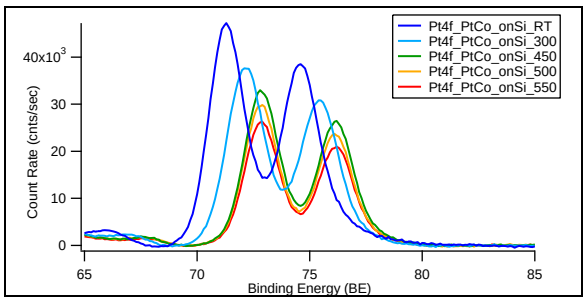

Figure 4.16: Pt4f photoelectron lines and PtCo sample grown on SiO_x substrate.

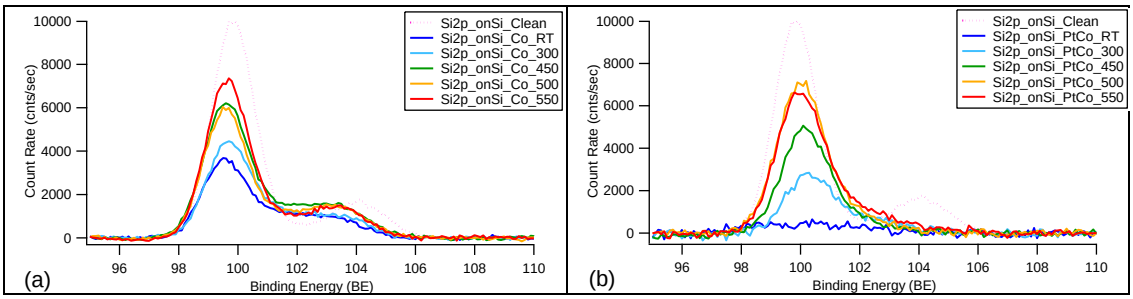

Figure 4.17: Si2p photoelectron lines of a) Co and b) PtCo samples grown on SiO_x substrate.

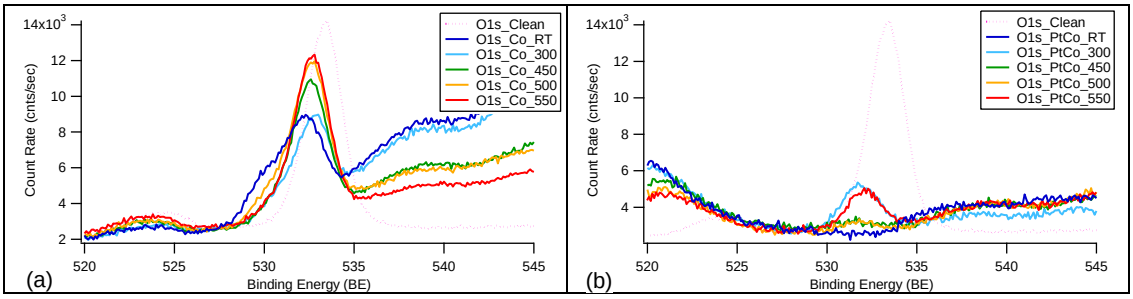

Figure 4.18: O1s photoelectron lines of a) Co and b) PtCo samples grown on SiO_x substrate.

A naturally oxidized silicon should have 2 different 2p peaks at 99,85 eV and 104,7 in XPS. These peaks are related to pure Si and SiO_2 respectively. Both peaks can be found in Si 2p spectra of the cobalt samples. However platinum 4f and 5s lines are close to the Si 2p line and SiO_2 2p lines get suppressed by these platinum peaks. Furthermore1s spectral line of oxygen is also close to the Pt 4p peaks. Main peak of the Pt 4p line and its satellites raise the background level of the spectrum around O1s line. Due to this high background level, O1s secondary electron background calculation becomes harder. The secondary background substraction methods are explained in chapter 3.2.1.1. Moreover, the oxygen content found in the sample is totally related to the oxidized silicon on the surface of the substrate which is low since the intensities of O1s emission line are lower. Due to low O1s spectral line and inaccurate background function, O1s peak fitting becomes unreliable. For these reasons, O1s lines could not been fitted.

On the other hand, the Co2p and 4f lines in high resolution window scans reveal interesting features. For the pure Co sample, the main trend in Co decreases by increasing temperature. However the sample preparation temperature is increased to 300°C from RT, the Co ratio. Furthermore, the asymmetric tail of the Co tends to lower with this increasing temperature. The increase in Co intensity may depend on this tail loss. To understand this mechanism, the curve fittings of the spectrum must be analyzed closely. The PtCo sample's spectra show even more interesting results. On the contrary of Co sample, Co 2p peak of the PtCo sample does not decrease with the increasing temperature from 300^0C to 550^0C. However, with the sample preparation temperature increased to 300^0C from RT, the Co ratio in the PtCo sample decreased. Moreover, the peak intensity tends to increase while increasing temperature. The tail loss of Co2p peak observed intensely in the PtCo. The

asymmetric tail of the Co 2p nearly disappears with first temperature increase (Figure 4.15). Moreover, the Pt4f peak from the same samples shifts towards higher binding energy while increasing temperature up to 450°C. Energy shift in photoelectron spectra may be related to the charges on the surface as well as related to the changes in the electronic structure. However, the charges on the surface will cause a shift for whole spectrum together, not only one peak. In this case, only platinum peaks are shifted which indicates for possible chemical bonding. Morgan et.al. reported that the bonding of Pt-Si formation leads to binding energy shift up to 1.7 eV with increasing temperature. The magnitude of energy shift reported in Morgan's study matches to the results in this study [50].

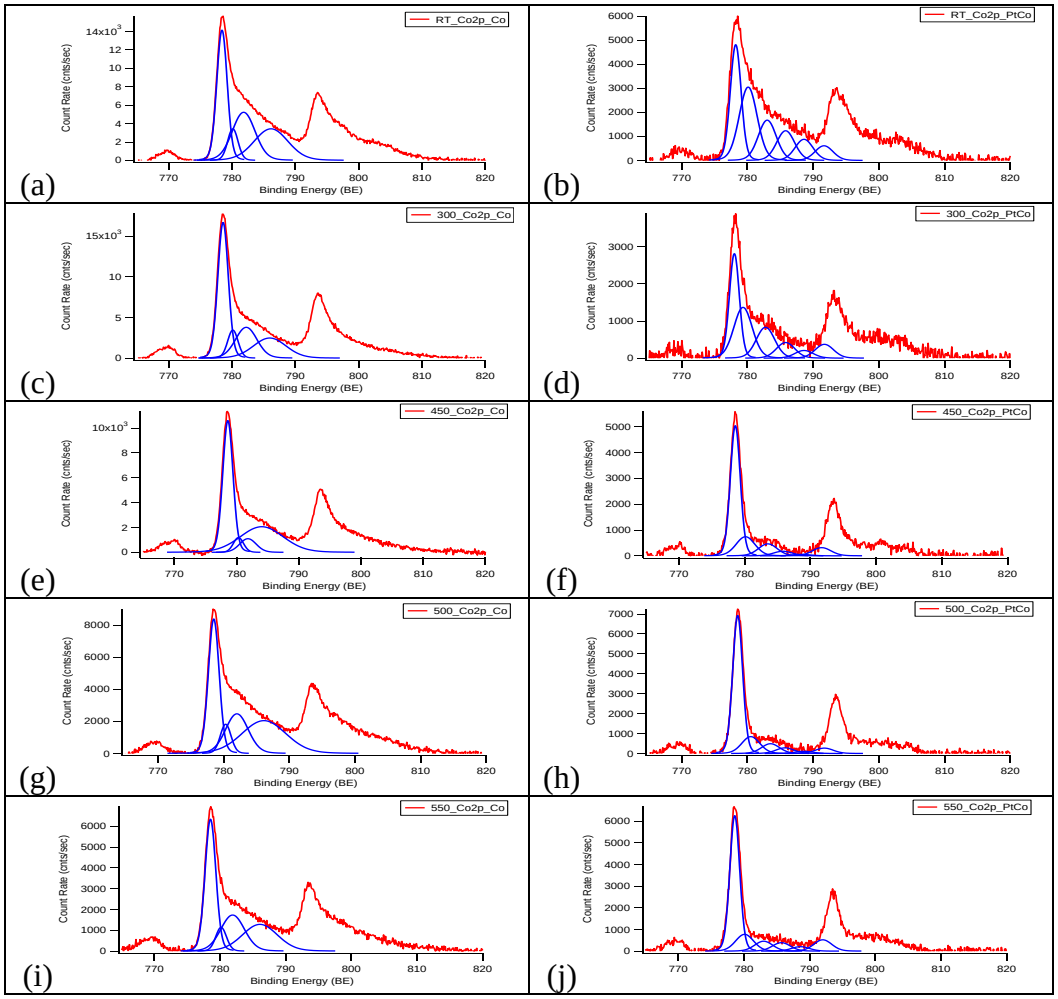

Figure 4.19: Curve fittings of Co2p lines of Co (left column) and PtCo (right column) samples on SiO_x for increasing substrate temperature (up to down).

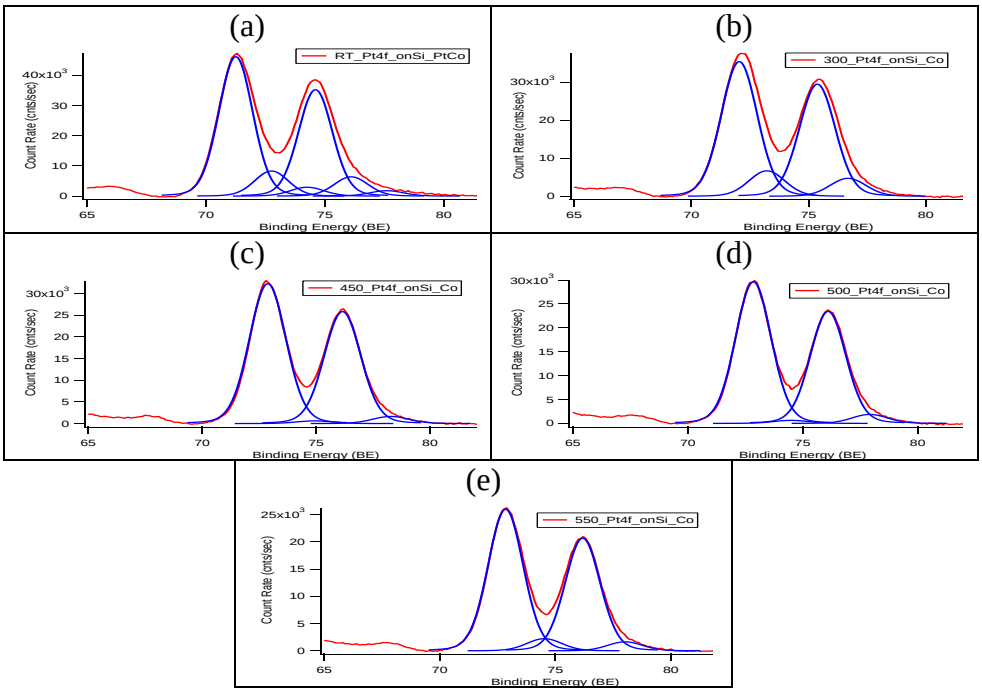

Figure 4.20: Curve fittings of Pt4f lines of PtCo samples on SiOx for increasing substrate temperature.

Table 4.3: Curve Fitting results and Energy shifts of Co and PtCo samples grown on SiO_x substrate.

	onSi					ΔBE				
	PtCo			Co		PtCo			Co	
	Si	Pt	Co	Si	Co	Si	Pt	Co	Si	Co
Clean	100,00%	0,00%	0,00%	100,00%	0,00%	0	-	-	-	-
RT	0,00%	68,53%	31,47%	38,42%	61,58%	-	0,1	0	0,1	0,23
300	28,81%	56,39%	14,80%	46,57%	53,43%	0,33	0,89	0,2	0,89	0,4
450	46,92%	40,73%	12,35%	66,55%	33,45%	0,21	1,73	0,35	0,73	0,4
500	57,07%	30,02%	12,91%	63,84%	36,16%	0,08	1,7	0,3	0,7	0,3
550	56,90%	29,07%	14,03%	77,23%	22,77%	0,06	1,7	0,4	0,7	0,34

Elemental compositions of the samples are calculated with equation (3.11) from the curve fitting results (Figure 4.19-4.21) by using the following atomic sensivity factors [49].

- ASF_{Co2p} =3,59
- ASF_{Pt4f} =5,575
- ASF_{Si2p} =0,399

The calculated elemental ratio and the energy shifts of core lines in XPS are given in Table 4.3 . Energy shifts are calculated by susbtracting the position of the main peak of the related element from a default binding energy. Default binding energies have been chosen as 95,85eV for Si, 778,2eV for Co and 71,15eV for Pt lines.

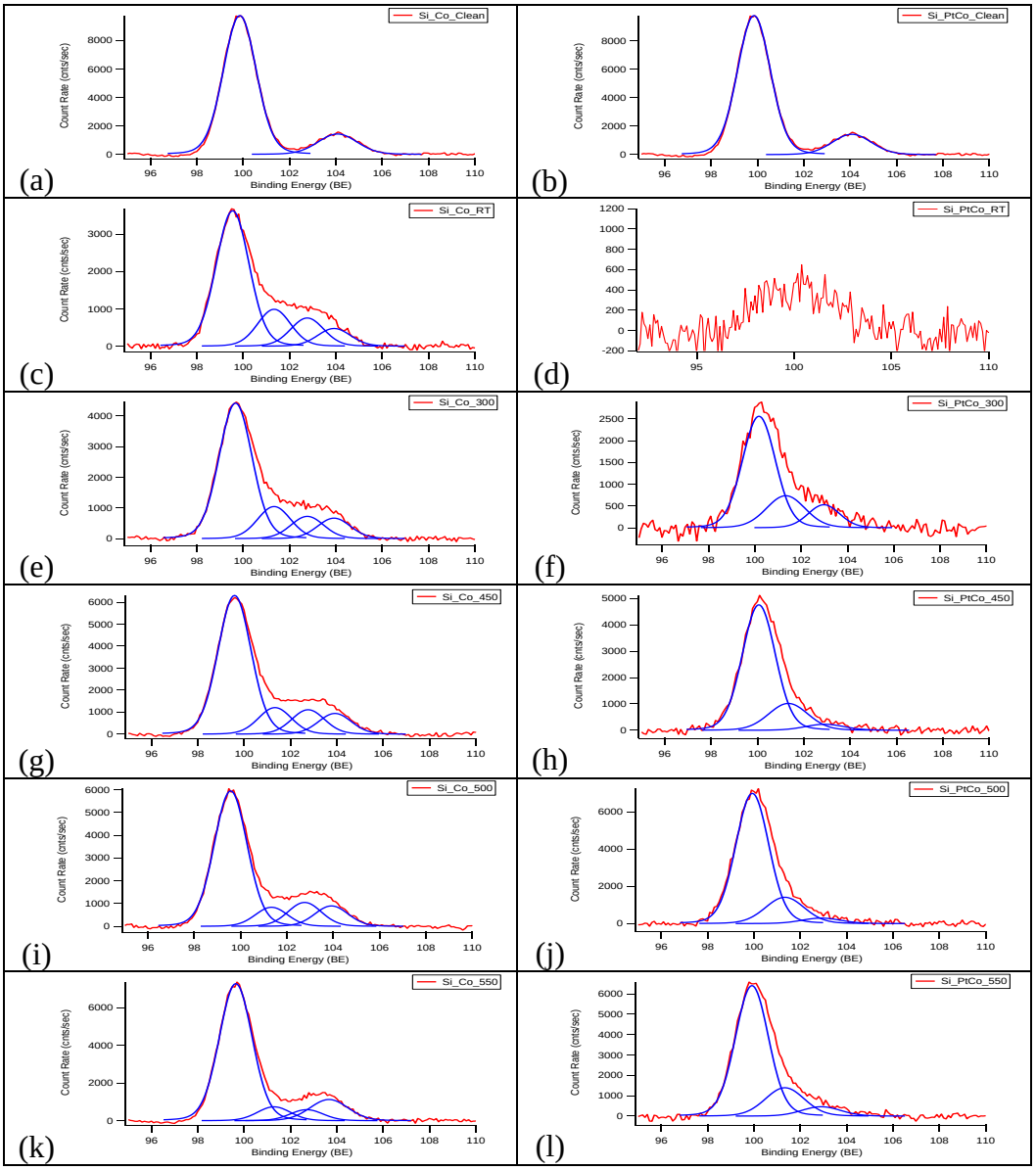

Figure 4.21: Curve fittings of Si2p lines of Co (left column) and PtCo (right column) samples on SiO_x for increasing substrate temperature (up to down).

The intensity of the Co2p from Co samples prepared on SiO_x increases while increasing the temperature up to 300^{o}C; however the calculations for stoichiometry show decrease in the Co ratio. It is related to the decrease of the asymmetric tail on

Co 2p peak. The intensity of the main peak may be increased but the decreasing in tail leads to greater loss in total area (Figure 4.19). The curve fitting results from PtCo samples show different trend (Figure 4.19-4.21). The Co ratio decreases to 15% from 30% while increasing temperature to 300^{o}C. However, this decrease stops, after the temperature of 300^{o}C while the tail intensity continues to decrease. The change of peak and tail area in Co main peak is given in Figure 4.22. On the other hand, Pt concentration of the surface continues to decrease while it goes up to 500^{o}C as Si concentration of the film behaves. The increment in Si intensity indicates either an agglomeration on surface or a diffusion of film through the substrate. Comparison of Pt ratio over Co does not change significantly while increasing temperature (Figure 4.25).

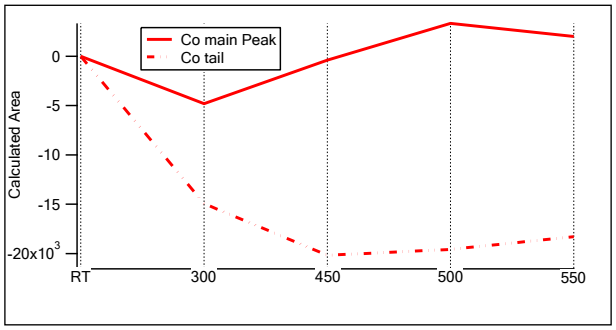

Figure 4.22: Comparison of the change in Co main peak intensity and its tail for PtCo sample on SiO_x substrate.

The asymmetric tail on Co 2p core main peak is a result of the unpaired electron above Fermi Level. The loss in this tail is interpreted as a redistribution of Co valance electrons. This redistribution might occur due to a formation of bonding or due to a change in electronic structure of Co under the temperature change. To understand this phenomenon, extra electronic structure analyses like UPS are required to resolve the reason of electronic effect.

The stoichiometry calculations of PtCo films prepared on different substrates show 7:3 ratio of Pt over Co at room temperature. This value is 20% lower than the expected Pt/Co ratio. In higher temperatures, the cobalt ratio in the films grown on SiO_x substrates is higher than films prepared on platinum single crystal. This case supports the conclusion about Co diffusion through Pt(111) substrate.

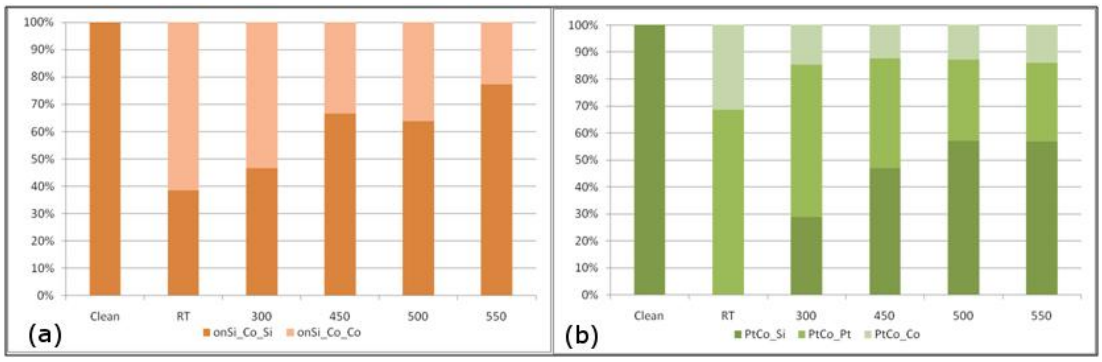

Figure 4.23: Elemental ratio of a) Co and b) PtCo films on SiO_x. Calculated by XPS results.

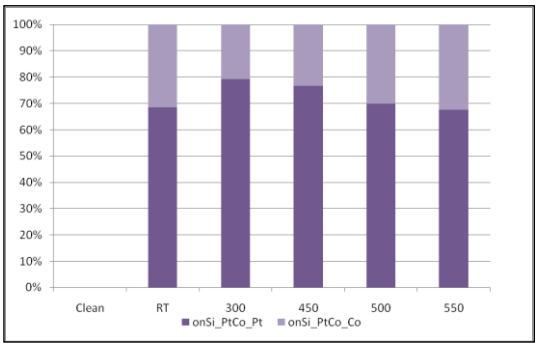

Figure 4.24: Pt/Co ratio of the PtCo film grown on SiO_x. Calculated by XPS.

The different behavior of Co and Pt on different substrates is interpreted as an interaction between Si and Co and Pt. The loss in Co tail was much more intense for PtCo sample on SiO_x than the Co sample grown on the same type of substrate. This difference indicates that the existence of Si and Pt, at the same time, increases the effect causing redistribution of electrons in fermi surface of Co atoms. This effect will be also investigated by the results of auger and ultraviolet spectroscopies.

4.3. UPS Results for Valance Structure Characterizations

UPS experiments are performed within the analytical chamber used for XPS analysis in-situ. The same energy analyzer has been used to analyze the photoemission electrons due to UV-excitation. The UV-light source is adjustable for polarized or un-polarized He-I or He-II discharges both. In this study, un-polarized He I light is used as the excitation source. Energy analyzer is adjusted for a fixed retarded ratio, iris opening and slit mode in order to ensure the same conditions for each analysis. However the intensity of light source depends on various parameters

such as He pressure, source voltage and the temperature of the source gun. In order to eliminate the deviations in different spectrum intensities due to unstable parameter for each uses, UPS spectra are normalized in every case.

A chemical bonding or a change in electronic structure of a material is mostly made by valance electrons. Thus understanding the valance structure is crucial in order to resolve the interactions between the substrates and the grown film, and also the interactions between Pt and Co in alloy films.

• The Samples Prepared on Pt(111)

UPS spectra for Cobalt and Platinum/Cobalt samples on Pt(111) substrate is given in Figure 4.25.

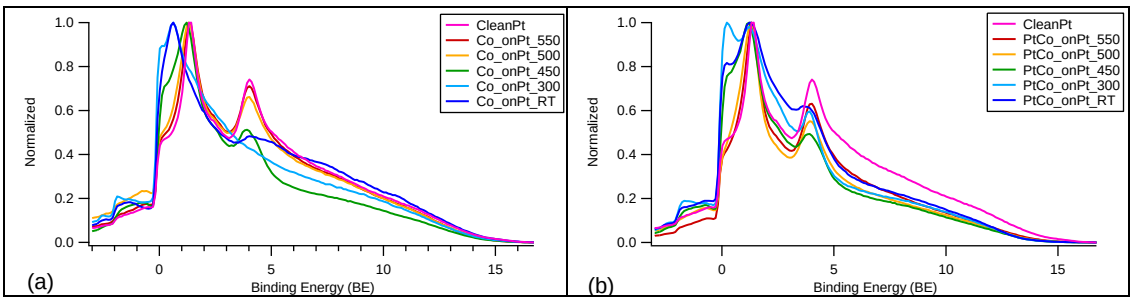

Figure 4.25: UPS spectra (HeI) of a) Co and b) PtCo samples prepared on Pt(111) at different temperatures.

The valance structures of PtCo and Co films prepared on single crystal platinum show nearly the same characteristics as pure platinum does, especially at higher temperatures. The Co sample grown on Pt (111) shows exactly the same electron distribution with pure platinum while the PtCo sample shows a little difference at far-fermi peak. At lower temperatures, Co peak is around 0eV can be seen in both samples. Co sample prepared on platinum single crystal shows a Co dominant electron distribution around Fermi but a small peak which is the far-fermi peak of platinum, is near to 4eV,. On the other hand, the valance structure of the Co sample prepared at 300°C loses its far-fermi peak and resembles to the pure Co valance levels.

Changes in the UPS spectrum from PtCo sample with respecting preparation temperatures are similar with Co samples results. However there are differences in fermi-away peaks with increasing temperature. At RT, PtCo valance structure is a

mixed form of Pt and Co characteristics with 3 peaks at 0eV, 1,5 eV and 4 eV. The peak in 4 eV is not sharp like in the spectrum of the Co sample prepared at RT. On the contrary of Co sample, the far-fermi peak is sharpened by increasing temperature up to 300°C, when the 0eV peak increases like in the Co sample. With increasing the sample preparation temperature to 450°C, both samples' valance spectra give mixed electron distributions of Pt and Co. In order to investigate the Pt-Co and Pt-PtCo interactions, the valance spectra of both samples for each temperature is shown in Figure 4.26.

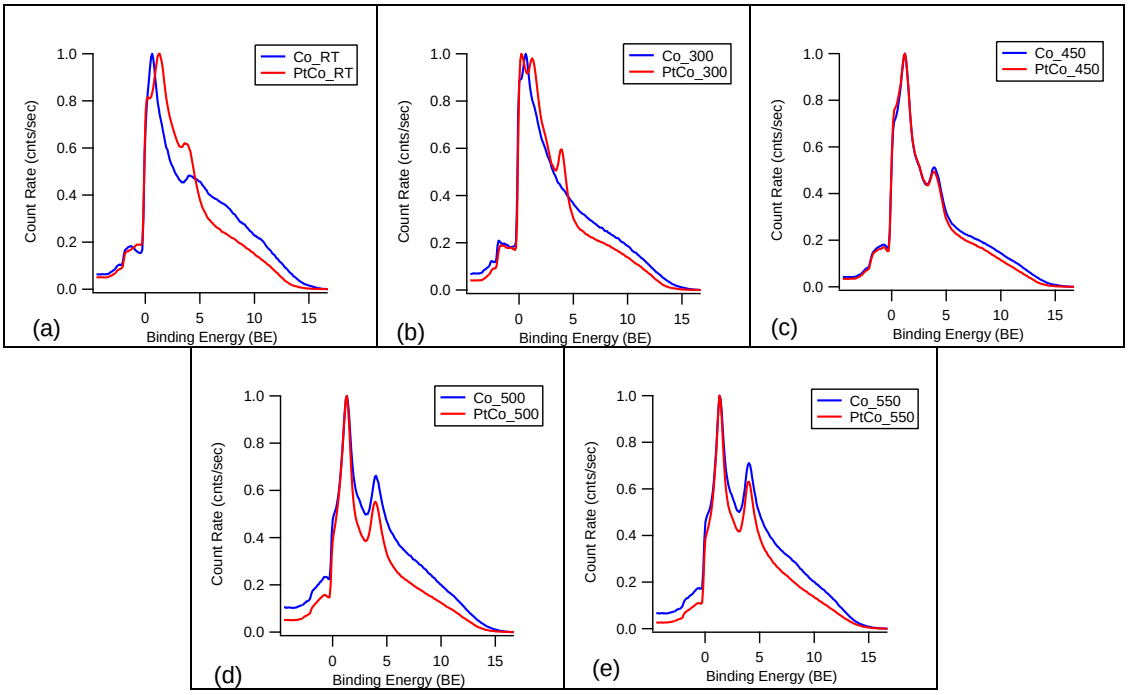

Figure 4.26: UPS comparisons of PtCo(red) and Co (blue) samples for sample preparation temperatures of a) RT, b) 300°C, c) 450°C, d) 500°C and e) 550°C.

The comparison of the samples at RT show a mixed feature with Co dominant at Co sample and a PtCo mixed structure at PtCo sample. This result is not surprising due to the difference of the films grown on the substrate and due to the lack of temperature for an interaction between Pt and Co. However, with the temperature increased up to 300°C, both the spectra take more stable shapes with sharpened peaks.

At higher temperatures (i.e. 500°C and 550), both spectra become nearly the same with pure Pt. On the other hand, the samples prepared below 500°C have different valance electron distribution especially around far-fermi peak. Both PtCo

and Co samples grown at 450°C, show exactly the same valance structure. This distribution is a superposition of both Pt and Co characteristics. As it is mentioned in previous chapter (4.2 XPS Results for Surface Characterizations), peak-fitting results of the pure Co and PtCo samples prepared on Pt(111) single crystal showed equal Pt/Co stoichiometry above 450°C (Table 4.2 and Figure 4.14). Furthermore valance band structures of both samples also give similar electronic configuration especially at 450°C. Above this temperature, the stoichiometry of the samples should be same. However their electronic configurations show little differences around 4 eV.

• The Samples Prepared on SiO_x

UPS spectra of Co and PtCo samples prepared on SiO_x are given in Figure 4.27.

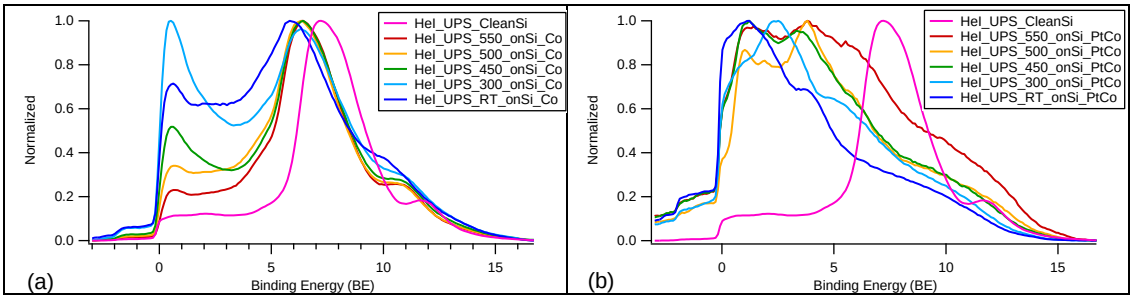

Figure 4.27: UPS spectra (HeI) of a) Co and b) PtCo samples prepared on SiO_x at different temperatures.

The valance electron distributions of the samples prepared on SiO_x substrate have different characteristics than the samples grown on platinum single crystal. Electronic structure of silicon is presented in both spectra. The valance spectrum of cobalt samples are made of two peaks; two peaks around 0 eV and 6.3-5,8 eV belonging to Co and Si respectively. Pure silicon peak at 7.1 eV shifted towards lower binding energy with the cobalt deposition on surface. This shift points out most likely, the formation of metallic surface than the SiO_x substrate because of cobalt deposition. Shifts on Si peak are proportional to the shifts of O1s showing Figure 4.18. Increasing the sample preparation temperature up to 300°C affected the samples just like the previous samples prepared on Pt(111). While the peak at the 0 eV increases, Si-peak decreases marginally and it is shifted towards higher binding energy. Furthermore, both peaks are sharp. Above this temperature, Si peak intensity

is increased to pure SiO_x level and stood same with increasing temperature. However, the increment in temperature leads a dramatic decrease in the peak at 0eV. This peak was related strongly to cobalt's electronic structure. At higher temperatures, peak at 0eV nearly disappears although the stoichiometric ratio of Co stands at 30%. Behavior of Co 2p peak in photoemission spectrum (XPS- showing Figure 4.15) under changing temperature matches to the behavior of the valance shape.

UPS spectra of the PtCo samples on SiO_x are much more complex than the any other samples. It depends on the contribution of various elements to the electronic structure (Pt, Co and Si). With each temperature change, the valance electron distribution of the sample undergoes through serious changes. The core level investigation of the samples showed strong electronic interaction between Pt, Co and Si with a dramatic loss in Co asymmetric tail and with shifts in Pt electron's binding energy. The shifts in Pt reagion are terminated when the temperature reaches to 450 °C (Table 4.3). In UPS, the peaks around 1.2 eV and 3.8eV do not shift significantly above 450°C. However, higher binding energy part of the spectrum increases at 550°C. This part of the spectrum is strongly related to Si. Furthermore, the Co related peak at 0eV also varies with changing temperature. These results point out that the formation between Pt, Co and Si vanishes at 450°C. Additionally, the electronic structure of Pt stands same after 450°C; yet Co and Si electronic structures continue changing even above this temperature.

4.4. AES Results for Elemental Calculations

AES measurements are also performed in the same analyze chamber with the same setup for UPS and XPS experiments but with an electron gun excitation source. Analyzer parameters of AES are adjusted for fixed values in order to have the same analysis conditions. Electrons with 2keV energy are used in the measurements. Taken auger spectra are differentiated and smoothed by the algorithm written in Igor workplace.

Auger spectroscopy gives similar information as XPS but with slightly different features. AES is much more surface sensitive comparing to XPS. Because of this difference in surface sensivity in both techniques, the film homogeneity can

be investigated by comparing the AES and XPS spectra. For stoichiometry calculations, the similar equation used for XPS is adapted with different sensivity factors called relative sensivity factor (RSF). RSF values chosen for the calculations are [49];

- 0,4 for oxygen
- 0,28 for silicon
- 0,23 for cobalt
- 0,28 for platinum

AES spectra of cobalt and platinum for Co and PtCo on Pt(111) and on the naturally oxidized Si(100) substrates are given in Figure 4.28, 4.29 and Figure 4.30-4.33 respectively.

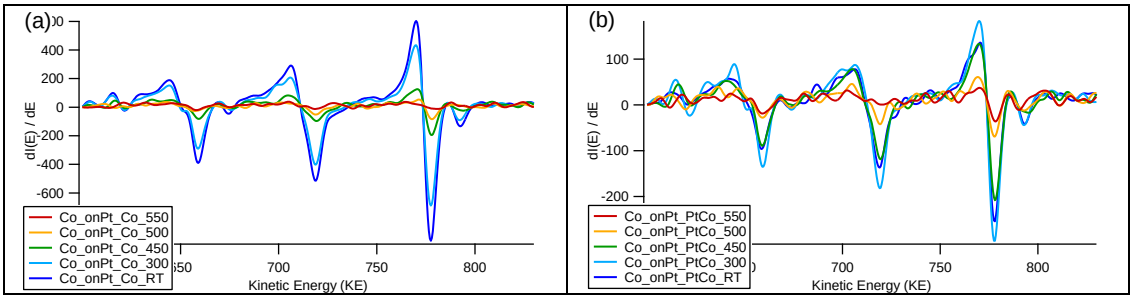

Figure 4.28: AES: spectra of cobalt for a) Co and b) PtCo samples prepared on Pt(111).

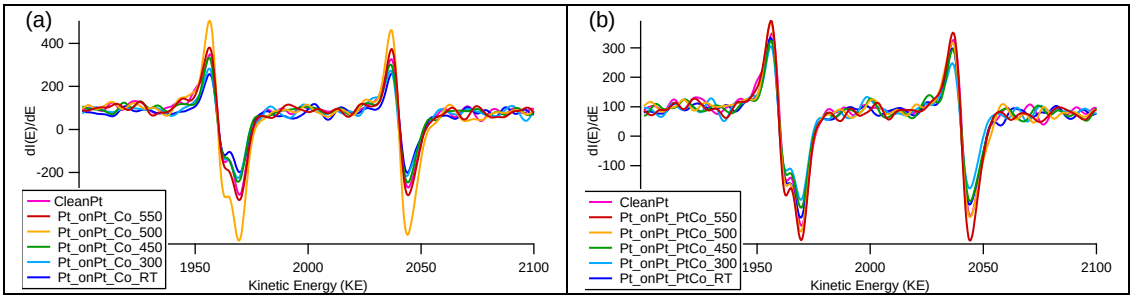

Figure 4.29: AES spectra of platinum for a) Co and b) PtCo samples prepared on Pt(111).

AES results show almost the same agreement as XPS results done for the investigating of spectral intensity but some little differences due to more surface sensivity. For example, the intensity of Pt auger spectrum of Co sample grown on

Pt(111) gives the highest intensity at 500°C while XPS results gave the highest intensity at the 550°C. Auger spectra of PtCo on Pt(111) , Co and PtCo on SiO_x, have the same trend as the XPS results. In both analysis results (i.e. XPS and AES), Co composition of the PtCo and Co samples on Pt(111) and PtCo sample on SiO_x decreases with the increasing temperature.

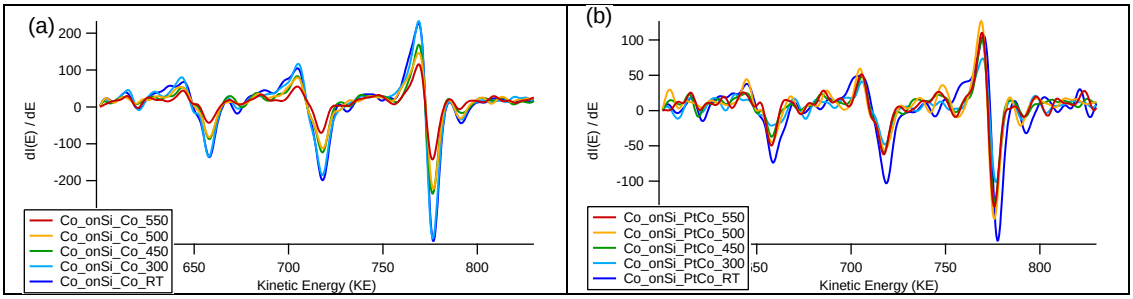

Figure 4.30: AES spectra of cobalt for a) Co and b) PtCo samples prepared on SiO_x.

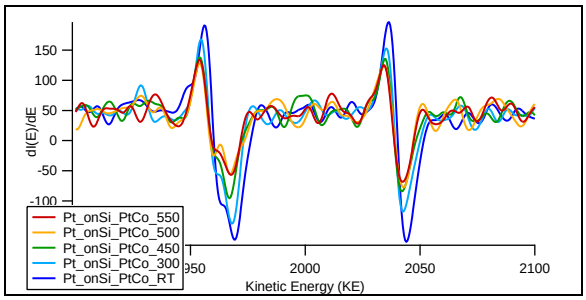

Figure 4.31: AES spectra of platinum for PtCo samples prepared on SiO_x.

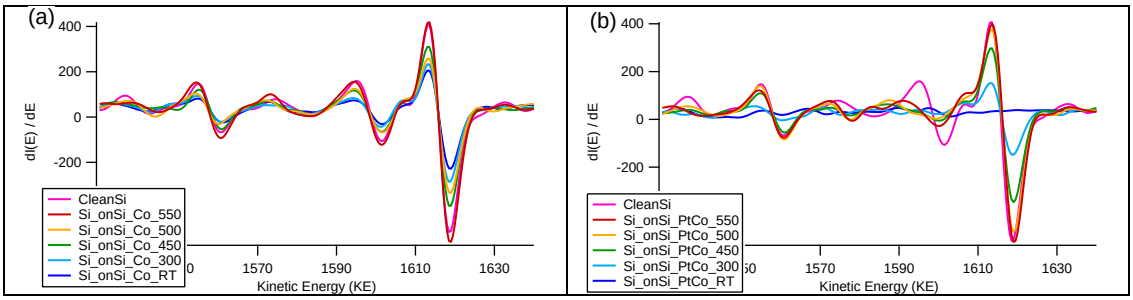

Figure 4.32: AES spectra of silicon for a) Co and b) PtCo samples prepared on SiO_x.

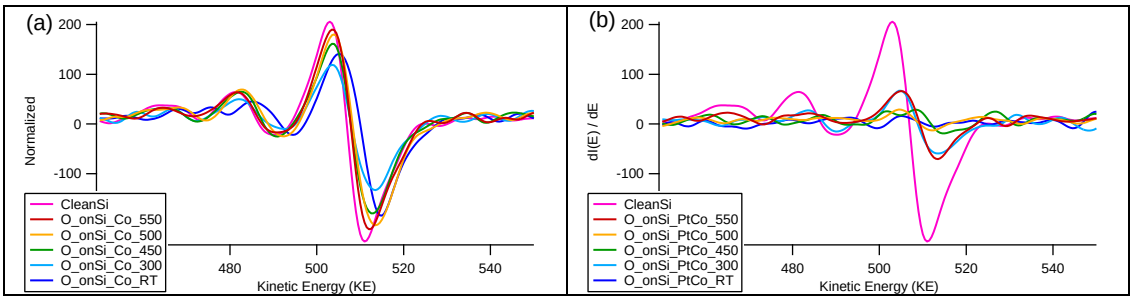

Figure 4.33: AES spectra of oxygen for a) Co and b) PtCo samples prepared on SiO_x.

Also in both analysis results, Co composition of PtCo sample prepared on SiO_x does not change significantly over changing the sample preparation temperature. Energy shift of the Pt4f spectral line of the PtCo sample on SiO_x for increasing temperature is also observed in both XPS and AES results İN-SİTU. The stoichiometry calculations are essential for a final statement.

Table 4.4: Pt/Co ratio calculated from auger spectra of Co and PtCo samples grown on Pt and Si substrate.

	onSi		onPt			
	PtCo		PtCo		Co	
	Pt	Co	Pt	Co	Pt	Co
Clean	0,00%	0,00%	100,00%	0,00%	100,00%	0,00%
RT	50,72%	49,28%	52,74%	47,26%	19,81%	80,19%
300	55,95%	44,05%	42,10%	57,90%	26,45%	73,55%
450	43,91%	56,09%	55,33%	44,67%	58,40%	41,60%
500	37,00%	63,00%	78,92%	21,08%	85,02%	14,98%
550	39,18%	60,82%	88,77%	11,23%	94,70%	5,30%

Results of the stoichiometry calculations of Pt/Co ratio of all samples are given in Table 4.4 and in Figure 4.34. Unlike the 7:3 ratios from XPS results, AES calculations show a ratio of 1:1 for both Pt:Co samples prepared on different substrates at room temperature. Above room temperature, there are of 5% difference between the stoichiometries calculated by both XPS and AES. This small variation can also be explained by the differences of the emission cross-section of both techniques. UPS and XPS done for PtCo and Co films prepared on Pt(111) substrate at 450°C give the same characteristic and elemental ratios.

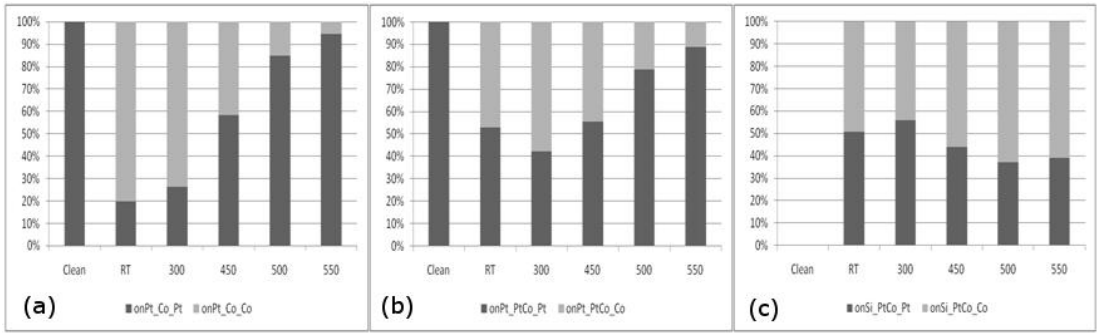

Figure 4.34: Pt-Co ratio of a) Co and b) PtCo samples prepared on Pt(111) and c) PtCo sample prepared on SiO_x substrate. Calculated by AES.

AES analysis of PtCo sample prepared on both SiO_x and Pt(111) substrates indicate different results with XPS. The Co composition of the PtCo on SiO_x is calculated as 1:1 for the room temperature. This composition was calculated 20% lower (Pt/Co – 7/3) with XPS results. Increasing the sample preparation temperature of PtCo on SiO_x did not change the Pt/Co ratio significantly.

4.5. LEED Results for Structural Characterizations

Low energy electron diffraction experiments are performed within the analyze chamber by the ErLEED optics and a CCD camera for image capturing. Electron energies from 90 to 310 eV are mainly scanned in the study (Figure 4.35).

LEED studies are essential for epitaxial film growth. Based on the diffraction of electron in 2-D surface, LEED is the most sensitive technique to study the surface symmetry of a structure. However, this extremely high surface sensitive technique requires in-situ sample preparation and analysis. LEED patterns, taken from substrate and films, will be used to understand the changes in the surface symmetry, quality of the epitaxial films and surface relaxations of the samples prepared on Pt(111) substrate.

Co and PtCo samples are prepared on the Pt(111) substrate at the same temperature. Both samples have the same surface symmetry with different epitaxy quality. For a perfect crystal structure, LEED patterns must be sharp, blurred patterns are the results of miss-locations of atoms in crystal. Below 450°C sample preparation temperature, the LEED patterns are blurry especially at Co samples.

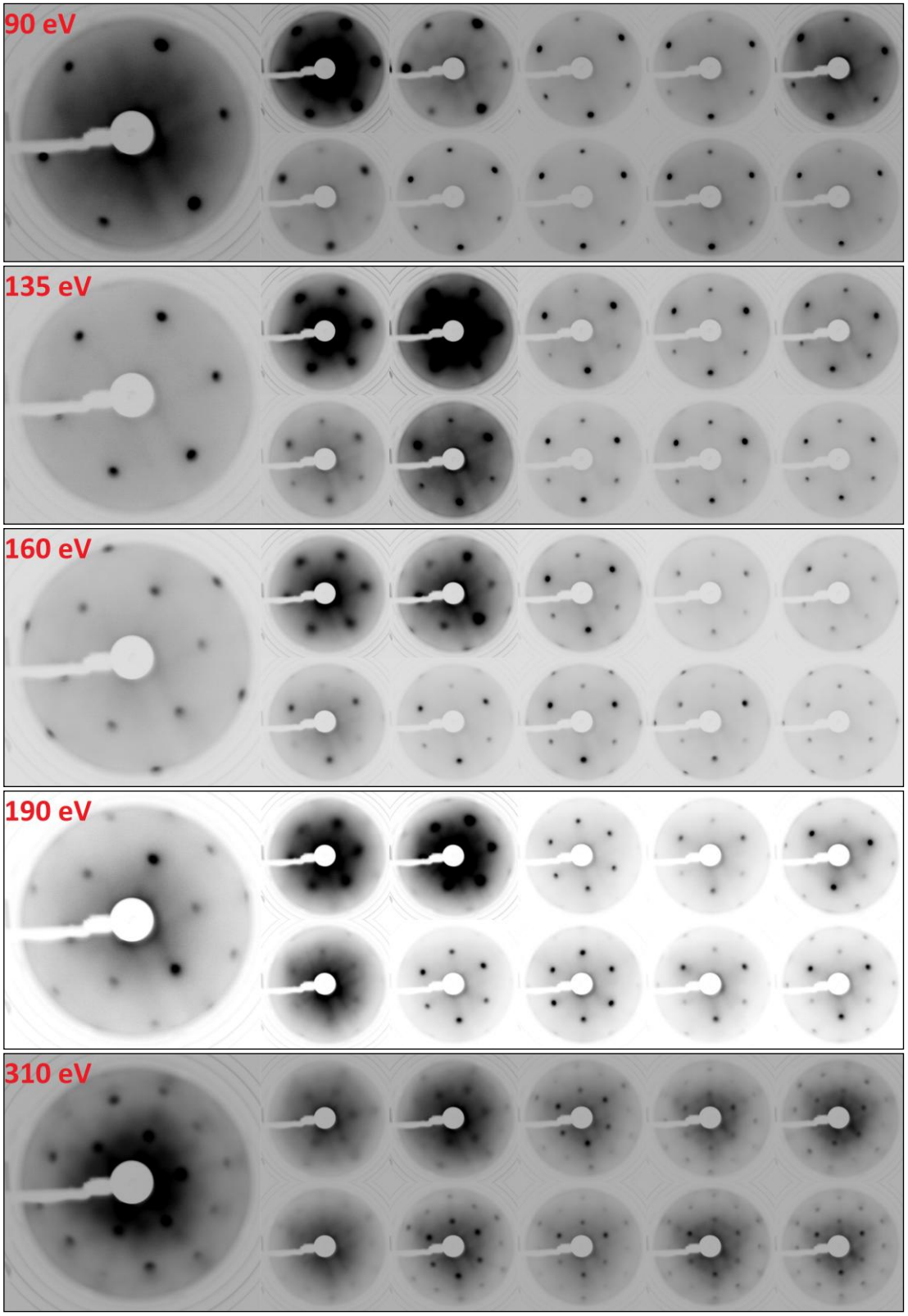

Figure 4.35: LEED patterns for different energies of Pt(111) substrate (left), Co (top) and PtCo (bottom) surfaces prepared at 550°C, 500°C, 450°C, 300°C and RT (right to left) substrate temperature.

It indicates that, for the samples prepared below 450°C, instead of pure Co, PtCo deposition helps the atoms to settle on lattice point and forms a well ordered crystal surface. On the other hand, the surface symmetry of the samples prepared at above 450°C is slightly different. The patterns taken from the samples prepared at lower temperatures are relaxed and the peaks intensities are not similar to clean Pt substrate and the samples prepared above 450°C. LEED patterns become sharp enough after 450°C which indicates a lower limit of annealing temperature for epitaxial film preparation of PtCo.

A PtCo of $L1_0$ phase has a symmetry group of 123:p4/mmm with atomic positions at [51, 52];

- Co @ $2e\left(0,\frac{1}{2},\frac{1}{2}\right)$
- Pt @ $1a(0,0,0)\ and\ 1c\left(\frac{1}{2},\frac{1}{2},0\right)$

, where $a = 3{,}806$ Å and $c = 3{,}684$ Å and $e = (a^2 + c^2)^{1/2}$ [53]. Figure 4.35 shows the positions of a $L1_0$ unit cell for PtCo. Diagram is calculated and sketched at ATOMS® V6 software.

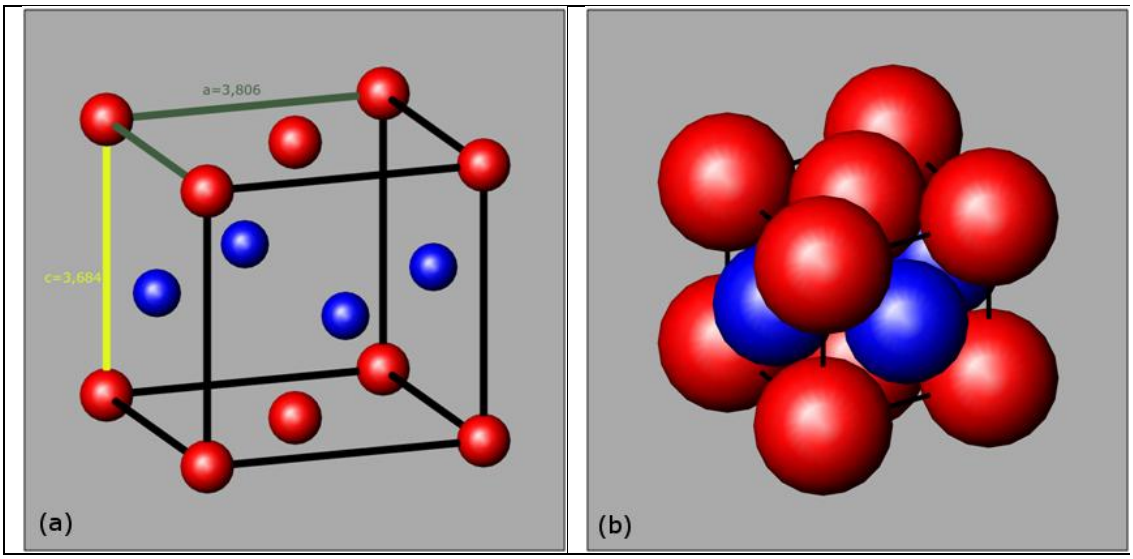

Figure 4.36: $L1_0$ crystal structure for PtCo, a)$r_{left} = r_{real}/4$, b) $r_{right} = r_{real}$.

Atomic radius (r_{real}) is taken, 1,39Å for Pt and 1,25Å for Co. From the structure sketched in Atoms software, the (111) surface of PtCo $L1_0$ is calculated (Figure 4.36). The surface has a hexagonal structure on an oblique lattice. The parameters of

the oblique lattice are $a = 2{,}6913$ Å , $b = 2{,}6485$ Å and $\theta = 59{,}46°$. LEEDpat® software has been used for LEED pattern calculations. The difference in atom types in the lattice will reflect as a difference in brightness in LEED points.

The patterns for clean Pt(111) surface nearly fits perfectly to the surfaces of the samples prepared at 500°C and at 550°C. It shows that the symmetry of these surfaces is the same each other. However, the sample prepared at 450°C shows different domain structure than at 500°C, 550°C and clean Pt(111).

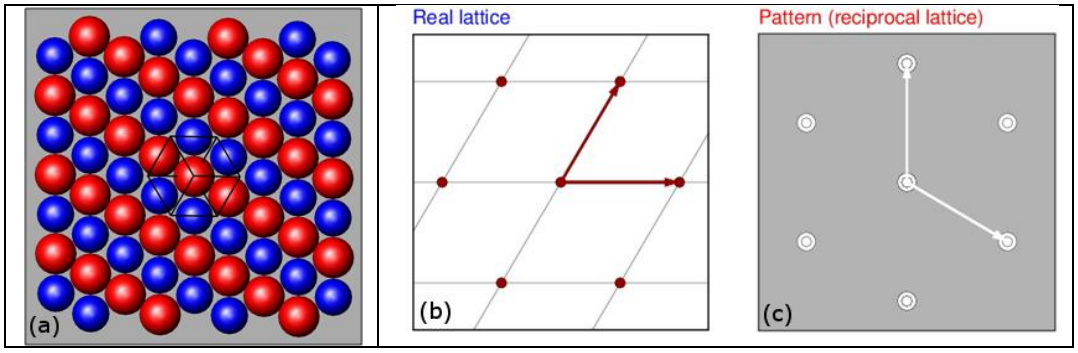

Figure 4.37: Real a) space and b) lattice and c) reciprocal lattice of PtCo surface.

However, the similarities of the surface indicate the crystal structures are the same for all the samples prepared above 450°C. Furthermore, the LEED patterns at 450°C have more relaxed pattern than the samples prepared at 500°C and 550°C. The LEED pattern is just a picture of reciprocal space points and the unit in reciprocal space is m^{-1}, thus a relaxation in pattern means a tightening in real space. This feature can be clearly seen at pattern taken by 190eV electron energies (Figure 4.38).

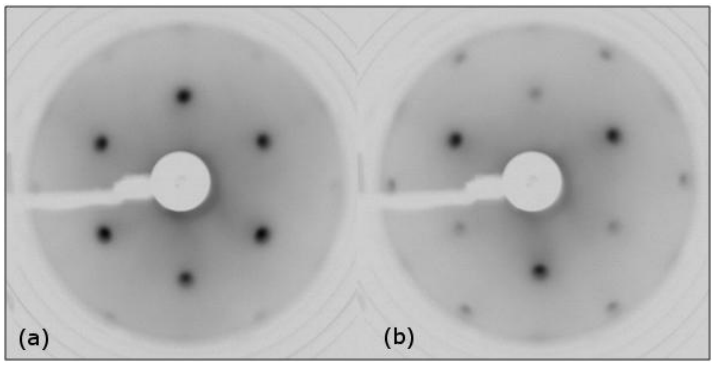

Figure 4.38: 190eV LEED pattern for PtCo samples prepared at a) 450°C b) 550°C on Pt(111).

Stoichiometry calculations were indicating higher Co ratio at 450° compare to the higher temperatures. Co has a smaller atomic radius compare to Pt (r_{Pt}=1,39Å, r_{Co}=1,25Å), thus the increase in cobalt ratio reduces the crystal parameters. The relaxation in LEED pattern is related with the increasing of the Co ratio. It also can be seen at lower temperature samples. The samples below 450°C have higher Co ratio and they have a more relaxed LEED pattern (Figure 4.35) even if the patterns are blurry due to the uncompleted surface.

5. DISCUSSION AND SUMMARY

The purpose of thesis is to investigate the behavior of cobalt as a function of preparation temperature on different substrates when it forms in alloy thin films with platinum. In previous studies, the photoemission analyzes indicated that the ratio of Cobalt became less than PtCo alloys. This type of unexpected variations is limited to the sensitivity of control-manner deposition for ultra-thin layer film technologies. PtCo thin films have potential applications in the magnetic films sensors having ultra-thin layers since it has perpendicular magnetization and high magnetic anisotropy. Some catalyze surfaces in hydrogen fuel cell applications are fabricated by using PtCo multiyear, since Pt ultra-thin layers covers the Co clusters so that the active surface area increase and the enthalpy energy for reaction decreases; however this phenomena would be investigated in range of molecular dimensions while thin layer of PtCo ought to be deposited in control-manner with high sensitivity.

- The Samples Prepared on Pt(111)

The selected ratio 50:50 of Co in alloy film of PtCo is used in this work and it is observed that the Co ratio reduces prominently. The samples prepared deliberately with Pt poor at room temperature even shows lower Co ratio. Although, the results of AES characterizations, done for PtCo films prepared on different substrates at room temperature, give PtCo elemental ratio of 1:1, XPS results done for the same samples pointed out PtCo ratio of 7:3. The differences between XPS and AES results are interpreted in first conclusion that the photoemission electron could be screened by secondary electrons but AES electrons might not be involved in the screening mechanism since they spend more time in the surface than the photoemission does.

The behavior of Co varies with function of preparation temperature on different substrates. The samples prepared on Pt(111) substrate, were investigated on their electronic, stoichiometric properties and their surface symmetries with the function of the substrate temperatures. It does not matter which substrate is used, the photoemission intensity of Co has been observed a dramatic drop with the function of the preparation temperature for both pure Co and PtCo samples. This drop in Co intensity could indicate a diffusion of Co atoms into the surface of Pt(111) crystal. This quick conclusion is supported by the results of photoemissions done after the

extending etching times and increasing the substrate temperature in order to clean the surface of Pt(111). After every experiment, the ultra-thin films on Pt(111) should be cleaned of and be prepared for next experiment. For every other cleaning cycle, the total etching time increases; also while etching, the reasonable high substrate temperature helps to clean the surface more efficiently. As mentioned above, it is observed that the photoemission intensity of Co in Pt Co films deposited on the surface is even getting less and less after every cleaning process with reasonably high substrate temperature.

It is also noticed that annealing temperatures used to prepare thin films in well-ordered have some effects on Co intensities of the films. Elemental ratio of Co and PtCo samples prepared on Pt(111) has been observed nearly equal at higher temperatures (450 °C and higher). Both XPS and AES calculations show the same trend in Pt/Co ratio while increasing preparation temperature. This last works indicate that two possible mechanisms cause to reduce Co intensity. Either the Co gets vaporized with the preparation temperature or gets diffused through the surface of the crystal substrate.

Furthermore analyze, UPS spectrum gives additional information about electronic structure near the fermi surface as supporting the conclusion. Valance band shapes coming from the surface ofCo and PtCo films on Pt(111) have different characteristics at room temperature. While Co films on Pt(111) substrate has a Co dominant valance-electronic structure, PtCo films shows a mixture of both structure as expected. Increasing in annealing temperature transforms the valance structure toward platinum like shape. Specifically at 450°C, the valance shapes of both samples overlap each other. Meanwhile, when the sample preparation temperature is increased more beyond 450°C, the elemental ratio of both samples stands the same; their electronic structure shows a minor differences. While the near-fermi peak (~ 1,3 eV) stands same for the sample prepared at 450°C , 500°C and 550°C , the far-fermi peak (~ 4 eV) shows lower electron population for PtCo sample, but the valance bands for both samples intends to become the same with increasing temperature. Surprisingly, clean Pt(111) substrate's the far-fermi peak has nearly equal electron population with Co sample instead of PtCo.

LEED analyses on Co and PtCo films on Pt(111) support the UPS results and show a good epitaxial films prepared for higher temperatures (450°C, 500°C and 550°C). LEED patterns of Co and PtCo films are similar to each other at these

temperatures. Although the patterns of the sample at 500°C and 550°C have nearly equal surface symmetry to clean Pt(111) surface, the surface structure of Co and PtCo films prepared at 450°C Co shows a relaxed LEED pattern with different domain structures than the other three surfaces (films prepared at RT, 500°C, 550°C) at do. The relaxation in surface points out a tightened crystal surface. It is known that Co has a lower atomic radius than Pt'. It is concluded that the higher Co Contents on the surface lead to relax surface parameter with different domain structure at 450°C preperation temperature.

All the results obtained from the sample prepared on Pt(111) indicates that some of Co atoms on the surface deposited clearly diffuse through the surface of Pt(111) crystal in some level. Meanwhile the rest of the Co atoms with Pt atoms make an ordered structure at 450°C, which is like Pt(111)'s but more relax and with different domains. At the higher temperature, the surface symmetry and elemental ratio stand almost same but the electronic structure shows differences.

- The Samples Prepared on The naturally Oxide surface of Si(111)

The behavior of Co behaves different in Co Films on SiO_x substrate. As observed on Pt(111), the photoemission intensity of Co decreases but it is not that strong as observed on Pt(111). However the tail on the Photoemission Peak of Co shows a decrease in some level due to the unoccupied electron energy levels above fermi surface. The decrease in the photoemission tail occurs between room temperature and 300°C (as preparation temperature). It also makes to rise the height of Co main peak, even higher than at RT. Above 300°C temperature, the shape of the peak stands same while its intensity gets lower. The variation on the photoemission peak of Co indicates a disturbance on the charge distribution around Co atoms in the surface. The peak positions of Co and Si in XPS do not change significantly with changing temperature. However, O1s peak shows a nearly 1eV shift towards higher binding energy when the temperature is increased up to 300°C from room temperature. The peaks of Co, Si and O in AES show the same intensity change as XPS results do, and the shift on the oxygen auger peak has the same trend as it has in XPS spectrum but with a higher magnitude.

UPS spectrum of Co films shows similar properties with XPS and Auger spectra. The near-fermi peak in UPS spectrum belongs to Co atoms while the far-fermi peak (~ 6 eV) is the contribution of Silicon from the substrate. With the

increase in temperature, it's clearly seen that the electron population near the fermi level is increased and the far-fermi peak shifted to higher binding energy in order to satisfy a more stable electronic structure on the surface. This change in near-fermi level may probably relate to the change in Co tail shape observed in XPS. It can be interpreted that Co interacts with the oxygen in the SiO_x substrate and it forms a new compound with independent electronic structure.

The results for The PtCo films on SiO_x substrate showed whole different features but the increase of Si peaks at XPS and AES spectra. Beside all results, the photoemission intensity of Co in XPS does not decrease. However, the decrease in the tail of Co2p peak is observed on PtCo films as observed for the Co films. Furthermore conclusion on the results, the decreasing on the photoemission of Co atoms is not observed and it indicates that there is no diffusion on the surface, but the variation on the tails of Co2p in XPS indicates a distribution on the charge distribution around Co atoms. Asymmetric Co2p photoemission line transforms to a typical voigt shaped peak. Additionally, there has been an energy shift of 1.7 eV in Pt4f line to the higher BE. These observations point out a formation of a different compound. The characterization of UPS were performed also supports the shift in the photoemission peak of Pt4f, although the UV photoemission spectroscopies are hard to be analyzed due to the arbitrary contributions of of Pt, Co, O and Si. On the other hand, the contribution of Si also varies with respect to preparation temperature, and it shifts arbitrarily. It might be interpreted that Si in the substrate has a role to occur a chemical bonding on the surface.

To understand the shift in Pt4f line and the shape of Co2p curve, it is necessary to compare the results coming from Pt(111) and SiO_x substrate with literature support. If the interaction was just between Co and Pt in PtCo films on SiO_x substrate, the similar behaviors would be observed for the samples prepared on platinum single crystal. Furthermore, the research done in literature shows that platinum and silicon can make a PtSi bond and this formation causes shifts the platinum 4f line for a 1,7 eV [50]. Additionally, the change in the tail of Co2p is also weakly observed in Co sample prepared on silicon substrates. Silicon has an electron affinity of 1,3895210 eV while Cobalt has 0,6633 eV; therefore, Co is not easily oxidized by oxygen from SiO_x substrate. However, JooHyung Kim and his friends showed that Co can form $CoSi_2$ so that the asymmetric tail of Co2p vanishes in XPS [54].

REFERENCES

[1] Artymowicz D.M., Lairson B.M.,Clemens B.M., (1996), "Formation of ordered tetragonal PtCo from epitaxial PtCo multilayers", Journal of Crystal Growth, 169(1), 83-88.

[2] David P., (2005), "Synthesis And Characterization Of Cobalt-Platinum Thin Films", Master Thesis, Louisiana State University and Agricultural and Mechanical College.

[3] Andreazza P., Pierron-Bohnes V., Tournus F., Andreazza-Vignolle C.,Dupuis V., (2015), "Structure and order in cobalt/platinum-type nanoalloys: from thin films to supported clusters", Surface Science Reports, 70(2), 188-258.

[4] Schierbaum K.D., Fischer S., Torquemada M.C., de Segovia J.L., Román E.,Martín-Gago J.A., (1996), "The interaction of Pt with TiO2(110) surfaces: a comparative XPS, UPS, ISS, and ESD study", Surface Science, 345(3), 261-273.

[5] Kang S.H., Sung Y.-E.,Smyrl W.H., (2008), "The Effectiveness of Sputtered PtCo Catalysts on TiO2 Nanotube Arrays for the Oxygen Reduction Reaction", Journal of The Electrochemical Society, 155(11), B1128-B1135.

[6] Erkovan M., (2010), "Investigation of Magnetic Properties and Crystallographic Structure of Transition Metal Ultra-Thin Films", Doctorate Thesis, Gebze Institute of Technology.

[7] Enghag P., (2008), "Encyclopedia of the Elements: Technical Data - History - Processing - Applications" 1st Edition, Wiley-VCH.

[8] Murth V.S.R., Gupta K.P., Jena A.K.,Murty G.S., (2003), "Structure & Properties Of Engineering Materials" 1st Edition, Tata McGraw-Hill.

[9] Nie X., Jiang J.C., Meletis E.I., Tung L.D.,Spinu L., (2003), "Synthesis, structure, and magnetic properties of ε-Co nanocrystalline thin films and annealing effects", Journal of Applied Physics, 93(8), 4750-4755.

[10] Sun S.,Murray C.B., (1999), "Synthesis of monodisperse cobalt nanocrystals and their assembly into magnetic superlattices (invited)", Journal of Applied Physics, 85(8), 4325-4330.

[11] Kitakami O., Sato H., Shimada Y., Sato F.,Tanaka M., (1997), "Size effect on the crystal phase of cobalt fine particles", Physical Review B, 56(21), 13849-13854.

[12] Coles B.R.,Phil D., (1964), "The Magnetic Properties of Platinum Metals and Alloys", Platinum Metals Rev., 8(1), 3.

[13] Massalski T.B., Murray J.L., Bennett L.H.,Baker H., (1986), “Binary alloy phase diagrams” 1st Edition, American Society for Metals.

[14] Capitan M.J., Lefebvre S., Calvayrac Y., Bessiere M.,Cenedese P., (1999), “Study of the chemical dependence of the effective pair potentials of Co-Pt alloy”, Journal of Applied Crystallography, 32(6), 1039-1049.

[15] Leroux C., Cadeville M.C., Pierron-Bohnes V., Inden G.,Hinz F., (1988), “Comparative investigation of structural and transport properties of L1 0 NiPt and CoPt phases; the role of magnetism”, Journal of Physics F: Metal Physics, 18(9), 2033.

[16] Sanchez J.M., Moran-Lopez J.L., Leroux C.,Cadeville M.C., (1989), “Magnetic properties and chemical ordering in Co-Pt”, Journal of Physics: Condensed Matter, 1(2), 491.

[17] Pearson W.B., (1958), “Handbook of Lattice Spacings and Structures of Metals and Alloys” 1st Edition, Pergamon Press.

[18] Xu X.-H., Yang Z.-G.,Wu H.-S., (2005), “A high (0 0 1)-oriented CoPt/Ag film deposited on glass substrate”, Journal of Magnetism and Magnetic Materials, 295(2), 106-109.

[19] Lairson B.M., Visokay M.R., Marinero E.E., Sinclair R.,Clemens B.M., (1993), “Epitaxial tetragonal PtCo (001) thin films with perpendicular magnetic anisotropy”, Journal of Applied Physics, 74(3), 1922-1928.

[20] Lairson B.M.,Clemens B.M., (1993), “Enhanced magneto-optic Kerr rotation in epitaxial PtFe(001) and PtCo(001) thin films”, Applied Physics Letters, 63(10), 1438-1440.

[21] Chang G.S., Lee Y.P., Rhee J.Y., Lee J., Jeong K.,Whang C.N., (2001), “Realization of a Large Magnetic Moment in the Ferromagnetic CoPt Bulk Phase”, Physical Review Letters, 87(6), 067208.

[22] Tohyama T., Ohta Y.,Shimizu M., (1989), “Tight-binding calculations of the electronic structure and magnetic properties in ordered TPt 3 (T=Ti, V, Cr, Mn, Fe and Co) alloys”, Journal of Physics: Condensed Matter, 1(10), 1789.

[23] Ohta Y., Miyauchi M.,Shimizu M., (1989), “A tight-binding calculation of the magnetic properties of TPt (T identical to 3d transition element) ordered alloys with CuAu structure”, Journal of Physics: Condensed Matter, 1(15), 2637.

[24] Kootte A., Haas C.,Groot R.A.d., (1991), “The electronic structure of ordered binary Co-Pt compounds”, Journal of Physics: Condensed Matter, 3(9), 1133.

[25] Lee Y.S., Rhee J.Y., Whang C.N.,Lee Y.P., (2003), “Electronic structure of Co-Pt alloys: X-ray spectroscopy and density-functional calculations”, Physical Review B, 68(23), 235111.

[26] Jyoko Y., Kashiwabara S.,Hayashi Y., (1996), “Preparation and characterization of electrodeposited Pt/Co multilayers”, Journal of Magnetism and Magnetic Materials, 156(1–3), 35-37.

[27] Seshan K., (2012), “Handbook of thin film deposition” 1st Edition, William Andrew.

[28] Bunshah R.F., (2001), “Handbook of hard coatings : deposition technologies, properties and applications, Materials science and processing technology series” 1st Edition, Noyes Publications.

[29] Chung Y.-W., (2001), “Fundamental Concepts In Ultrahigh Vacuum, Surface Preparation, And Electron Spectroscopy” 1st Edition, Academic Press.

[30] (2013), https://en.wikipedia.org/wiki/Electron_spectroscopy. (Acces Date :01/05/2015).

[31] John C. Vickerman I.S.G., (2009), “Surface analysis : the principal techniques” 2nd Edition, Wiley.

[32] K.K. Kolasinski K.W.K., (2012), “Surface Science: Foundations of Catalysis and Nanoscience” 1nd Edition, John Wiley & Sons.

[33] Chung Y.-W., (2001), “Photoelectron Spectroscopy” 1st Edition, Academic Press.

[34] Einstein A., (1905), “The photoelectric effect”, Ann. Phys, 17(132), 4.

[35] Niemantsverdriet J.W., (2007), “Spectroscopy in catalysis : an introduction” 1st Edition, Wiley-VCH.

[36] D. Briggs M.P.S., (1990), “Practical Surface Analysis, V1: Auger and X-ray Photoelectron Spectroscopy” 2nd Edition, John Wiley & Sons Ltd.

[37] John F. Moulder J.C., (1992), “Handbook of X-Ray Photoelectron Spectroscopy: A Reference Book of Standard Spectra for Identification and Interpretation of XPS Data” 1sth Edition, Perkin-Elmer Corp.

[38] Végh J., (2005), “On analyzing the intrinsic processes through the Shirley background correction procedure”, Surface science, 577(2), 220-228.

[39] Végh J., (2006), “The Shirley background revised”, Journal of electron spectroscopy and related phenomena, 151(3), 159-164.

[40] Hesse R.,Denecke R., (2011), “Improved Tougaard background calculation by introduction of fittable parameters for the inelastic electron scattering cross-section in the peak fit of photoelectron spectra with UNIFIT 2011”, Surface and Interface Analysis, 43(12), 1514-1526.

[41] Maddams W., (1980), “The scope and limitations of curve fitting”, Applied Spectroscopy, 34(3), 245-267.

[42] Schönfeld E.,Janßen H., (2000), “Calculation of emission probabilities of X-rays and Auger electrons emitted in radioactive disintegration processes”, Applied Radiation and Isotopes, 52(3), 595-600.

[43] Chung Y.-W., (2001), “Auger Electron Spectroscopy” 1st Edition, Academic Press.

[44] Wandelt K., (1986), “LJ Clarke: Surface Crystallography—An Introduction to Low Energy Electron Diffraction”, Berichte der Bunsengesellschaft für physikalische Chemie, 90(1), 98-99.

[45] VanHove M.A., Weinberg W.H.,Chan C.-M., (2012), “Low-energy electron diffraction: experiment, theory and surface structure determination” 1st Edition, Springer Science & Business Media.

[46] Chung Y.-W., (2001), “Low-Energy Electron Diffraction” 1st Edition, Academic Press.

[47] Öztürk O., (2002), “Growth and Structure of Ultra-Thin Epitaxial Chromium and Iron Oxide Films on Silver(001) and Silver(111): A Comprehensive Study Accomplished by X-Ray Photoelectron Diffraction and Low Energy Electron Diffraction”, Doctorate Thesis, University of Missouri-Rolla.

[48] NIST (2015) Atomic Spectra Database (version 5.2), G. National Institute of Standards and Technology, MD.

[49] Wagner C.D., Davis L.E., Zeller M.V., Taylor J.A., Raymond R.H.,Gale L.H., (1981), “Empirical atomic sensitivity factors for quantitative analysis by electron spectroscopy for chemical analysis”, Surface and Interface Analysis, 3(5), 211-225.

[50] Morgan S.J., Williams R.H.,Mooney J.M., (1992), “An XPS study of thin Pt and Ir silicide overlayer formation on Si(100)2 X 1 surfaces”, Applied Surface Science, 56–58, Part 1, 493-500.

[51] Klein C., Hurlbut C.S., Dana J.D.,Mineraloge G., (1993), “Manual of mineralogy” 1st Edition, Wiley New York.

[52] Wyckoff R.W.G.,Wyckoff R.W., (1960), “Crystal structures” 1st Edition, Interscience New York.

[53] Greenwood H.W., (1930), “Dana's manual of mineralogy. By W. E. Ford. 14th edition. Pp. x + 476. London: Chapman & Hall; New York; J. Wiley & Sons, 1929. 20s”, Journal of the Society of Chemical Industry, 49(4), 84-84.

[54] Kim J., Yang J., Lee J.,Hong J., (2008), “Memory characteristics of cobalt-silicide nanocrystals embedded in HfO2 gate oxide for nonvolatile nanocrystal flash devices”, Applied Physics Letters, 92(1), 13512-13512.

BIOGRAPHY

Baha Sakar was born at May 1985, in Istanbul, Turkey. He graduated from Erenköy Elementary School, Lycée Français Saint-Benoît d'Istanbul and Fenerbahçe Highschool. He got bachelor's degree from Gebze Institute of Technology at 2012 in Physics and started to pursue a master degree in same university. Since October 2014, he works as a research assistant in Physics Department of the Gebze Technical University.